

The Use of Small Cells to Reduce Radiation Heat Transfer in Foam Insulation

by

Mark D. Mozgowiec

B.S. Lehigh University
(1988)

Submitted to the Department of Mechanical Engineering
in partial fulfillment of the requirements for the degree of

Master of Science in Mechanical Engineering

at the

MASSACHUSETTS INSTITUTE OF TECHNOLOGY

June 1990

© Massachusetts Institute of Technology 1990

Signature of Author
Department of Mechanical Engineering
May 23, 1990

Certified by
Leon R. Glicksman
Professor, Mechanical Engineering
Thesis Supervisor

Accepted by
Ain A. Sonin
Chairman, Departmental Committee on Graduate Studies

MASSACHUSETTS INSTITUTE
OF TECHNOLOGY

AUG 14 1990

LIBRARIES

ARCHIVES

The Use of Small Cells to Reduce Radiation Heat Transfer in Foam Insulation

by

Mark D. Mozgowiec

Submitted to the Department of Mechanical Engineering
on May 23, 1990, in partial fulfillment of the
requirements for the degree of
Master of Science in Mechanical Engineering

Abstract

A model which predicts the radiative component of heat transfer in foam insulation based on foam density and cell size has been improved. The model assumes that thermal radiation is attenuated by cell walls and by struts, or linear elements formed by three-way intersections of cell walls. If struts are assumed to attenuate all radiation, the extinction coefficient is inversely proportional to the mean cell diameter and proportional to the square root of the foam density. After finding that cell walls have significant absorptivity, the model was expanded to include cell walls for two limiting cases: optically thin and optically thick cell walls. If the foam consists of optically thin cell walls only, the extinction coefficient is found to be proportional to density but independent of cell size. The optically thick expression is more complicated but simplifies to the optically thin expression when certain assumptions are made.

Experiments were devised to measure the Rosseland mean extinction coefficient from computer analysis of spectrometer data. The foams were also measured for density and mean cell diameter. Two extinction coefficients were determined for each foam from measured transmissivities of thin foam slices. The first coefficient was determined from a best-fit line on a plot of transmissivity vs. slice thickness. The second coefficient was also determined from a line which fit the data but was also constrained to have a transmissivity of unity for zero thickness. Each coefficient was then plotted against a parameter defined by the square root of foam density divided by cell diameter. The theoretical curve for optically thin cell walls fit the data well for only the best-fit definition.

Polyurethane foams were then mixed in the lab with the ultimate goal of determining factors which encourage small cell size without increasing foam density. Foam mixing experiments were carried out to test the practicality of observing foam cell growth with a microscope. From these experiments it was determined that foam could be viewed through a thin sheet of insulated glass. The insulation is necessary to prevent boundary heat transfer effects from affecting cell size.

Thesis Supervisor: Leon R. Glicksman
Title: Professor, Mechanical Engineering

Acknowledgements

This research could not have been possible without funding from the Environmental Protection Agency. Special thanks go to Dean Smith from the EPA for his interest in this project.

Many foam industries were also instrumental in this research. In particular I would like to thank Deb Bhattacharjee from Dow, Jim Mish from ICI, and the Asahi and Fisher-Paykel corporations for their supply of necessary raw materials and information. My introduction to foam mixing was made possible by a visit to Mobay Corp. in Pittsburgh. Special thanks to John Szabat, Don Wysocki, and Chris Aranowski for their help.

Of course, special thanks must be given to Dr. Glicksman, who provided the encouragement and direction to make this project successful.

Finally, I'd like to thank Mom and Dad for their continued love and support.

Contents

Abstract	2
Acknowledgements	4
Nomenclature	7
1 Introduction	13
1.1 Background	15
1.2 Concurrent Foam Projects	18
2 Radiation Theory and Model	20
2.1 Background Theory—Absorbing Media	20
2.2 Foam Radiation Model	22
2.2.1 Assumptions	23
2.2.2 Extinction Coefficient—Struts	23
2.2.3 Extinction Coefficient—Cell Walls	25
3 Radiation Experiments	31
3.1 Description of Foams	32
3.2 Cutting Foam Slices	32
3.3 Collecting Transmission Data	35
3.4 Sample Thickness Measurement	39
3.5 Cell Diameter Measurement	41
3.5.1 The Scanning Electron Microscope	41

3.5.2	Cell Diameter Analysis	43
3.6	Computer Analysis of Spectrometer Data	47
4	Results	54
4.1	Extinction Coefficient Data	54
4.2	Force-Fit vs. Best-Fit Methods	57
4.3	Comparison of Cell Wall Photographs	62
4.4	Error Analysis	65
4.4.1	Transmission Data	65
4.4.2	Foam Slice Thickness	66
4.4.3	Cell Diameter Calculations	66
4.4.4	Density	69
4.4.5	Further Considerations	69
5	Foam Production	73
5.1	Background	74
5.1.1	Foam Chemistry	74
5.1.2	Foam Dynamics and Cell Size Control	76
5.1.3	Foam Board Production	78
5.2	Foam Mixing Experiments	78
5.2.1	Preliminary	80
5.2.2	Boundary Experiments	81
5.2.3	Suggested Viewing Apparatus	94
6	Conclusions	99
A	Computer Code with Input and Output	101
B	Summarized Extinction Coefficient Data for Polyurethane Foams	113
	References	115

Nomenclature

LATIN

<i>a</i>	absorption coefficient, strut length, integration variable
<i>A</i>	area
<i>C</i>	constant, projected area per unit length
<i>d</i>	cell diameter
<i>e</i>	radiative emissive power
<i>f_s</i>	fraction of solid polymer in struts
<i>F</i>	blackbody fraction
FTIR	Fourier transform infrared spectrometer
<i>i</i>	radiative intensity
<i>I</i>	source function
<i>k</i>	thermal conductivity, summation counter
<i>K</i>	extinction coefficient
<i>ℓ</i>	mean chord length
<i>L</i>	length, thickness
<i>n</i>	number of intersections
<i>P</i>	number of intersection points, pressure
<i>q</i>	heat flux
<i>r</i>	radius
<i>S</i>	surface area

SEM scanning electron microscope
 t thickness
 u variable of integration
 V volume
 W work
 x horizontal distance
 y length of line through a sphere

GREEK

α absorptivity
 γ surface tension
 δ void fraction
 Δ difference
 η wavenumber
 θ angle
 λ wavelength
 ρ density
 σ Stefan-Boltzmann constant
 σ_s scattering coefficient

SUBSCRIPTS/SUPERSCRIPTS

<i>b</i>	blackbody
<i>eff</i>	effective
<i>f</i>	foam
<i>g</i>	gas component
<i>L</i>	per unit length
<i>LHS</i>	left-hand side
<i>m</i>	mean
<i>max</i>	maximum
<i>p</i>	peak
<i>r, rad</i>	radiative component
<i>R</i>	Rosseland mean
<i>RHS</i>	right-hand side
<i>v</i>	per unit volume
<i>w</i>	for one cell wall
λ	wavelength-specific
0	boundary condition
1, 2	beginning and ending, or denoting constants in Planck's law
	parallel
\perp	perpendicular

List of Figures

1-1	Transmission through polyurethane membranes	16
1-2	Foam cell and strut cross-sectional photographs	17
2-1	Radiative interaction among high-absorptivity cell walls	28
3-1	Sketch of Isomet saw	34
3-2	Comparison of acceptable and unacceptable FTIR backgrounds	37
3-3	Sample FTIR spectrum	38
3-4	Sketch of paper micrometer	40
3-5	Comparison of optical microscope and SEM photographs	42
3-6	Cell wall and strut cross-sections	44
3-7	Model for integration in cell diameter analysis	46
3-8	SEM photo with grid overlay for calculating cell size	48
3-9	Force-fit vs. best-fit definitions of the extinction coefficient	50
3-10	Input file for FORTRAN program	52
4-1	Extinction coefficient data from force-fit slopes	55
4-2	Extinction coefficient data from best-fit slopes	56
4-3	Data of Cunningham and Sparrow with new theory	58
4-4	Illustration of nonzero intercept on transmissivity plot	60
4-5	Comparison of transmissivity plots for two foams	61
4-6	SEM photos of foam samples cut with the Isomet saw and a razor blade	63
4-7	Comparison of cell wall cross-sections for the same foam	64

4-8	Optical microscope photograph of foam slice cross-section	67
4-9	Test line passing close to a strut	68
4-10	Best-fit extinction coefficient data with error bars	70
5-1	Comparison of elongated and cross-linked polymer molecules	75
5-2	General method of manufacturing foam board	79
5-3	Cross-sectional photographs of free-rise surface skin	82
5-4	Sketch of void formation in lab-blown foams	83
5-5	Sketch of foam blown in cardboard box	85
5-6	Sketch of foam blown in plastic box	86
5-7	SEM photographs of foam cells from foam blown in plastic box	87
5-8	Comparison of cell sizes as seen through the bottom of unheated and heated Pyrex dishes	89
5-9	Sketch of thin-glass viewing experiment	91
5-10	Comparison between cell sizes at glass surface and 1/2" up from surface, thin-glass viewing experiment	92
5-11	Comparison between cell sizes at glass surface and 1/2" up from surface, thin-glass viewing experiment, over hole	93
5-12	Proposed microscope setup for viewing foam	95
A-1	Original ASCII transmissivity file from Nicolet IR44 spectrometer	103
A-2	Transmissivity file modified for input into FORTRAN program	104
A-3	Sample program output	105

List of Tables

3.1	Comparison of saw gage and paper micrometer for measuring foam slice thicknesses	53
4.1	Extinction coefficient, density, and cell diameter data for polyurethane foams	71
4.2	Cell wall thicknesses for eight foams	71
4.3	Uncertainty in transmissivity	72
4.4	Error in paper micrometer measurements	72
4.5	Final results of error analysis	72
5.1	Data for foam blown in plastic box.	97
5.2	Density measurements for Pyrex dish foams	97
5.3	Cell diameter data for foams blown in heated and unheated Pyrex dishes.	97
5.4	Cell diameter data for foams blown in the container of Figure 5.9.	98
B.1	Summarized extinction coefficient data	113
B.2	Comparison of best-fit and predicted extinction coefficients	114

Chapter 1

Introduction

Closed-cell polyurethane foam is currently the best form of insulation available commercially. Its relative ease of mass production makes it suitable for the manufacture of major appliances and in the building industry. A typical polyurethane foam insulation manufactured in panels for buildings has an R-value between 6 and 7 per inch thickness. This means that an inch thick slab of such foam would insulate as well as 5.6 inches of a typical softwood [1]. The exceptional insulating quality of the foam is due to the use of a low-conductivity gas, known as a blowing agent, trapped in a closed-cell matrix of a low-conductivity polymer.

The gas used in most foam insulations is some sort of chlorofluorocarbon (CFC), most likely CFC-11. Until recently CFC's have been recommended and used widely in the foam industry because of their low conductivity and chemical stability. This stability has become an environmental concern, however, since CFC's released into the atmosphere will not break down until they reach the upper atmosphere. The decomposition generally takes place in the ozone layer, where released chlorine tends to break down ozone molecules. The gas is released from the foam by diffusion through the cell walls. Concern over the environmental impact of CFC's has led to worldwide restrictions of its use in the foam industry as well as in other industries. The problem now facing foam manufacturers is how to produce foams with similar thermal qualities in the absence of

CFC's, which have the lowest conductivities of any possible blowing agent.

The purpose of the following report is to provide the basis for one solution to this problem: the reduction of the average cell size in the foam to decrease radiation heat transfer. Though often overlooked, thermal radiation heat transfer is important in foams, since it typically comprises 25 to 30 percent of the total heat transfer [2]. Because of the importance of radiation, research was begun at MIT to study radiative behavior in foam insulation. The intent is to use this study to suggest and test methods of reducing radiative heat transfer without significantly increasing conduction. The project described here is a continuation of that research.

The project is divided into two distinct phases. The first has been completed, and involves a study of the effects of cell size on radiative properties of polyurethane foam. This is a continuation of research done at MIT on radiation heat transfer by Mark Schuetz, Mark Sinofsky, and Mark Torpey, who experimentally obtained for various polymeric foams a property known as the extinction coefficient. This property measures how much radiation is transmitted through a sample of the material as a function of the thickness of the sample. In the current project this coefficient will also be experimentally determined for several foams, and will be plotted as a function of cell diameter and foam density. The relationship obtained will then be compared with a formula derived by Glicksman and Torpey [3], and modifications will be made to the formula to account for any significant effects that were previously neglected.

The second phase is currently in progress and will be continued in future research. In this phase, polyurethane foam will be observed on a microscopic scale as it is being formed. This involves the mixing of foam component chemicals obtained from the industry, and the filming of cell nucleation and growth as the foam is formed. The foam will be filmed with the aid of an inverted biological microscope specially rigged for this purpose. A brief study of polymer chemistry and classical bubble nucleation theory will also be required. The objective is to learn what factors are important in governing the final cell size and how to control this process through physical or chemical means.

1.1 Background

Heat transfer in foams is composed of three separate mechanisms: conduction through the solid polymer, conduction through the gas, and radiation. In the past, models with simplified cell geometry have been proposed to account for the different mechanisms, but many of these have neglected radiation and have thus proved inaccurate. The heat transfer was generally underestimated by these models. Others such as Skochdopole [4] and Doherty et al. [5] included radiation but assumed cell walls were opaque, so the radiation contribution in their models is still quite small. Schuetz [6] tested this assumption by measuring the transmissivity of two polyurethane membranes: one from the surface of a foam “bun” which was allowed to rise freely without constraint, and one from a chemically altered foam which produced large cells (about 5 mm mean diameter). The membranes had thicknesses of 1.5 and 36 μm , respectively. As can be seen from the transmission spectra in Figure 1.1, the free rise bun film had an average transmissivity of about 80 percent. Since the cell wall thickness for a typical polyurethane foam is less than 1 μm , cell walls must be taken as highly transparent. Radiation was thus recognized as a significant mode of heat transfer, and was found to account for most of the earlier underestimations of the total heat transfer.

In estimating radiation heat transfer in foams others, such as Williams and Aldao [7], recognized that the cell walls are highly transparent, but neglected the effect of struts. Struts are the intersections of three cell walls which form a framework of linear elements with approximately triangular cross-sections. A actual strut cross-section, along with a photograph of foam cells at lower magnification, is shown in Figure 1.2. Since the dimension of the strut side is much greater than the thickness of a cell wall (typically 60 times greater), the struts are expected to absorb most of the radiation. Glicksman and Torpey [3] derived a formula for the extinction coefficient which assumes transparent cell walls and blackbody struts. The relation obtained is presented in Chapter 2 and states that the extinction coefficient is directly proportional to the square root of the foam density and inversely proportional to the mean cell diameter.

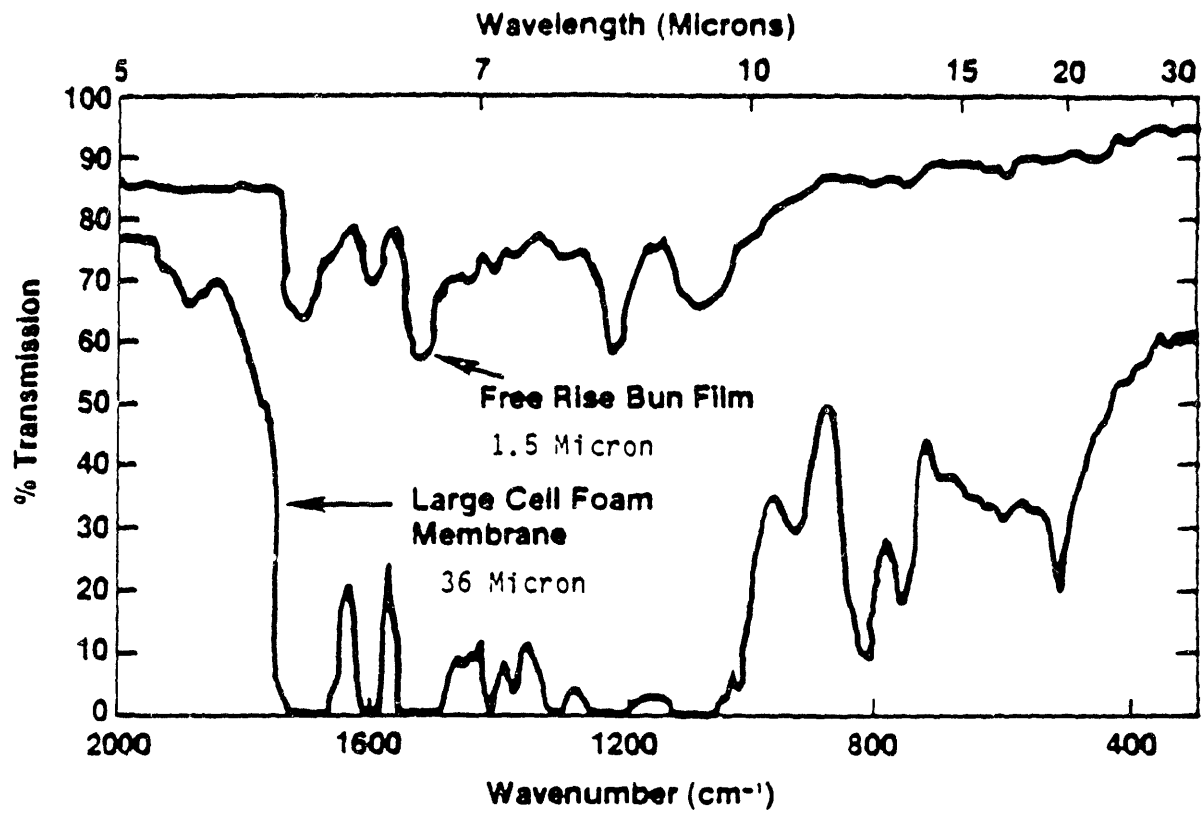


Figure 1-1: Transmission through polyurethane membranes [6].

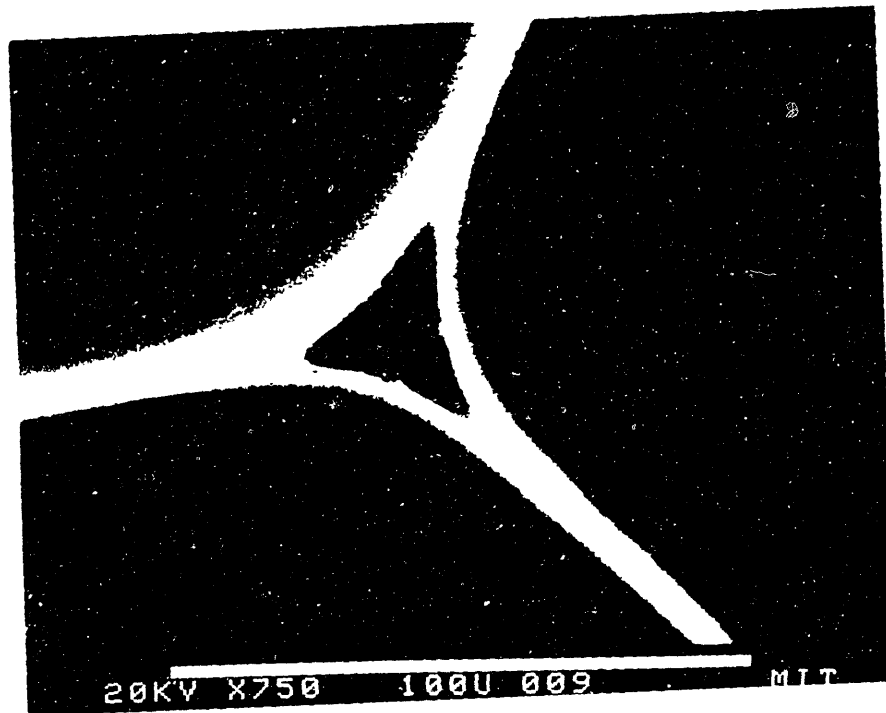
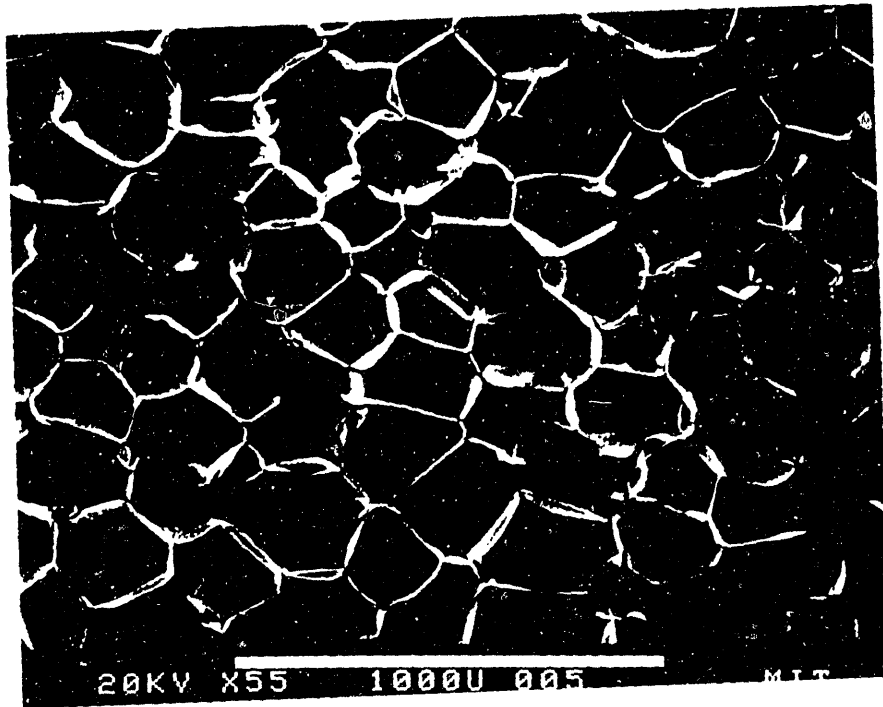


Figure 1-2: SEM photograph of foam cells (top, 55X) and strut cross-section (bottom, 750X).

The extinction coefficient can then be incorporated into a model to predict heat transfer from all three mechanisms. The model which is currently used is presented by Schuetz and Glicksman [2] and begins with a basic expression of Fourier’s Law for heat flux:

$$q = -k_{eff} \frac{dT}{dx} \quad (1.1)$$

The k_{eff} is an effective conductivity accounting for all modes of heat transfer, which can be broken down into components for each mode:

$$k_{eff} = k_g + \left(\frac{2}{3} - \frac{f_s}{3}\right)(1 - \delta)k_s + \frac{16\sigma T_m^3}{3K} \quad (1.2)$$

where k_g and k_s are the gas and solid conductivities, and δ is the void fraction, or the volume percentage of gas in the foam. The parameter f_s represents the fraction of solid polymer in the struts, typically between 0.75 and 0.9. The solid contribution (second) term was derived assuming either cubical cells or isotropic foam with randomly-oriented struts, and the effects of conduction through cell walls and conduction through struts were combined. The final term is known as the “radiative conductivity” and contains the extinction coefficient K in its denominator. The radiative heat flux is thus a strong function of the mean foam temperature T_m and is directly proportional to the mean cell diameter, since the expression derived by Glicksman and Torpey is

$$K = C \frac{\sqrt{\rho}}{d} \quad (1.3)$$

where C is a constant. The radiative conductivity is then

$$k_{rad} = \frac{16\sigma T_m^3 d}{3C\sqrt{\rho}} \quad (1.4)$$

By using this expression as the last term in Eqn. (1.2), it can be seen that reducing the cell size will reduce the radiative heat transfer without affecting solid conduction, as long as f_s and δ are kept constant.

1.2 Concurrent Foam Projects

This research is part of a broader scope of work being done at MIT on improving the thermal performance of foam insulation. The research involves factors affecting all three

modes of heat transfer. One such project analyzes foam aging, or the diffusion of the low-conductivity gas out of the foam and its replacement with air, which decreases thermal performance. Another project seeks to reduce solid conduction by inserting vacuum panels as a conduction barrier. Finally, in addition to the present study, radiation reduction is also being attempted through the addition of small flakes of submicron thickness to the foam chemicals. These flakes would be opaque to thermal radiation, while having conductivities close to or less than the solid polymer.

Chapter 2

Radiation Theory and Model

The following chapter will present a model which predicts radiative heat transfer in foam insulation from material properties and cell geometry. Fundamental concepts of absorbing media relevant to the model will first be reviewed. These concepts are presented assuming a homogenous isotropic medium; when the foam model is presented this assumption will be modified to account for voids in the foam. All radiative properties will be given as wavelength-specific to eliminate the assumption of a gray medium, or one in which properties are independent of wavelength. For more information or a more detailed analysis, the reader is referred to Siegel and Howell [8].

2.1 Background Theory—Absorbing Media

The most important radiative property in the model is the extinction coefficient (K_λ), which is defined by examining a thin slice of an absorbing medium of thickness dx and observing the change in intensity of radiation passing through the slice:

$$di_\lambda = -K_\lambda i_\lambda dx \quad (2.1)$$

Assuming that the medium does not emit its own radiation, the solution to the differential equation is

$$\tau = \frac{i_\lambda(x)}{i_{0\lambda}} = C e^{-K_\lambda L} \quad (2.2)$$

where τ is the transmissivity of a finite thickness L of the medium, and i_0 is the intensity of the incoming radiation, normal to the plane of the slice. The constant in front of the exponential is often taken as unity so that zero thickness would produce a transmissivity of one. This is not always the case, however, as will be seen in Chapter 3.

The extinction coefficient represents how well the medium attenuates radiation, and is actually the reciprocal of the mean free path of a photon. It can be expressed as the sum of two coefficients which denote two methods of attenuation:

$$K_\lambda = a_\lambda + \sigma_{s,\lambda} \quad (2.3)$$

where a_λ is the coefficient due to absorption and $\sigma_{s,\lambda}$ is due to multidirectional scattering. The dimensionless quantity KL in the exponential of Eqn. (2.2) is called the optical thickness of the medium. As seen in (2.2), the higher the optical thickness, the less radiation is transmitted. If $KL \gg 1$, an object is said to be optically thick, in which case a significant amount of radiation is absorbed and re-emitted as well as transmitted. If the presence of emission and scattering are taken into account, Eqn. (2.1) becomes

$$\frac{di_\lambda}{dx} + K_\lambda i_\lambda(x) = K_\lambda I_\lambda(x, \omega) \quad (2.4)$$

where I_λ is called the source function and includes the effects of emission and scattering, which is a function of direction (solid angle ω) as well as position. In the most general case this is a complex integro-differential equation, but can be solved by making simplifications. One of these is a diffusion approximation, which holds for optically thick media and assumes radiative equilibrium with isotropic scattering. Siegel and Howell provide a complete derivation to obtain a simplified expression for the heat flux with this approximation. One form of this expression is

$$q = -\frac{4}{3K_R} \frac{de_b}{dx} \quad (2.5)$$

If e_b , the blackbody emissive power, is expressed as σT^4 , the expression becomes

$$q = -\frac{16\sigma T^3}{3K_R} \frac{dT}{dx} \quad (2.6)$$

where the coefficient of dT/dx is the radiative conductivity k_{rad} discussed in Chapter 1. This equation is one form of the Rosseland diffusion equation, where K_R (the wavelength subscript will be dropped) is the Rosseland mean extinction coefficient and is given by

$$\frac{1}{K_R} = \frac{\int_{\Delta\lambda} (1/K_\lambda) (\partial e_{\lambda b} / \partial e_b) d\lambda}{\int_{\Delta\lambda} (\partial e_{\lambda b} / \partial e_b) d\lambda} \quad (2.7)$$

which is the general form for evaluation over a given wavelength interval. The $\partial e_{\lambda b} / \partial e_b$ can be evaluated by differentiating the Planck blackbody emissive power distribution after setting $T = (e_b / \sigma)^{1/4}$:

$$\frac{\partial e_{\lambda b}}{\partial e_b} = \frac{\pi C_1 C_2 \sigma^{1/4}}{2 \lambda^6 e_b^{5/4}} \frac{\exp[(C_2/\lambda)(\sigma/e_b)^{1/4}]}{(\exp[(C_2/\lambda)(\sigma/e_b)^{1/4}] - 1)^2} \quad (2.8)$$

where C_1 and C_2 are the constants specified in Planck's Law. After rewriting the equation in terms of temperature, we obtain:

$$\frac{\partial e_{\lambda b}}{\partial e_b} = \frac{\pi C_1 C_2}{2 \sigma T^5 \lambda^6} \frac{\exp(C_2 T / \lambda)}{[\exp(C_2 T / \lambda) - 1]^2} \quad (2.9)$$

Since the expression is quite complex, it cannot be integrated analytically when substituted into Eqn. (2.7). Computer techniques are required to obtain a numerical solution; such a technique was used to calculate K_R from experimental data, and will be described in Chapter 3.

2.2 Foam Radiation Model

From Eqn. (2-6) it can be seen that the extinction coefficient is the only material property necessary to determine the radiative heat flux. This property must now be derived as a function of foam cell geometry. The goal is to relate K to cell size, and thus verify that reducing cell size, while keeping other properties constant, will significantly reduce the radiative heat transfer. The effects of struts and cell walls on attenuating radiation will be treated separately and then added, since an uncoupled relationship is assumed.

2.2.1 Assumptions

The following model makes many simplifying assumptions about cell geometry and radiative behavior. Foam cells are taken to be uniform, constant in geometry, and isotropic (not elongated). The fraction of polymer in struts (f_s) is also assumed to be the same in all foams. It should be noted that a cell is assumed to be a pentagonal dodecahedron in this analysis, while the technique for calculating mean cell diameter in Chapter 3 assumes spherical cells.

The analysis also makes two assumptions about radiative behavior, the first of which is the neglect of scattering. This is based on experiments which show that most of the attenuated radiation is absorbed rather than scattered, and that the scattered radiation is only moderately forward oriented [6]. The foam can then be treated as isotropically scattering, which will produce an error of 10 to 15 percent in radiative heat flux calculations [2]. The second assumption is that the struts can be treated as black bodies, which was verified by measurements of the transmissivity of a thin polyurethane film, along with the reflectivity of a thicker sample [9]. These measurements were used to obtain the spectrum of the real and imaginary portion of the index of refraction, which were then used in the Mie equations. The solution to the Mie equations was then integrated over wavelength to obtain a Rosseland mean extinction coefficient, which was compared to the coefficient obtained assuming a black body. When the analysis was carried out for cylinders with the same diameter as strut dimensions, the two extinction coefficients agreed within ten percent. This produced an efficiency factor near unity, so the black body strut assumption was validated.

2.2.2 Extinction Coefficient—Struts

The extinction coefficient was predicted by Glicksman and Torpey on the assumption that struts are primarily responsible for absorption in foams, since struts are taken as black bodies and cell walls have a high transmissivity. Cell walls were thus neglected in their analysis, which will be summarized here. For a more detailed description, the

reader is referred to Torpey [10].

The analysis begins by representing the foam as a matrix of randomly oriented struts in the form of pentagonal dodecahedra. From Hottel and Sarofim [11], the basic relation for the extinction coefficient for randomly spaced linear elements is

$$K = CL_vQ \quad (2.10)$$

where C is the projected area of a strut per unit length and L_v is the length of strut per unit foam volume. After assuming that the efficiency factor Q is unity, it now remains to obtain relations for C and L_v in terms of more basic foam characteristics. For a triangular strut, the average area projected normal to the strut axis per unit length is

$$C = .955a \quad (2.11)$$

where a is the length of one side of an equilateral triangle. The parameter L_v can be expressed in terms of the mean cell diameter d by assuming a cell geometry. The pentagonal dodecahedron was found the most representative of a foam cell [17], in which case the relation is

$$L_v = \frac{8.62}{d^2} \quad (2.12)$$

where d is the diameter of a sphere occupying a volume equivalent to that of the dodecahedron. The strut side length a can then be expressed by relating the strut volume per unit foam volume to the overall foam density. This requires knowledge of the strut cross-sectional area, which Torpey found to be equal to approximately two-thirds the area of an equilateral triangle formed by strut vertices, due to concave sides (see Figure 1.1). The density relationship is then

$$0.29a^2L_v\rho_s = f_s\rho_f \quad (2.13)$$

where f_s is the fraction of solid material in the struts, and ρ_f , ρ_s are the foam and solid polymer densities, respectively. The previous three equations can be manipulated from values substituted in to (2.10) to obtain

$$K' = 5.23 \frac{\sqrt{f_s\rho_f/\rho_s}}{d} \quad (2.14)$$

The notation K' indicates that this is still an intermediate value, since it assumes all struts are perpendicular to the heat flow direction. Eqn. (2-14) can be multiplied by a factor, obtained through integral analysis, which accounts for random orientation of struts. After inserting this factor, along with assuming values of 0.8 for f_s and 1.242 g/cm^3 for polymer density, the final relation becomes

$$K_{struts} = 3.29 \frac{\sqrt{\rho_f}}{d} \quad (2.15)$$

All values are expressed in the CGS system, giving K in cm^{-1} . The parameter $\sqrt{\rho}/d$ will be used in subsequent plots of experimental data.

2.2.3 Extinction Coefficient—Cell Walls

Though the cell wall has a small absorptivity, it was decided that it was significant enough to derive a model for the extinction coefficient for cell walls. An uncoupled relationship is assumed, so the extinction coefficient for struts would be added to that for cell walls to obtain the final value. The value for cell walls was calculated for two limiting cases: one assuming an optically thin ($Kt \ll 1$) cell wall and one assuming optically thick ($Kt \gg 1$).

Optically Thin Cell Walls

The derivation of the extinction coefficient for highly transparent cell walls is quite simple, because radiation absorbed and re-emitted by cell walls is small compared to the transmitted radiation from an outside source. If reflectivity is neglected, Eqn. (2.2) can be approximated by assuming $K_w t \ll 1$, where K_w is the extinction coefficient for a single wall:

$$\tau = e^{-K_w t} \approx 1 - K_w t \quad (2.16)$$

where the constant in (2.2) is taken as one. The foam can then be represented as a matrix of these cell walls of identical thickness, oriented in random directions and forming the faces of isotropic, uniform cells. If the extinction coefficient for the cell wall is known, then the ratio of the overall value of K to that for one cell wall is simply the mass ratio

of a volume of foam with cell walls only to an equivalent volume of solid polymer, or, in terms of densities:

$$K_{walls} = \frac{(1 - f_s)\rho_f}{\rho_s} K_w \quad (2.17)$$

The value $(1 - f_s)$ is the fraction of solid polymer in the cell walls and accounts for the neglecting of struts in this model. An important result of this equation is that the extinction coefficient for optically thin cell walls is independent of cell size. A value for K_{walls} by first noting that many rigid polyurethane foam insulations have densities in the area of 32 kg/m^3 . Also, from the data of Schuetz, it was calculated that the extinction coefficient for a typical cell wall is 1633 cm^{-1} . After substituting these values and the previous values of f_s and ρ_s , we obtain $K = 8.4 \text{ cm}^{-1}$. Adding this to K_{struts} evaluated at the above foam density, we obtain the final extinction coefficient as a function of cell diameter (d in cm , K in cm^{-1}):

$$K = \frac{.589}{d} + 8.4 \quad (2.18)$$

The diffusion approximation can be used with this value of K even though cell walls are assumed optically thin. This is because in a typical slab of foam board, thermal radiation must travel through at least 50 cell walls, which means that the medium has an optical thickness of at least 5. Thus the Rosseland diffusion equation is appropriate for foam slabs with a thickness of one inch or more.

High absorptivity walls

The opposite limiting case will now be presented: where each cell wall can be treated as optically thick, but not necessarily near opaque. In this case a cell wall will not be significantly affected by walls more than a few cell diameters away. While this is generally not the case with foam insulations, it will provide additional insight into the radiative behavior of foams. Upon making certain approximations, the solution presented here should approach the optically thin solution.

The analysis begins with a formula from stereology, or the determination of three-dimensional geometry from one- or two-dimensional data. The relation was first derived

of a volume of foam with cell walls only to an equivalent volume of solid polymer, or, in terms of densities:

$$K_{walls} = \frac{(1 - f_s)\rho_f}{\rho_s} K_w \quad (2.17)$$

The value $(1 - f_s)$ is the fraction of solid polymer in the cell walls and accounts for the neglecting of struts in this model. An important result of this equation is that the extinction coefficient for optically thin cell walls is independent of cell size. A value for K_{walls} by first noting that many rigid polyurethane foam insulations have densities in the area of 32 kg/m^3 . Also, from the data of Schuetz, it was calculated that the extinction coefficient for a typical cell wall is 1633 cm^{-1} . After substituting these values and the previous values of f_s and ρ_s , we obtain $K = 8.4 \text{ cm}^{-1}$. Adding this to K_{struts} evaluated at the above foam density, we obtain the final extinction coefficient as a function of cell diameter (d in cm , K in cm^{-1}):

$$K = \frac{.589}{d} + 8.4 \quad (2.18)$$

The diffusion approximation can be used with this value of K even though cell walls are assumed optically thin. This is because in a typical slab of foam board, thermal radiation must travel through at least 50 cell walls, which means that the medium has an optical thickness of at least 5. Thus the Rosseland diffusion equation is appropriate for foam slabs with a thickness of one inch or more.

High absorptivity walls

The opposite limiting case will now be presented: where each cell wall can be treated as optically thick, but not necessarily near opaque. In this case a cell wall will not be significantly affected by walls more than a few cell diameters away. While this is generally not the case with foam insulations, it will provide additional insight into the radiative behavior of foams. Upon making certain approximations, the solution presented here should approach the optically thin solution.

The analysis begins with a formula from stereology, or the determination of three-dimensional geometry from one- or two-dimensional data. The relation was first derived

by Saltykov [12] in 1945 and is presented by Underwood [13]:

$$L = \frac{2}{S_v} \quad (2.19)$$

where S_v is the surface to volume ratio of the cell geometry, and L is the average intersected length (between cell walls) of a random line passing through the foam. A simple diagram of cell wall interactions using the parameter L is shown in Figure 2.1, where α and τ are the absorptivity and transmissivity for the single wall. The cell wall being analyzed is perpendicular to the overall direction of heat flow. An energy balance will be used to calculate the net radiative flux in the positive x -direction. Both q_{LHS} and q_{RHS} represent the radiation emitted from other cell walls in the vicinity of the wall in question, and e_{b0} is the blackbody emissive power at the local temperature. The quantities can be taken as monochromatic or for a gray medium. Neglecting reflected radiation, the energy balance is

$$q_r = \alpha e_{b0} + \tau q_{LHS} - q_{RHS} \quad (2.20)$$

The first term denotes the energy emitted by the cell wall itself, which would be absent in the optically thin case.

The task now remains to express q_{RHS} and q_{LHS} in terms of blackbody emissive power, taking into account the direction of the incident radiation. To begin this analysis, the incoming radiative flux from a given direction can be written as a Taylor series in terms of blackbody intensity:

$$q'_{RHS} = \alpha [i_{b0} + \frac{di_b}{dx}(L \cos \theta) + \frac{1}{2} \frac{d^2 i_b}{dx^2} (L \cos \theta)^2 + \dots] \quad (2.21)$$

where the q' notation denotes a directional quantity. This expression only applies to radiation from the layer of cell walls one cell diameter or less away. To account for cell walls in farther layers, additional Taylor series must be added to (2.21), with $L \cos \theta$ replaced by $2L \cos \theta$, $3L \cos \theta$, etc. Also, for small cell diameters, the terms after the first derivative can be assumed insignificant and dropped. After making these additions and

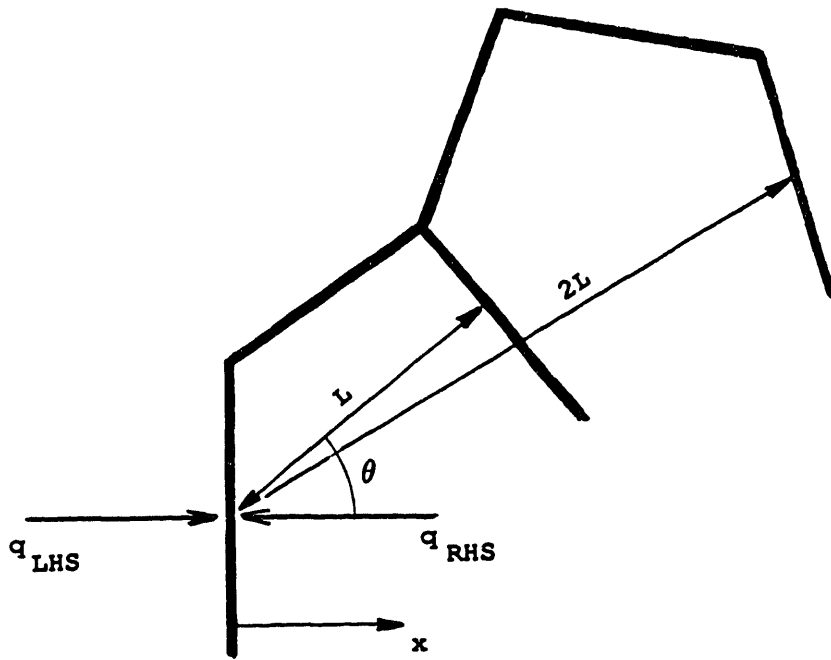


Figure 2-1: Radiative interchange among high-absorptivity cell walls.

integrating over all solid angles $d\omega$, the heat flux is

$$q_{RHS} = \alpha \int_{2\pi} (i_{b0} + \frac{di_b}{dx} L \cos \theta) \cos \theta d\omega + \alpha \tau \int_{2\pi} (i_{b0} + \frac{di_b}{dx} 2L \cos \theta) \cos \theta d\omega + \dots$$

or

$$q_{RHS} = \alpha \sum_{k=1}^{\infty} \tau^{k-1} \int_{2\pi} (i_{b0} + \frac{di_b}{dx} kL \cos \theta) \cos \theta d\omega \quad (2.22)$$

The increasing powers of τ come about because radiation must pass through $k - 1$ cell walls if the source of radiation is k cells away. The integrals can be evaluated by using cylindrical coordinates where $d\omega = \sin \theta d\theta d\phi$, setting θ from 0 to $\pi/2$ and ϕ from 0 to 2π . After evaluating the integrals, (2.22) becomes

$$q_{RHS} = \alpha e_{b0}(1 + \tau + \tau^2 + \dots) + \frac{2}{3} \alpha L \frac{de_b}{dx} (1 + 2\tau + 3\tau^2 + \dots) \quad (2.23)$$

Since the summation in the first term is $1/(1 - \tau) = 1/\alpha$, the first term is simply e_{b0} . The expression for q_{LHS} is similar, but the second term is negative, since the two fluxes are in opposite directions, and thus the sign of the gradient changes. The expressions for q_{RHS} and q_{LHS} can be substituted into Eqn. (2.20) to obtain

$$q_r = -\frac{2}{3} \alpha L \frac{de_b}{dx} (1 + 3\tau + 5\tau^2 + \dots) \quad (2.24)$$

The series in brackets sums to $(\tau + 1)/(\tau - 1)^2$. Substituting this and $\tau = 1 - \alpha$, we obtain

$$q_r = -\frac{4}{3} L \frac{de_b}{dx} \left(\frac{1}{\alpha} - \frac{1}{2} \right) \quad (2.25)$$

Since the medium is optically thick, this equation can be equated to the Rosseland diffusion equation; the extinction coefficient can be expressed as

$$K_R = \frac{1}{L} \frac{2\alpha}{2 - \alpha} = \frac{S_v \alpha}{2 - \alpha} \quad (2.26)$$

This equation can be rewritten in terms of cell diameter by first using an expression for the fraction of material in cell walls presented by Reitz:

$$f_w = 1 - f_s = \frac{S_v t}{1 - \delta} \quad (2.27)$$

The surface to volume ratio S_v is taken as $3.46/d$ if the cells are pentagonal dodecahedra, and δ , the void fraction, is defined by

$$\delta = \frac{\rho_s - \rho_f}{\rho_s - \rho_g} \approx 1 - \frac{\rho_f}{\rho_s} \quad (2.28)$$

if the foam gas density ρ_g is small compared to the foam and solid polymer densities. After substituting $1 - e^{-K_w t}$ for the absorptivity and $3.46/d$ for S_v , Eqn. (2.26) becomes

$$K_{walls} = \frac{3.46}{d} \frac{1 - e^{-K_w t}}{1 + e^{-K_w t}} \quad (2.29)$$

where t is obtained from Eqn. (2.27).

To check the validity of the previous equation, one can see what happens in the optically thin limit. If the absorptivity can be approximated by $K_w t$ then Eqn. (2.26) becomes

$$K_{walls} = \frac{S_v K_w t}{2 - K_w t} \quad (2.30)$$

In the optically thin limit, the denominator approaches 2. In addition, the value $S_v t$ in the numerator represents twice the cell wall volume per unit foam volume, recalling that each wall is shared by two cells. The final form is then

$$K_{walls} = \frac{\rho_f}{\rho_s} (1 - f_s) K_w,$$

giving the same result derived earlier in Eqn. (2.17).

Chapter 3

Radiation Experiments

As stated earlier, the purpose of the following experiments is to check the validity of the radiation model and provide a basis for its modification if necessary. The data should demonstrate a simple relationship between the extinction coefficient and a cell diameter-density parameter. The experiments will follow the same general procedure as previous radiation tests at MIT, but some changes will be made to balance feasibility and accuracy.

The radiation experiments conducted separately by Schuetz, Sinofsky, and Torpey at MIT center around the determination of the extinction coefficient. The general procedure is as follows. A sample of foam is first sectioned into slices thin enough to have transmissivities detectable by a standard infrared spectrometer (for most foams the thickness is well below .1 in). The slice thicknesses are then measured with a micrometer, verifying that the thicknesses vary over a considerable range. Transmissivity measurements are then taken with an infrared spectrometer, which displays data of transmissivity vs. wavenumber. The extinction coefficient is then calculated by some variation of the equation $K = -\ln \tau/t$, where τ is the transmissivity and t is the sample thickness. From this equation one obtains the extinction coefficient as the slope of a line fitting τ vs. t data for all foam slices on a semilog plot.

3.1 Description of Foams

In October and November of 1988, the Heat Transfer Laboratory at MIT received a number of fresh foam samples from numerous manufacturers in the United States and overseas. These sources consisted of: Dow, Mobay, ICI, Asahi, and Fisher-Paykel. All foams were rigid low-density polyurethane and polyisocyanurate, and were intended for use as thermal insulation for buildings or in appliances such as refrigerators. Except for one foam tested, all samples had densities in the area of 31 kg/m^3 ($\pm 20\%$). The exception was a small-celled sample with a density of 50 kg/m^3 . The mean cell diameters of the foams were calculated to be in the range of .2 to .6 mm. It was desired to obtain foams with cell sizes below .2 mm, but, as noted earlier, such foams cannot be practically produced on an appreciable scale [14].

Some foams could not be tested because they contained many large voids several cell diameters across. The presence of these voids would seriously affect the accuracy of the transmissivities obtained by the spectrometer, since the infrared beam generated in the spectrometer may easily be smaller than a large void in a foam slice. Some other samples could be tested despite the presence of large voids. The voids occur mainly in a thin layer near the facings at the surface of the foam board sample, and are the result of thermal stresses during manufacture. In all foams, care was taken to cut slices from regions away from the foam boundaries.

3.2 Cutting Foam Slices

To begin the experiments, cylindrical plugs were cut from each acceptable foam with a hole saw fixed on a drill press. These plugs would eventually be cut into slices for spectrometer analysis, but initially they were weighed and had length and diameter measurements taken to determine density. A Mettler balance was used, which was accurate to .1 mg. It was necessary to find a scale with at least 1 mg accuracy, since the foam plugs weighed were often less than 1 gram.

The plugs were then taken to an Isomet low-speed saw to prepare slices for the spectrometer. A sketch showing the basic features of the Isomet is shown in Figure 3.1a. The blade used for cutting is circular is a thin disk of 5 in. diameter, and is set to rotate at about 160 rpm for cutting foam. The edge of the blade is diamond-tipped for cutting hard objects and has a squared tip (rather than pointed). The squared tip provides greater precision when an even cut is required. A metal arm which holds the sample on one end pivots down towards the edge of the blade, and can accomodate weights to provide additional force of the sample on the blade. A gage attached to the arm moves it horizontally, moving the sample towards or away from the blade to produce a certain cut length. The primary application of the Isomet low-speed saw is for cutting metals, so normally the blade must be running through a reservoir of lubricant to prevent excessive heat generation. In cutting foam samples, such lubrication is not required and in fact would be harmful, since the lubricant remains on the foam slices and will invariably affect radiative properties.

Ten slices were typically cut for a given foam, with thicknesses ranging from .018 in to .065 in. All slices were cut in planes perpendicular to the heat flow direction that the manufacturer intended. To cut foam slices on the Isomet, a simple chuck had to be constructed to hold the foam plug on the arm, shown in Figure 3.1b. The chuck was constructed of plexiglass and consists of an open-ended cylindrical container with a hole in the bottom. A bolt passes through this hole and a hole in the arm and is fastened. To ensure a firm fit on the chuck, the plugs were cut slightly undersized in diameter and one end of each plug was wrapped with electrical tape. The fit must be tight enough to ensure that the plug will not give way when it first touches the blade, as the force of the blade will tend to tilt the sample and cause an uneven cut. The saw gage was adjusted after each cut for a new thickness, usually .003 in or .004 in thicker than the last. To account for the width of the blade, .012 in had to be subtracted from each apparent gage thickness to obtain the actual thickness. It should be noted, however, that even after this adjustment, the final gage measurement of the actual thickness was found to be highly

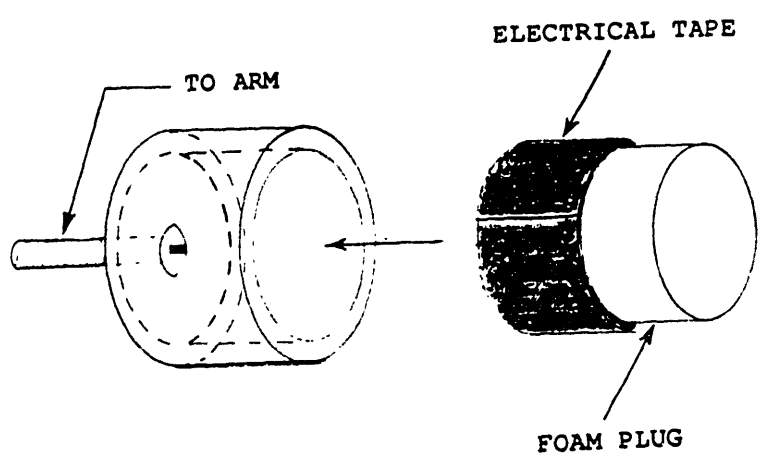
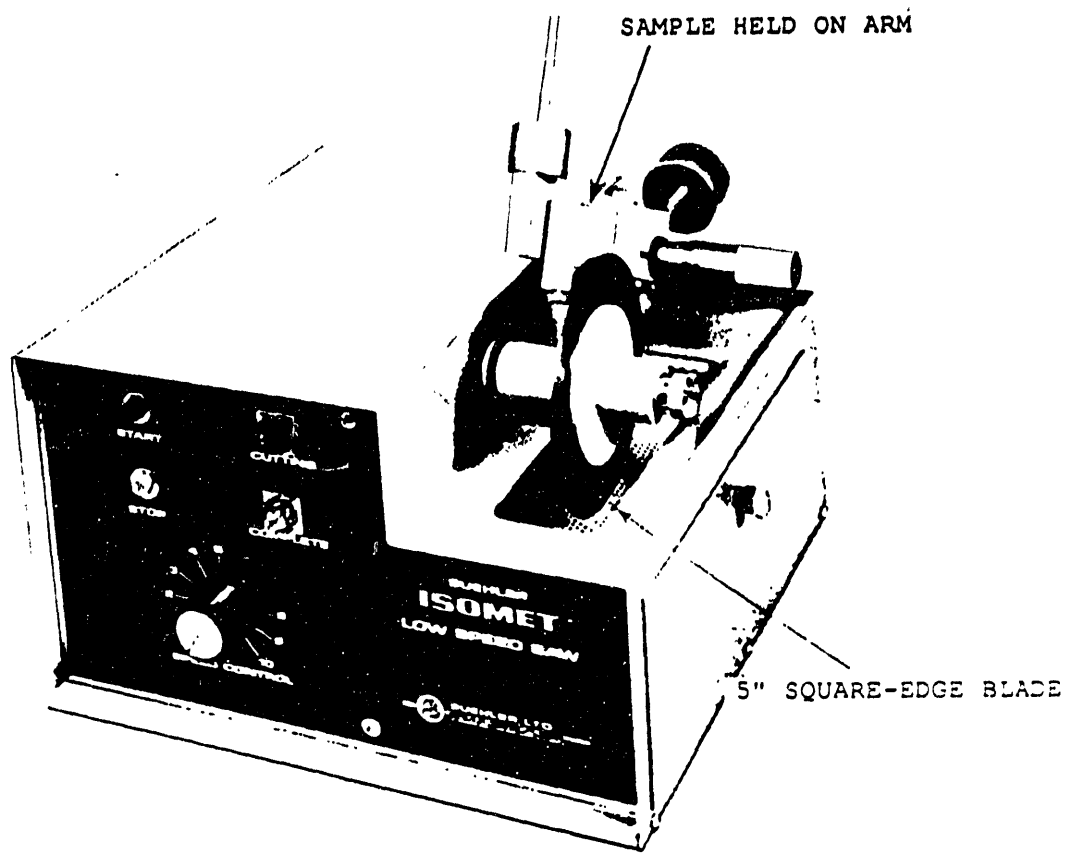


Figure 3-1: Sketch of (a) Isomet saw, (b) chuck with foam plug.

inaccurate when the slices were measured by other means, as will be seen later.

Despite the inaccuracy of the gage, the Isomet saw gives the advantage of an even cut for thicknesses as low as .02 in. The variation of thickness with location was less than .002 in for 90 percent of the slices measured. The main problem encountered with slices cut with the Isomet is that despite the general evenness of the surface, there are more small-scale effects that may cause problems in later tests. The tearing and compression of surface cells may be significant, especially when torn cell walls collect on the blade as flakes and redeposit on the foam slices. In Chapter 4 the possible effects on transmissivity will be discussed.

3.3 Collecting Transmission Data

After cutting, the foam slices were taken to Fourier Transform Infrared Spectrometer (FTIR) for transmissive analysis. The FTIR used was a Nicolet IR44, and included a personal computer attachment with software capable of displaying and manipulating the transmission data in a number of ways. The spectrometer basically consists of a high-temperature source emitting infrared radiation, which is collected by mirrors into a thin beam. This beam passes through the sample, and a finite solid angle of radiation leaving the sample is then collected by another series of mirrors. The chamber containing the sample is sealed and purged of water and carbon dioxide. After the beam leaves the sample, a prism breaks the beam into spectral elements so the detector can measure the intensity of transmitted radiation as a function of wavenumber, or the reciprocal of wavelength.

To obtain transmissivity data, the spectrometer must take a ratio of the intensity of the beam passing through a sample in dry air to the intensity of a beam passing through dry air only. The intensity spectrum of the beam through dry air is called the "background" and is recorded first. To obtain a background, one must first set the number of times the intensity will be recorded to obtain an average ("scans") and the size

of the wavenumber interval that will be assigned an intensity (“resolution”). After these parameters are set, the command is given to begin scanning to produce the background. The background should appear similar to Figure 3.2a when displayed, provided that at least ten minutes have passed between closing the chamber to outside air and recording the background. If less time were allowed for the chamber to purge, the background will show wavenumber bands where the presence of water and carbon dioxide reduce the intensity, resulting in the less smooth curve of Figure 3.2b. Once a proper background spectrum is achieved and stored in memory, the chamber is opened and the the first foam slice is placed in the path of the beam. The chamber is given time to purge, and the command is then given to run a “sample”. In this case the spectrometer measures intensity as before, but when the sample spectrum is displayed, the vertical axis of the plot displays transmissivity rather than intensity. The intensities for this and subsequent samples are compared to the same original background, so only one background need be taken regardless of the number of samples analyzed. A typical sample spectrum for polyurethane foam is shown in Figure 3.3. The wavenumber range displayed can be adjusted to any interval within 400 to 4800 cm^{-1} (25 to 2.1 μm wavelength).

The data for the transmissivity-wavenumber plot is stored in binary form, but can be converted to a more usable numerical form. A certain command saves a sample spectrum as ASCII characters, which can be stored in a data file and read as numbers by a computer program in a high-level language. The ASCII file is described in detail in Appendix A and consists of a series of numbers and words describing the plot characteristics, followed by the transmissivities for successive wavenumber intervals. If a single mean transmissivity is desired over a certain wavenumber band, the “integrate” command can be used. This command is used with starting and ending wavenumbers as arguments, and returns the value of the area *above* the spectrum shown in Figure 3.3 to a horizontal line at a transmissivity of one. The units of the area are obtained by multiplying the units of wavenumber by the transmissivity on a zero-to-one scale. Thus, if the spectrum in Figure 3.3 were a horizontal line at 25 percent transmissivity, the value returned by

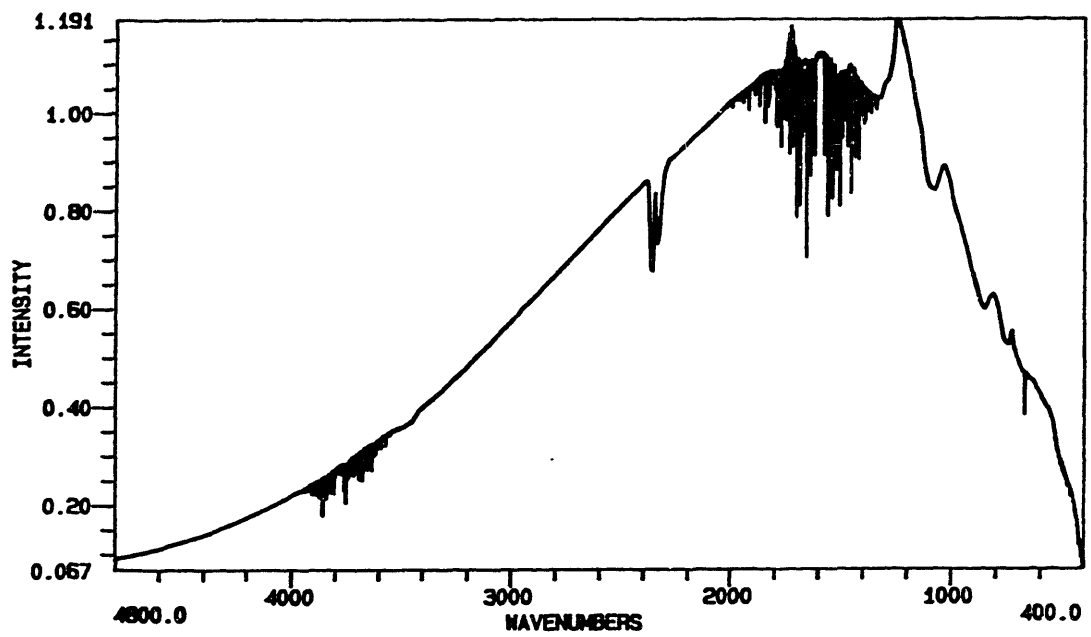
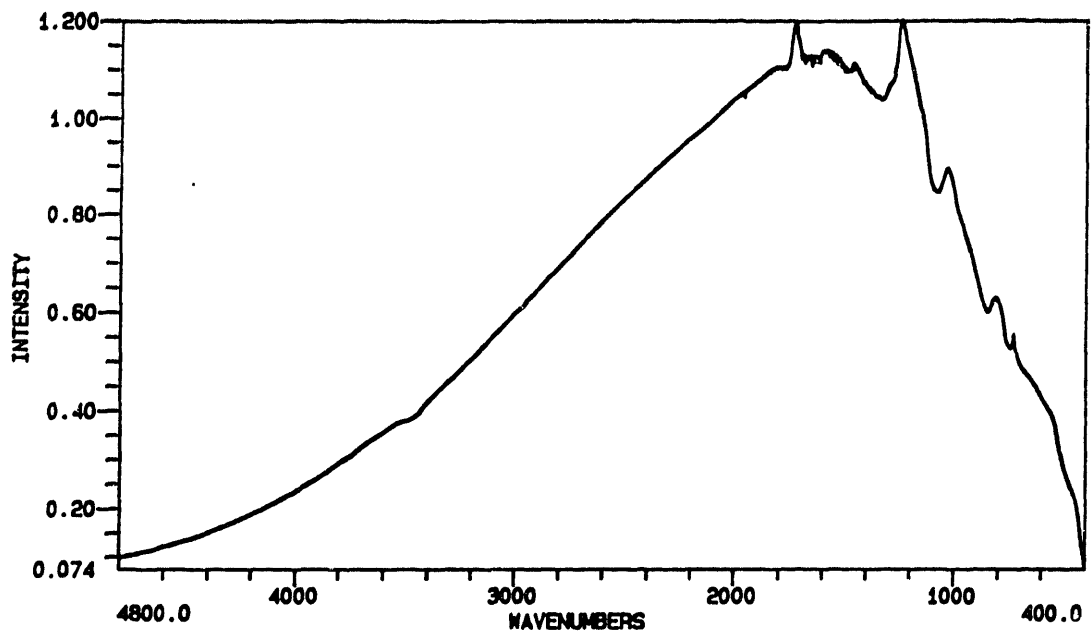


Figure 3-2: Comparison of (a) acceptable and (b) unacceptable FTIR backgrounds.

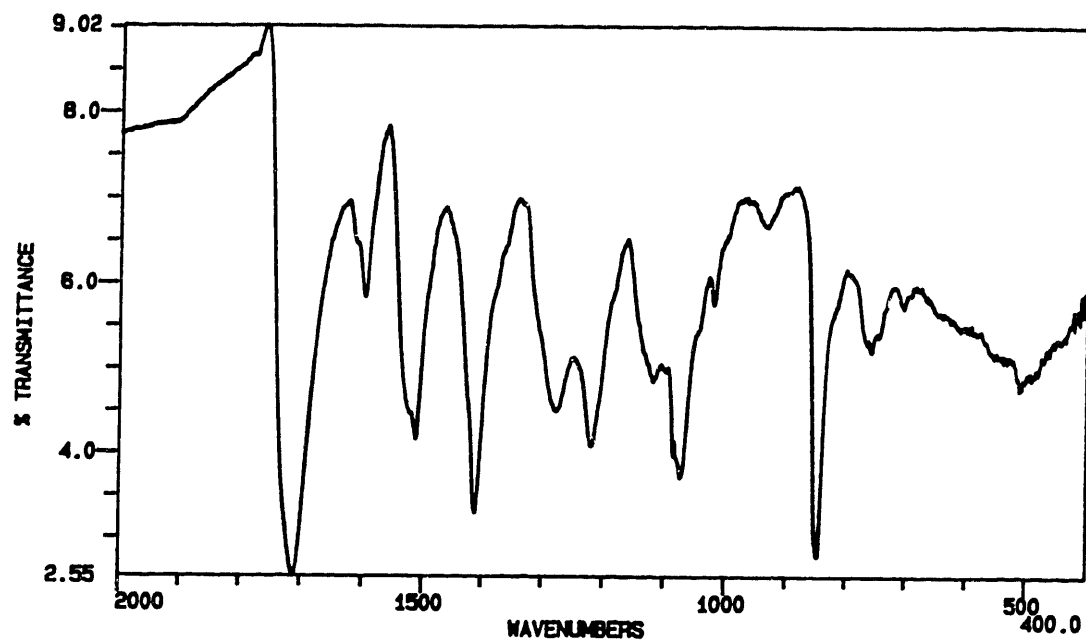


Figure 3-3: Sample FTIR spectrum for .033 in thick polyurethane foam slice. Density: .0300 g/cm^3 . Cell diameter: .31 mm.

the “integrate” command for the 400-2000 cm^{-1} wavenumber range would be $(2000 - 400)(1 - .25) = 1200$. This value is labeled by the spectrometer as the “peak area”. The average transmissivity can then be calculated from

$$\bar{\tau} = 1 - \frac{A_p}{\eta_2 - \eta_1} \quad (3.1)$$

where A_p is the peak area, and η_1, η_2 are the beginning and ending wavenumber, respectively.

3.4 Sample Thickness Measurement

A Starrett paper micrometer was used to check the thicknesses which were read from the gage on the Isomet saw. A paper micrometer has basically the same features as a regular micrometer caliper, but the paper micrometer has a larger measuring surface area, and one of the measuring surfaces is allowed to swivel (see Figure 3.4). These features minimize local compression of the foam, and thus minimize any underestimation of the foam thickness. The gage was slowly turned until the slightest resistance was felt, and the thickness was read off to the nearest thousandth of an inch, the smallest division on the gage.

Table 3.1 compares the slice thicknesses as recorded by the saw gage with those measured with the paper micrometer for a particular foam sample (all tables will appear at the end of each chapter). In some cases the two measurements differ by as much as 20 percent. In most cases the paper micrometer thickness was lower than the saw gage thickness. The discrepancy is probably due to a distortion that takes place when the foam slices are being cut. The Isomet saw is not intended to cut materials as delicate as plastic foam, so it is possible that the foam is stretched slightly as the blade comes in contact with the plug. Because of this possibility, the paper micrometer measurements were used for later calculations.

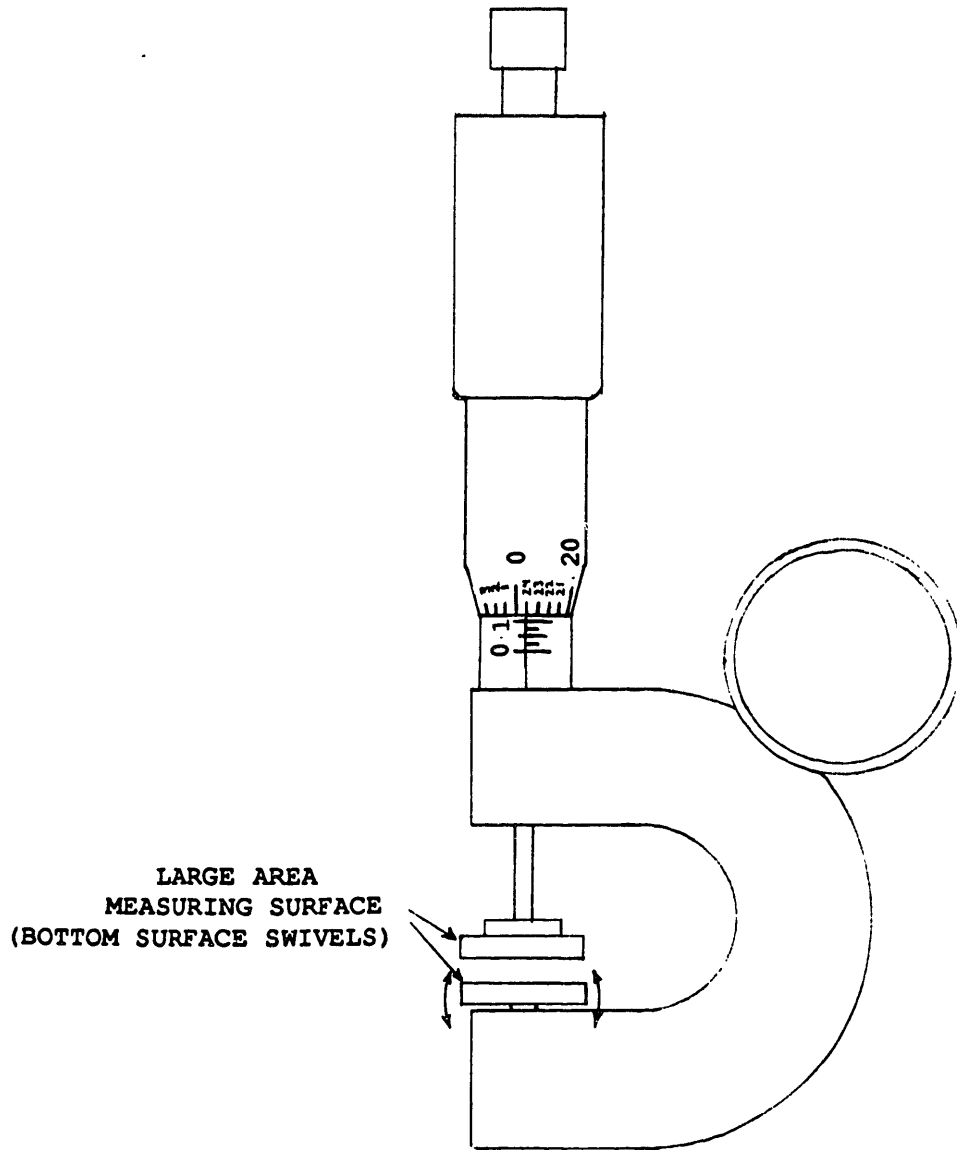


Figure 3-4: Sketch of paper micrometer.

3.5 Cell Diameter Measurement

3.5.1 The Scanning Electron Microscope

The final procedure to be performed on the foam slices was the determination of a mean cell diameter for each foam. This required a microscope that provides at least a 50X magnification, a low depth of field to view cells only on a surface layer, and a high contrast. Most conventional optical microscopes were found to be inadequate, so eventually an Amray AMR1000 scanning electron microscope (SEM) was used. Although the SEM was initially used well below its magnification limits (at least 100,000X), the picture quality proved to be ideal for cell size analysis. Figure 3.5 shows a comparison between an SEM photograph and a photograph from an optical microscope, showing the clarity provided by the SEM. The advantage in picture quality stems from the method that the specimen was prepared and viewed in the SEM.

Three slices were chosen from each foam for viewing. One square with 1 cm sides was cut from each slice and was attached to the surface of a small metal stub with two-sided tape. The foam specimens were then taken to a sputtering machine to be coated with a thin layer of gold, which allows them to be viewed in the SEM. The gold-coated foam is then placed in the SEM specimen chamber, and the chamber is brought to a vacuum. A beam of electrons is focused by a series of electromagnetic lenses on the sample and scans a small area. The gold coating causes the electrons to reflect off the specimen surface, where they are attracted onto a collector. Because the gold coats only the exposed surface of a sample, the electron beam can only "see" at most the top two layers of cells. By contrast, an optical microscope uses reflected or transmitted light which may pass through many layers of uncoated cells, making the distinction between the layers unclear and producing an overall brighter picture with less contrast.

Because of the advantages of the SEM, it was used extensively in determining the geometric characteristics of the foams. In addition to the slices, each foam was viewed in two planes parallel to the intended heat flow direction to determine the amount of cell

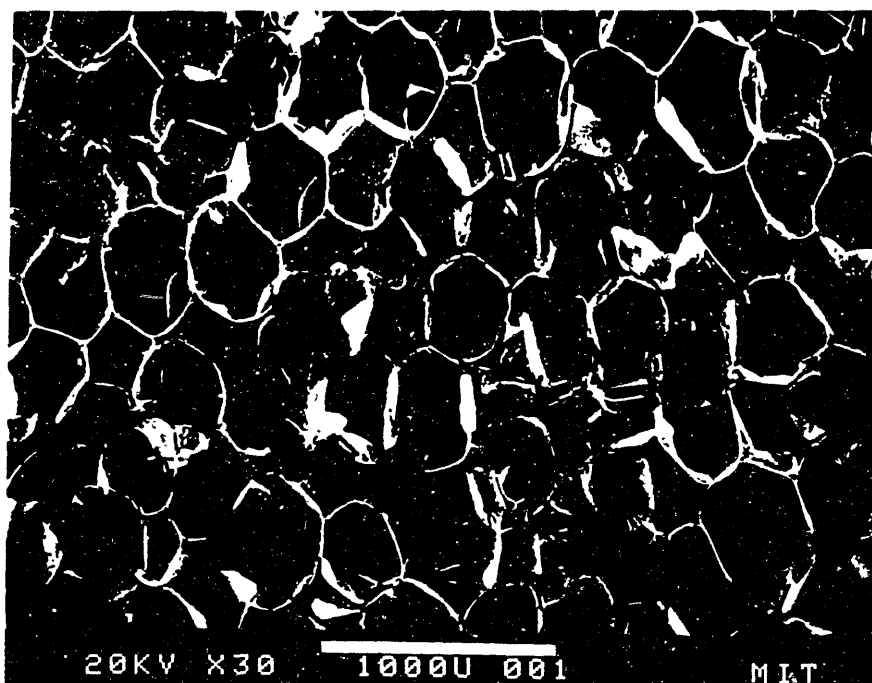
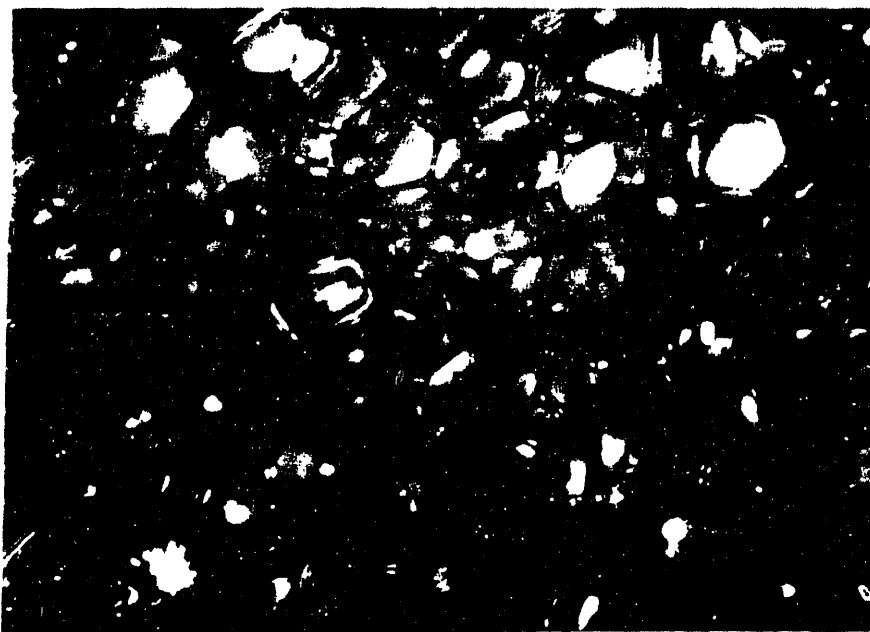


Figure 3-5: Comparison of optical microscope (top) and SEM (bottom) photographs of the same foam, both at 30X magnification.

elongation in three dimensions. Photographs were also taken at much higher magnifications (750X to 10,000X) to observe cell wall and strut cross sections. Figure 3.6 shows typical cell wall and strut photographs. For each foam photographs were taken of two cell wall cross-sections to check uniformity of wall thickness, and also to determine the fraction of polymer in struts (f_s) for each foam, which could be compared to the value of 0.8 assumed for f_s in the radiation model.

3.5.2 Cell Diameter Analysis

It was necessary to find a statistical method of calculating cell size from an analysis of SEM photographs such as in Figure 3.5a. As late as 1970, there was no adequate visual method developed to determine a mean cell diameter. Cell sizes were determined either indirectly using complex volume displacement methods or by drawing lines on microscope photographs and representing the cell size as the average distance on the lines between cell walls. The latter method had already been found inappropriate by Schael [15], who used a volume displacement technique instead.

The flaw in using the average distance between cell walls (mean chord length) as the mean cell diameter is that the method works only if the line passes through the center of every cell it intersects, and that the center of every cell intersected lies in the plane of the photograph. In a real foam this cannot occur, since the cells are in random positions and may be intersected far from their centers. This phenomenon is illustrated in Figure 3.6. In this way the the mean chord length will always be considerably smaller than the actual cell diameter. Michalski and Hubeny [16] assumed spherical cells and integrated chord lengths over the diameter of a circle, and derived that the cell diameter is 1.27 times the average length of a random line drawn through the cell. Though an improvement, this result is still incomplete since it only accounts for two dimensions; it still incorrectly assumes that the center of every cell lies in the plane of the photograph. ASTM Standard D3576 attempts to correct this by using the same integral analysis, but applying it twice to account for three-dimensional cells. The mean cell diameter is

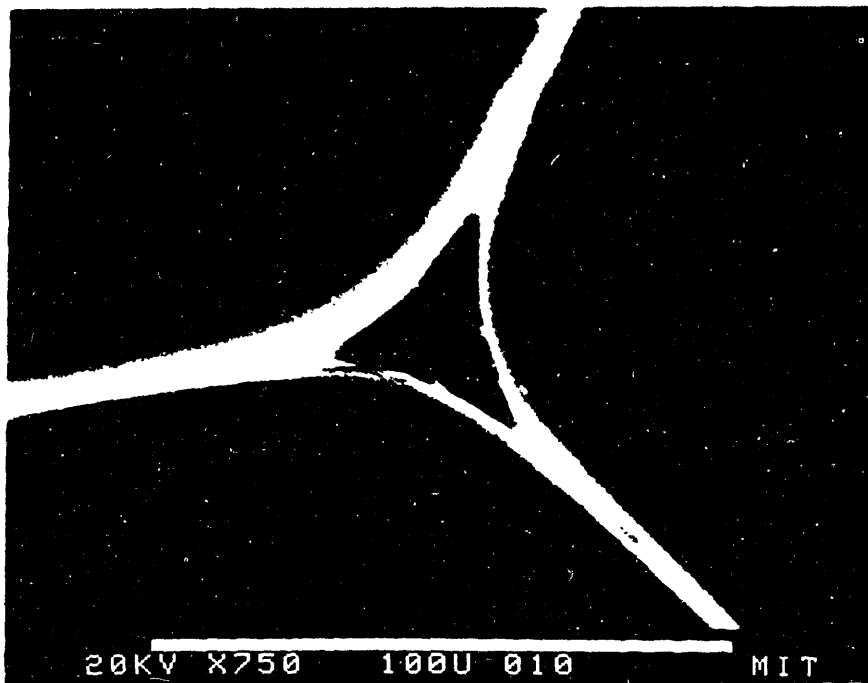
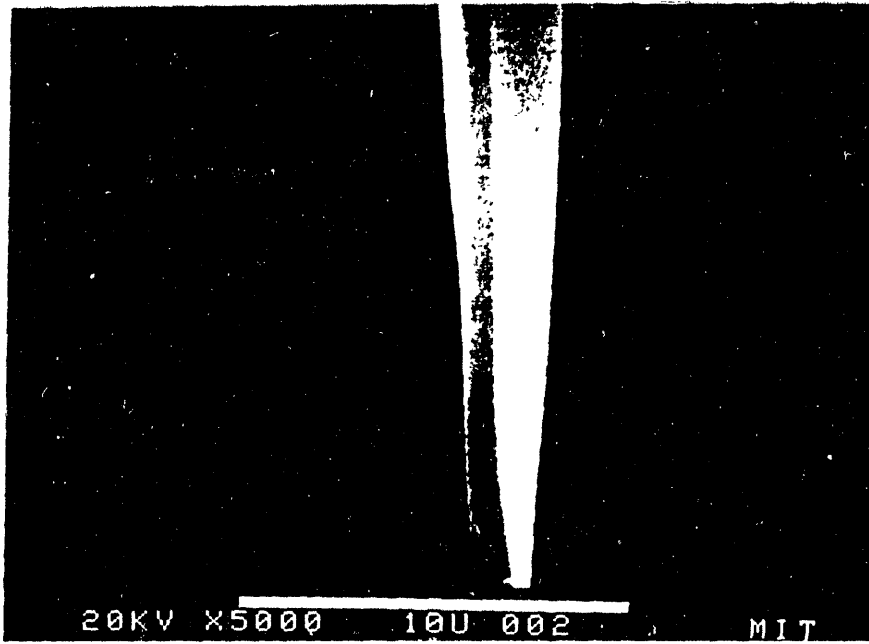


Figure 3-6: SEM photographs of cell wall (top, 5000X) and strut (bottom, 750X) cross-sections.

now derived as 1.62 (1.27x1.27) times the mean chord length. This technique was used initially for these experiments and also in previous foam analyses at MIT. Reitz [17] used techniques developed by Underwood [13] to obtain expressions for the mean cell diameter for cells approximated as: cubes, pentagonal dodecahedra, truncated octahedra, and rhombic octahedra. Except for cubes, his assumptions of non-spherical shapes produced constants of proportionality (to multiply by mean chord length) higher than the 1.62 reported above.

Both the Reitz and the ASTM formulas were used until a new relation was obtained through two different derivations, both of which assume uniform spherical cells. Like the other two methods, the mean cell diameter is proportional to the mean chord length, but the constant of proportionality is 1.5 (7.5 percent less than that of the ASTM method). Because of their simplicity, the two derivations will be shown here.

Whereas the ASTM method squares the result of an integration over a circle, the first derivation uses one integration over a sphere, using the model in Figure 3.7. The length of a line drawn through a sphere is weighted with respect to the area of a differential ring of area $2\pi a da$ on a disk of area πr^2 through the center of the sphere. The expression for the average value of y is

$$\bar{y} = \frac{1}{\pi r^2} \int_0^r y \cdot 2\pi a da = \frac{1}{r^2} \int_0^r \sqrt{r^2 - a^2} \cdot 2a da \quad (3.2)$$

The integral can be solved by substituting $u = \sqrt{r^2 - a^2}$, obtaining

$$\bar{y} = \frac{1}{r^2} \int_0^{r^2} \sqrt{u} du = \frac{2}{3}r \quad (3.3)$$

If $r = d/2$ and $\bar{y} = \bar{\ell}/2$ where $\bar{\ell}$ is the mean chord length, then

$$d = 1.5\bar{\ell} \quad (3.4)$$

The second derivation is based on concepts of stereology, using Eqn. (2.19):

$$S_v = 2/\bar{\ell}$$

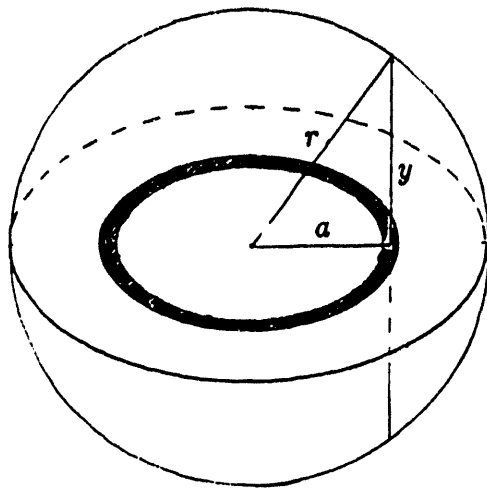


Figure 3-7: Model for integration over a sphere in cell diameter analysis.

where S_v is a surface to volume ratio. Using spherical geometry to determine S_v ,

$$\frac{2}{\bar{\ell}} = S_v = \frac{\frac{1}{2}\pi d^2}{\frac{1}{6}\pi d^3} \quad (3.5)$$

The surface area is halved because each surface of a cell is shared with another cell. Cancelling and solving for d , we obtain

$$d = 1.5\bar{\ell}$$

The technique used to implement this equation is illustrated in Figure 3.8. In this case a photograph with elongated cells will be used to demonstrate the adjustment made to the mean chord length for anisotropic geometry. A rectangular grid was constructed on a transparency so that seven vertical and seven horizontal lines could be superimposed over the photograph. For each line the number of intersections with a cell wall to obtain $P_L = 1/\bar{\ell}$. An average value of P_L was then calculated for the horizontal lines and for the vertical lines. To account for elongated cells, a weighted average P_L was calculated according to a formula derived by Underwood:

$$P_L = 0.785(P_L)_\perp + 0.215(P_L)_\parallel \quad (3.6)$$

where $(P_L)_\perp$ is the value for the short dimension and $(P_L)_\parallel$ is the value for the long dimension. The mean cell diameter is then calculated by $d = 1.5/P_L$.

3.6 Computer Analysis of Spectrometer Data

The next step in the procedure was to obtain extinction coefficients from spectrometer data. The main problem was how to account for a nongray medium when using the transmission spectrum to calculate K . Three different techniques were used in previous projects in the Heat Transfer Laboratory, all of whom graphically analyzed the transmission spectra printed out from a spectrometer. Schuetz broke each spectrum into bands of approximately constant transmissivity and calculated a Rosseland mean extinction coefficient using a technique from Ozisik [18]. Sinofsky [19] also broke spectrum into bands,

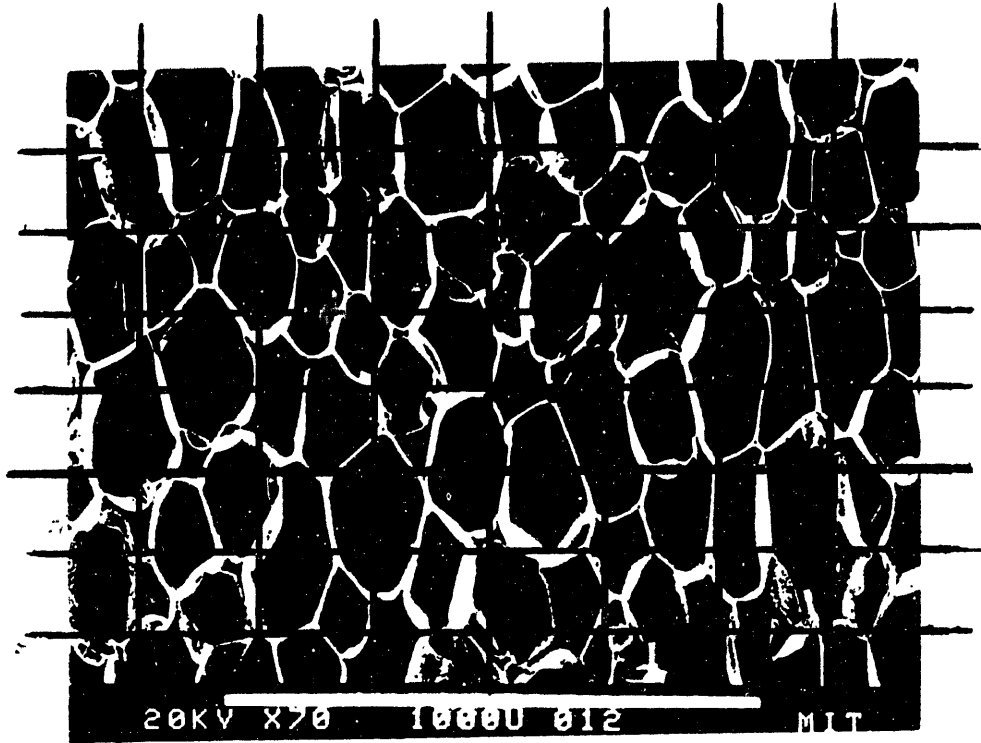


Figure 3-8: SEM photograph with grid overlay for calculating cell size. Magnification: 70X.

but instead calculated a Planck mean coefficient by using a band approximation:

$$K^{-1} = \sum_i K_{\lambda_i}^{-1} (F_{i+1} - F_i) \quad (3.7)$$

where F is the blackbody fraction from $\lambda T = 0$ to the given value. Torpey used no integral formula, since he assumed the transmissivity to be constant with wavelength, and read an average transmissivity from the spectrum.

It was first decided to take advantage of the integration command on the FTIR software to quickly find the extinction coefficient. The average transmissivity can be obtained from Eqn. (3.1) for each foam slice, and the ten data points for $-\ln \bar{\tau}$ vs. sample thickness (t) can be plotted. Two different values of K can be calculated, depending on the definition of the extinction coefficient. An illustration of the two definitions is shown in Figure 3.8, which shows typical data points for a polyurethane foam. The data show a linear relationship, as do the data for all of the foams. If the extinction coefficient is defined by $\tau = \exp(-Kt)$, then a sample thickness of zero must produce a transmissivity of unity, or $\ln \tau = 0$. A line must be determined which fits the data as closely as possible but which is also forced through the origin. If the extinction coefficient is defined by $\tau = C \exp(-Kt)$ where $0 < C < 1$, then a line can fit the data without passing through the origin, since a graph of $-\ln \tau$ vs. t will have an intercept of $-\ln C$. Since each definition had its own advantages and disadvantages, both were employed until it could be determined which was correct.

To obtain the most precise value, it was decided that the Rosseland mean extinction coefficient (K_R) should be used. Since the transmission data could be stored in the FTIR in numerical form, a computer program was written which numerically integrates the data to obtain K_R . The program calculates K_R from Eqn. (2.7):

$$K_R = \frac{\int_{\Delta\lambda} (\partial e_{\lambda b} / \partial e_b) d\lambda}{\int_{\Delta\lambda} (1/K_\lambda) (\partial e_{\lambda b} / \partial e_b) d\lambda} \quad (3.8)$$

Since the FTIR transmission data are recorded with respect to wavenumber (reciprocal wavelength), the numerator integral becomes, from Eqn. (2-9),

$$\int_{\Delta\lambda} \frac{\partial e_{\lambda b}}{\partial e_b} d\lambda = \int_{\Delta\eta} \frac{\pi C_1 C_2 \eta^4}{2 \sigma T^5} \frac{\exp(C_2 \eta T)}{[\exp(C_2 \eta T) - 1]^2} d\eta \quad (3.9)$$

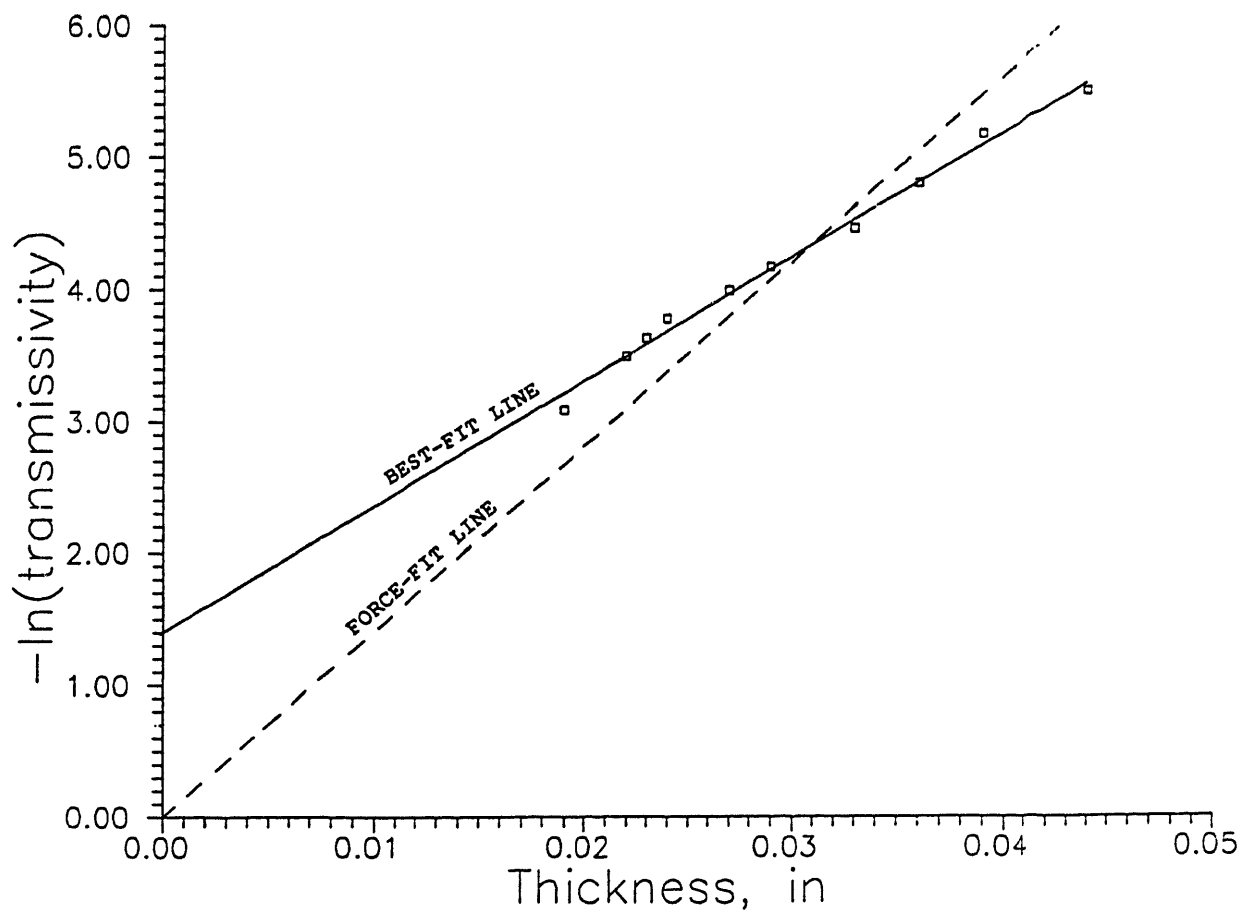


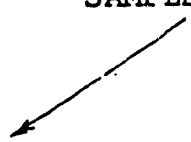
Figure 3-9: Force-fit vs. best-fit slopes for calculating the extinction coefficient.

A FORTRAN program was written to evaluate the above integral numerically by inputting the FTIR data files for all ten slices of a given foam, listed in its entirety in Appendix A. The limits of integration were chosen as $400\text{-}2000\text{ cm}^{-1}$ (25 to 5 μm wavelength) and room temperature (528° R) was chosen for T. These choices are compatible, since 82 percent of blackbody radiation intensity at room temperature is emitted in the chosen wavenumber range. The wavenumber interval was broken up into 270 smaller intervals for the integration.

The ASCII files represented in Figure 3.3 had to be modified for input to the computer program. After recording the "FIRST PT", "LAST PT", and "# POINTS" to calculate the wavenumber interval length, all of the initial information prior to the list of transmissivities was erased. A number representing the sample thickness in inches was added to the top of the file, resulting in the listing shown in Figure 3.9.

To calculate a wavenumber-specific extinction coefficient (K_λ), the program inputs the sample thickness and the transmissivity at a given wavenumber for each of the ten foam slice files into a subroutine. The subroutine actually calculates two different values of K_λ which represent the two definitions discussed earlier, the force-fit and best-fit coefficients. The program outputs these values for each wavenumber interval along with a correlation coefficient to determine how well the force-fit and best-fit methods fit the data. Once both sets of K_λ 's have been integrated over the wavenumber range to obtain two values of K_R , the program prints the two K_R 's along with the average correlation coefficients for each. A sample output is shown in Appendix A after the program listing. It can be seen from this output that any assumption of the foam as a gray medium is inaccurate, since the extinction coefficient varies considerably with wavenumber.

SAMPLE THICKNESS (in)



.035					
.081	.082	.081	.083	.086	.082
.085	.085	.084	.078	.080	.080
.081	.080	.081	.079	.082	.081
		.			
		.			
		.	761 ROWS OF TRANSMISSIVITIES		
		.			
		.			
.035	.034	.033	.033	.034	.033
.033	.035	.036	.034	.034	.036

Starting wavenumber: 4800 cm^{-1}

Ending wavenumber: 400 cm^{-1}

Figure 3-10: Input file for FORTRAN program. Each transmissivity represents a wavenumber interval of $.965 \text{ cm}^{-1}$.

Saw gage thickness, in	Paper micrometer thickness, in
.060	.053
.056	.052
.054	.056
.052	.053
.048	.045
.045	.043
.042	.041
.039	.039
.036	.036
.033	.028

Table 3.1: Comparison of saw gage and paper micrometer for measuring foam slice thicknesses.

Chapter 4

Results

4.1 Extinction Coefficient Data

The data for K vs. $\sqrt{\rho}/d$ must be separated into two groups: force-fit calculation of K , shown in Figure 4.1, and best-fit calculation, shown in Figure 4.2. The lower line represented in both plots is the theory which assumes transparent cell walls and blackbody struts, and the upper line is the revised theory, which includes the effect of optically thin cell walls. Recall that the final equation for the extinction coefficient is

$$K = K_{struts} + K_{walls} = 3.29 \frac{\sqrt{\rho}}{d} + 263\rho \quad (4.1)$$

when the foam density is included as a variable. If all foam densities are assumed to be $.032 \text{ g/cm}^3$, the effect of cell walls is to move the lower line vertically 8.4 cm^{-1} (K_{walls}). As stated earlier, all foams except the far right data point in Figures 4.1 and 4.2 have densities within 20 percent of this value.

Obviously, the theoretical line fits the best-fit data more accurately than the force-fit data, despite the fact that the force-fit data seem to correlate better with a straight line. The complete set of data with both sets of extinction coefficients is shown in Table 4.1. The table shows the average correlation coefficients r which indicate the quality with which the force-fit and best-fit methods relate the $-\ln \tau$ vs. t data for each foam.

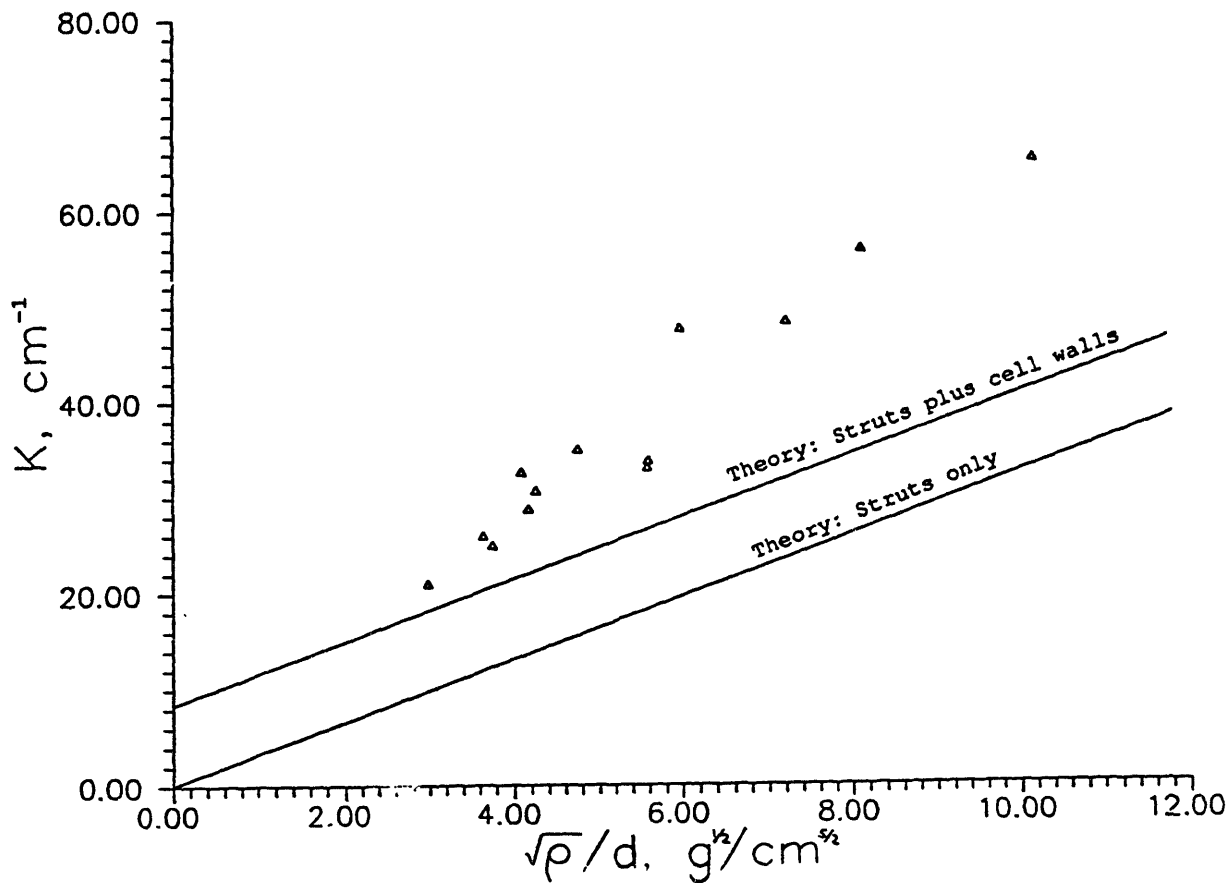


Figure 4-1: Extinction coefficient data from force-fit slopes. Theoretical line assumes a foam density of $.032 \text{ g/cm}^3$. All data points have densities within twenty percent of this value except for the point at the far right, which has a density of $.050 \text{ g/cm}^3$.

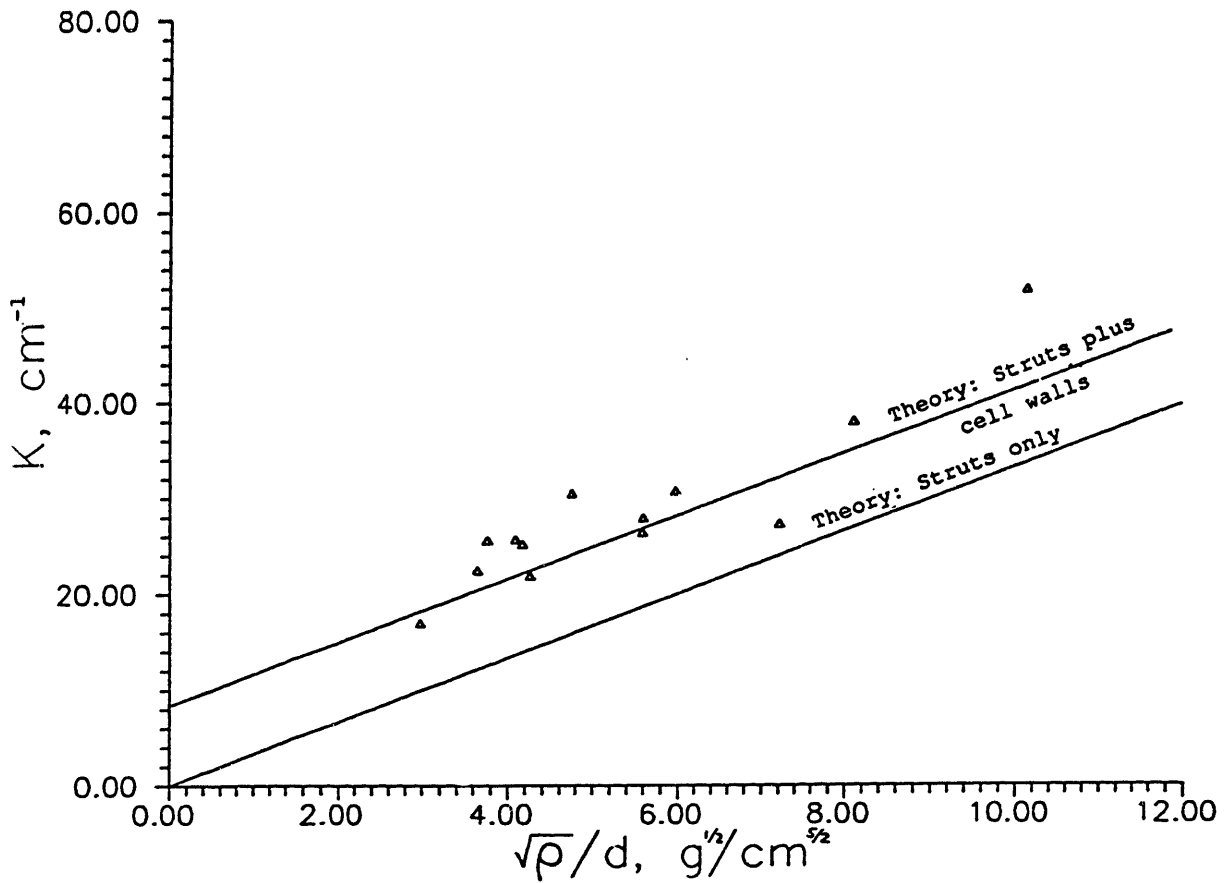


Figure 4-2: Extinction coefficient data from best-fit slopes. Density assumptions are the same as in Figure 4.1, and the far right point is again the exception.

Obviously, the best-fit values of r should be higher than the force-fit values, and in this case the best fit method showed a considerably better correlation. Reasons for this will be examined in the next section.

To further validate the theory, Eqn. (2.18) was applied to the data of Cunningham and Sparrow [20], who measured radiative conductivity vs. cell size for polyurethane foams of constant density. The radiative conductivity was obtained by measuring the overall foam conductivity, and then subtracting calculated values of solid and gas conductivity. This technique introduced a high amount of scatter in the data, since there are numerous uncertainties involved in calculating the solid and gas conductivities. The data were plotted and compared with a theoretical line for transparent cell walls. To express radiative conductivity in terms of cell diameter, either Eqn. (2.15) or (2.18) is inserted into the expression for k_{rad} . If cell walls are assumed transparent, the relation is

$$k_{rad} = \frac{16\sigma T^3}{3(0.751/d)} \quad (4.2)$$

where σ is expressed in $W/(m^2K^4)$, T in degrees K , and d in m. Eqn. (4.2) states that $k_{rad} \propto d$, so the equation is linear. If the effect of cell walls is added, the relation becomes

$$k_{rad} = \frac{16\sigma T^3}{3\left(\frac{0.751}{d} + 8.4\right)} \quad (4.3)$$

or $k_{rad} \propto d/(0.751 + 8.4d)$, which means that the radiative conductivity reaches a certain asymptotic value as the cells become larger. The two curves are drawn over the data of Cunningham and Sparrow in Figure 4.3. The slight bending of the data points indicate that the cell walls have a significant effect on radiative heat transfer.

4.2 Force-Fit vs. Best-Fit Methods

The initial method of calculating K proved valuable in illustrating certain phenomena. The average transmissivity from the spectrometer software could be plotted as $-\ln \tau$ vs. sample thickness to demonstrate the accuracy of fit of the line whose slope should be the

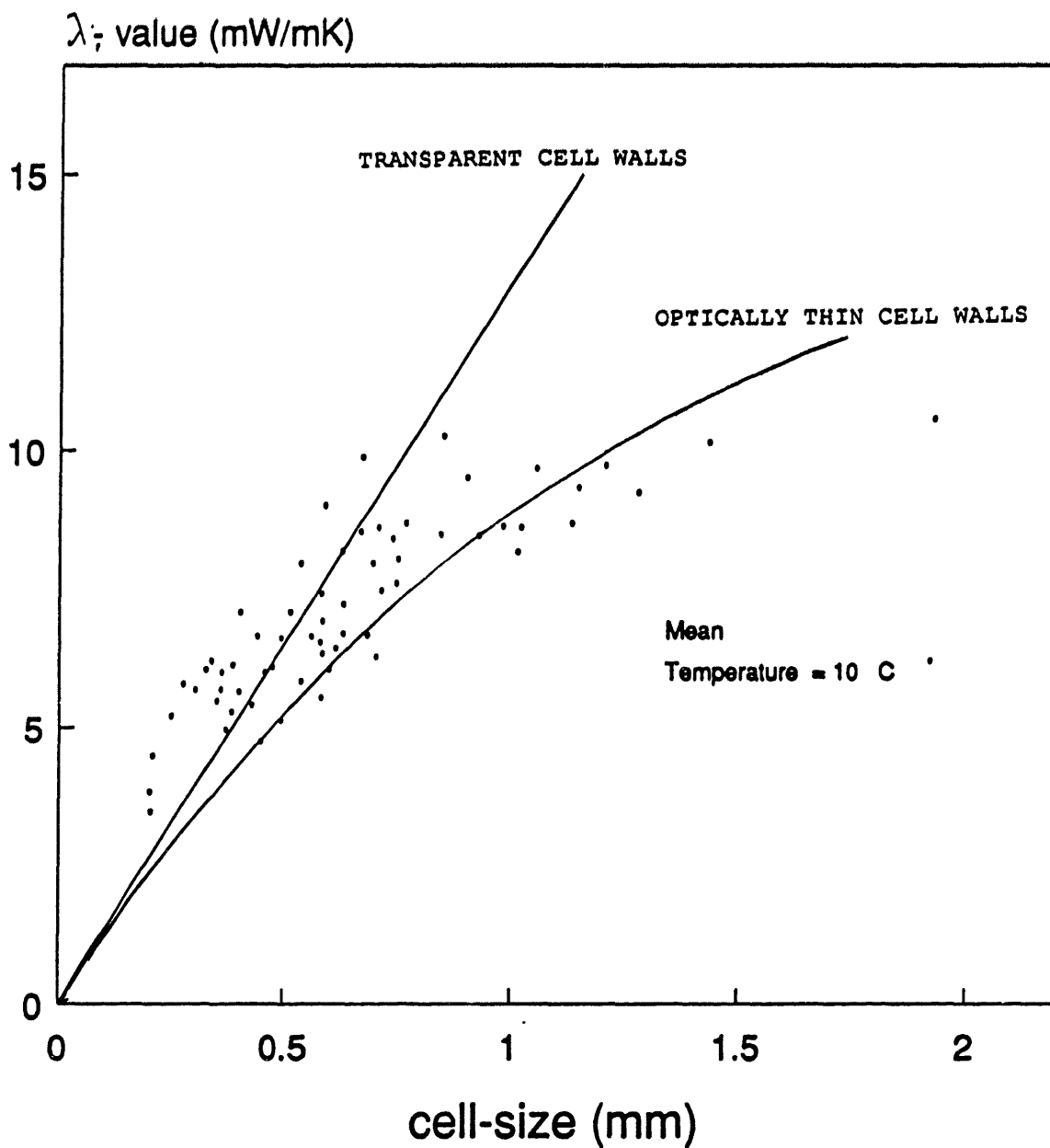


Figure 4-3: Data of Cunningham and Sparrow [20] with theoretical curves for transparent and optically thin cell walls, for a constant foam density of $.032 \text{ g/cm}^3$.

extinction coefficient. The primary question that these plots raise is whether a line forced through the origin or a best-fit line should be used to obtain the extinction coefficient.

Logically, the equation for transmissivity should be $\tau = e^{-Kt}$; at thickness $t = 0$ there is no medium and thus τ should equal one. In this case a plot of $-\ln \tau$ vs. t would be required to pass through the origin. From many of the plots generated, however, this does not seem to be the case. Many of the foams analyzed produce plots similar to Figure 4.4. The solid line fits the points well, but does not intercept the vertical axis near the origin. The intercept is $-\ln \tau = 1.424$, which corresponds to a transmissivity of 0.24 for zero thickness. If a line was drawn which best fit the data while being forced through the origin (the dotted line in Figure 4.4), it is readily seen that many points will be a great distance away from the line. The correlation coefficient would thus be considerably lower than that for a best-fit line. Another problem with using a force-fit slope can be seen from Figure 4.4. If more data points were added to the right of the given ones, the slope of the force-fit line would have to decrease to move the line closer to the new data. The extinction coefficient would then be dependent on the thickness range of slices analyzed, which is not compatible with the definition of K .

Though the best-fit slopes relate the data better, the method still does not explain certain phenomena. An example is the comparison of plots for two different foams, shown in Figure 4.5. By the best-fit method, the two foams have extinction coefficients very close to each other. However, the line fitting the lower set of data nearly passes through the origin, while the line in the upper set of data has a high intercept, corresponding to a transmissivity for zero thickness. Despite the similar values of K , the second foam should attenuate radiation much better than the first, since the value of $\sqrt{\rho}/d$ for the second foam is almost twice that of the first. It would seem that from this example that the force-fit extinction coefficient would be the better indicator of radiative behavior.

There is one possible physical explanation for the nonzero intercepts, which deals with the manner in which the foam slices were cut. The Isomet saw provides an even cut of constant thickness, but tears parts of surface cells in the process. This phenomenon is

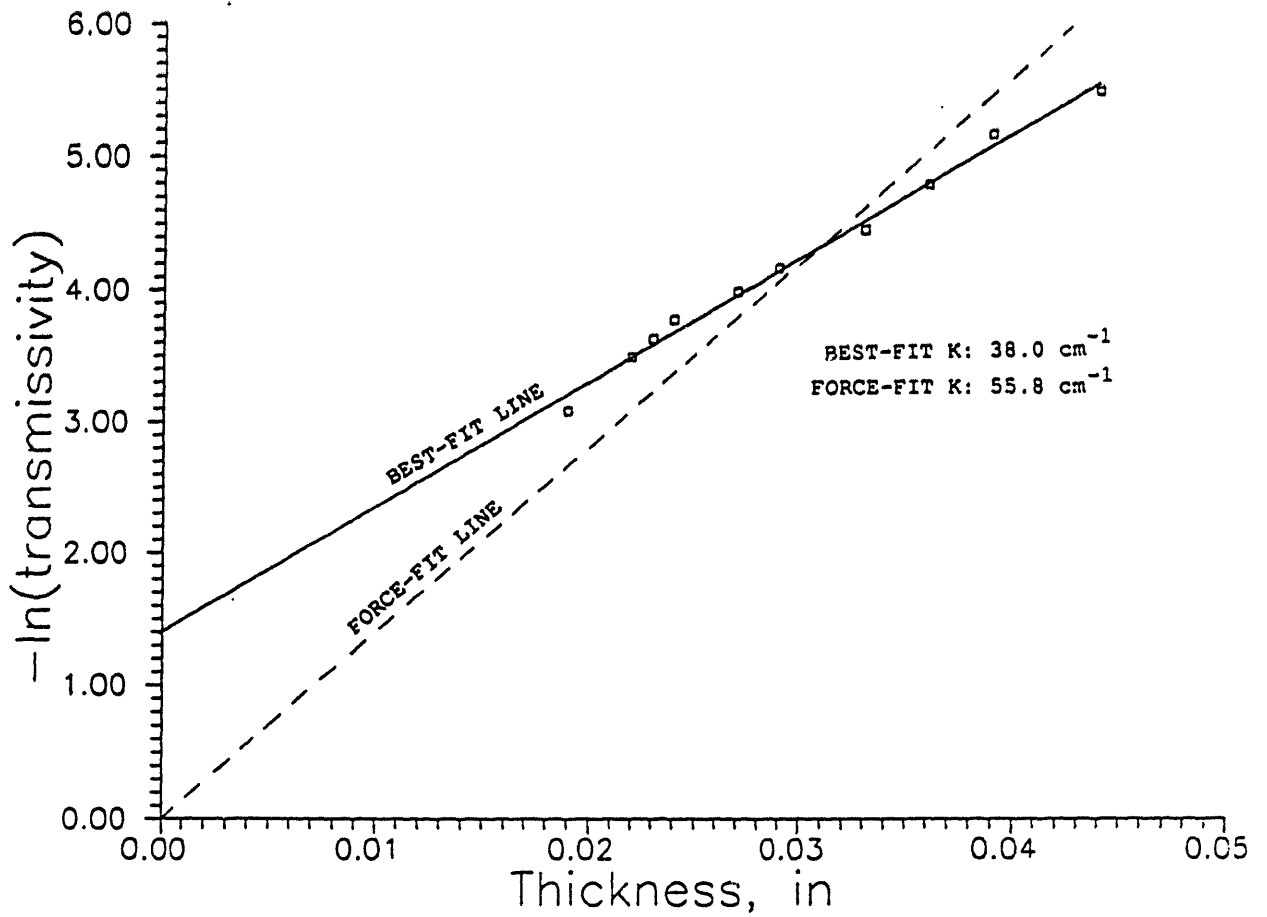


Figure 4-4: Illustration of nonzero intercept on plot of $-\ln \tau$ vs. t . The foam represented is number 1a from Appendix B.

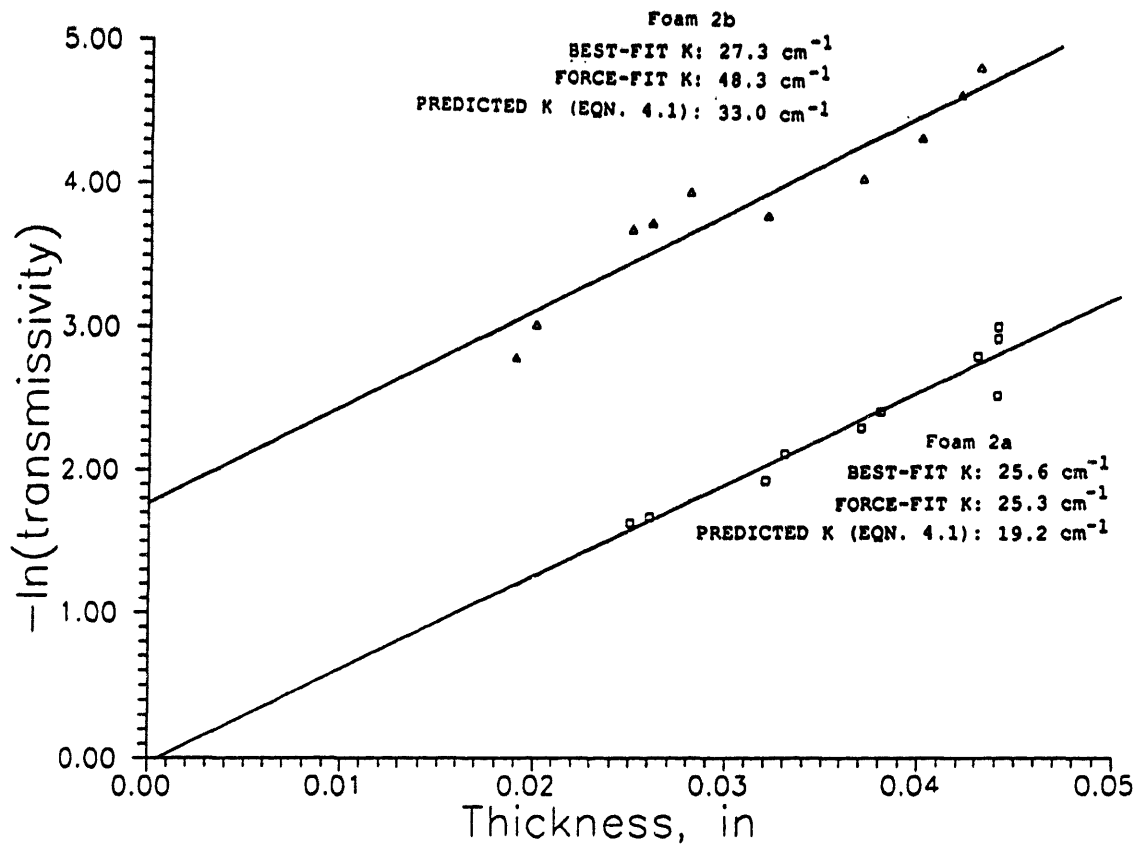


Figure 4-5: Comparison of transmissivity plots for two foams. Upper set of data points: $\sqrt{\rho}/d = 7.21 \text{ g}^{1/2}/\text{cm}^{5/2}$. Lower data: $\sqrt{\rho}/d = 3.76 \text{ g}^{1/2}/\text{cm}^{5/2}$. Foam numbers listed are from Appendix B.

illustrated in Figure 4.6, which compares a foam sample cut with an Isomet saw to that cut with a razor blade. As a result, an artificial layer of torn cell walls and struts can be deposited on the surface of each side of the foam slices. By “artificial” it is meant that these layers do not represent the rest of the foam in radiative properties. As foam slices cut on the Isomet get thinner, the thickness of these layers do not change, and thus a certain fraction of radiation is always absorbed when a test is run in a spectrometer. The transmissivity of the slice approaches that of the outer layers as the slice thickness approaches zero, creating a nonzero positive intercept on a graph on a graph of $-\ln \tau$ vs. t .

This explanation is questionable, however, because it does not explain how the foams from Figure 4.5 could have similar extinction coefficients; by the above explanation, the intercepts should be similar but the values of K should be different. It also does not explain how some of the intercepts should be so high on the vertical axis. The upper data of Figure 4.5 suggest that two outer layers on each of the foam slices analyzed has a transmissivity of 0.17; that it could be that low is highly unlikely.

4.3 Comparison of Cell Wall Photographs

Measurements were taken of cell wall thickness for each photograph described in Chapter 3. These measurements were used for comparison with the results of Reitz, who found that a typical cell wall is $0.5 \mu\text{m}$ thick. The measurements were also used to calculate the fraction of solid polymer in struts from Eqn. (2-27):

$$f_s = 1 - \frac{S_v t}{1 - \delta}$$

The calculation of f_s for each foam could not be carried out with only two cell wall photographs, however, since great disparity often appeared between the two thicknesses. Table 4.2 lists cell wall measurements taken for eight foams, and a comparison between two cell wall photographs for the same foam is shown in Figure 4.8. A difference of this magnitude was quite unexpected, since it was assumed to this point that cell walls were

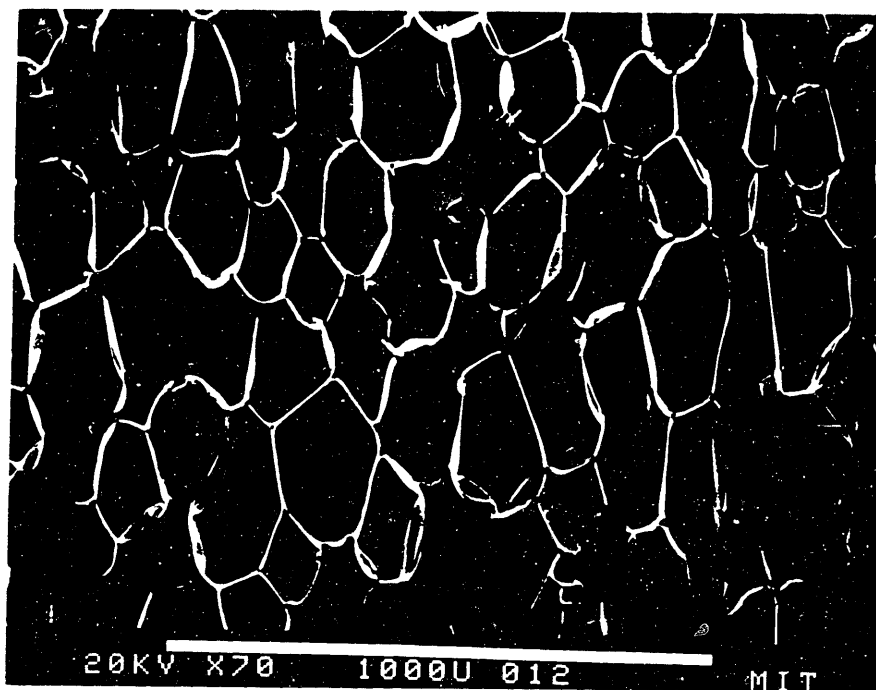
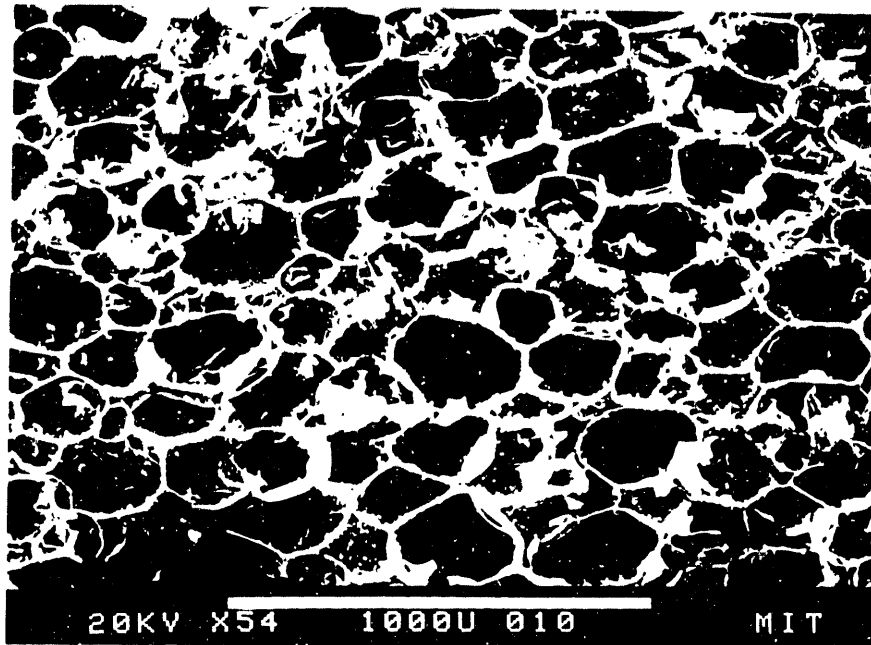


Figure 4-6: SEM photographs of foam samples cut with the Isomet saw (top, 54X) and a razor blade (bottom, 70X).

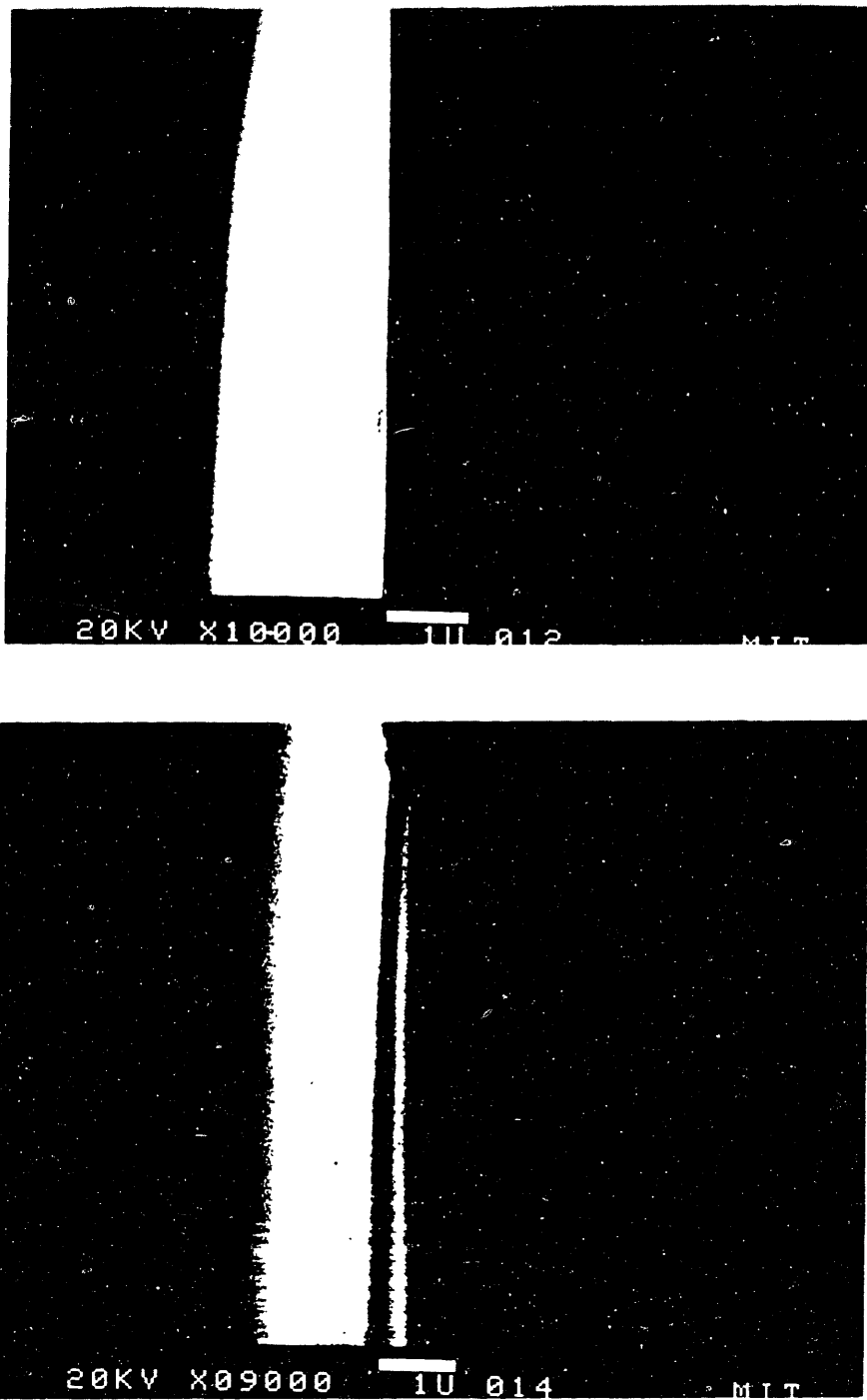


Figure 4-7: Comparison of cell wall cross-sections for the same foam of $.0268 \text{ g/cm}^3$ density and $.4 \text{ mm}$ cell diameter. Top magnification: 10,000X. Bottom magnification: 9,000X.

of uniform thickness. Apparently the effects of local stress variations in foam formation are more significant than originally thought. The thickness of a cell wall may be highly dependent on the area of the wall, and uneven distribution of certain chemicals in the uncured foam mixture may locally affect the surface tension, which would also affect wall thickness.

To obtain an accurate average wall thickness, at least five high-magnification photographs would have to be taken for each foam. This is a problem, since obtaining clear cell wall photographs is a time-consuming process which requires constant zooming in and out of high magnification to find a cut cell wall with a proper "head-on" orientation for viewing. In addition, the adjustment of focus and image contrast at high magnification was a delicate process. As a result it was decided to average all of the values in Table 4.2 to obtain one cell wall thickness for use in Eqn. (4.4). This was done to avoid calculating f_s for each foam from only two wall thicknesses. Since density and cell diameter are also required for this equation, the values from Table 4.1 were also averaged to obtain a single density and cell size. The average wall thickness was $0.38 \mu\text{m}$, which produced a value of 0.826 for f_s for a cell diameter of .36 mm and a density of $.031 \text{ g/cm}^3$. This value is reasonably close (three percent) to the value of 0.8 assumed in the foam radiation model.

4.4 Error Analysis

It was expected that there would be considerable uncertainty in the foam data in spite of the precautions taken. To produce a set of error bars on the plots of Figures 4.1 and 4.2, the uncertainty was analyzed for four separate quantities: sample thickness, transmissivity, cell diameter, and foam density.

4.4.1 Transmission Data

The error in the extinction coefficient was broken up into errors in transmissivity and sample thickness. The error in transmissivity was subsequently broken up into error due

to the spectrometer and error due to the variation of transmissivity with position on the foam slice. A simple experiment was devised to determine the relative importance of each effect. To begin, a foam slice was placed in the spectrometer and a sample was run. Four additional samples were run five minutes apart on the same foam slice without moving it. Four more samples were then run, each time slightly moving the sample in its holder. The transmissivities were obtained for each trial using the “integrate” command. Two standard deviations were calculated: one for the transmissivity data when the sample was moved for each trial, and one when the sample was kept still. The results are shown in Table 4.3, and indicate that the error from moving the sample is at least one hundred times that when the sample is left in place. The error in the spectrometer due to changing beam conditions was therefore neglected.

4.4.2 Foam Slice Thickness

The paper micrometer is an adequate instrument for measuring foam slices, but there is still a significant error which must be recognized. This error is due to the possibility of compressing the foam, and as a result the micrometer will tend to read values smaller than the actual thickness. To estimate the uncertainty, thin strips were cut from random foam slices and photographed in cross-section with an optical microscope. Typical photographs are shown in Figure 4.9. A paper clip of known thickness was also photographed to calibrate the magnification. The slice thicknesses were measured from the pictures, and the slices were then remeasured using the paper micrometer. The comparison of the two sets of measurements is shown in Table 4.4. As expected, the negative error was greater than the positive, and no deviation was greater than eleven percent.

4.4.3 Cell Diameter Calculations

Unlike the previous two measurements, the error in the cell diameter measurements could not be determined by experiment. It was instead estimated by assuming that the primary source of error was in counting the number of intersections of a test line with a cell wall. It

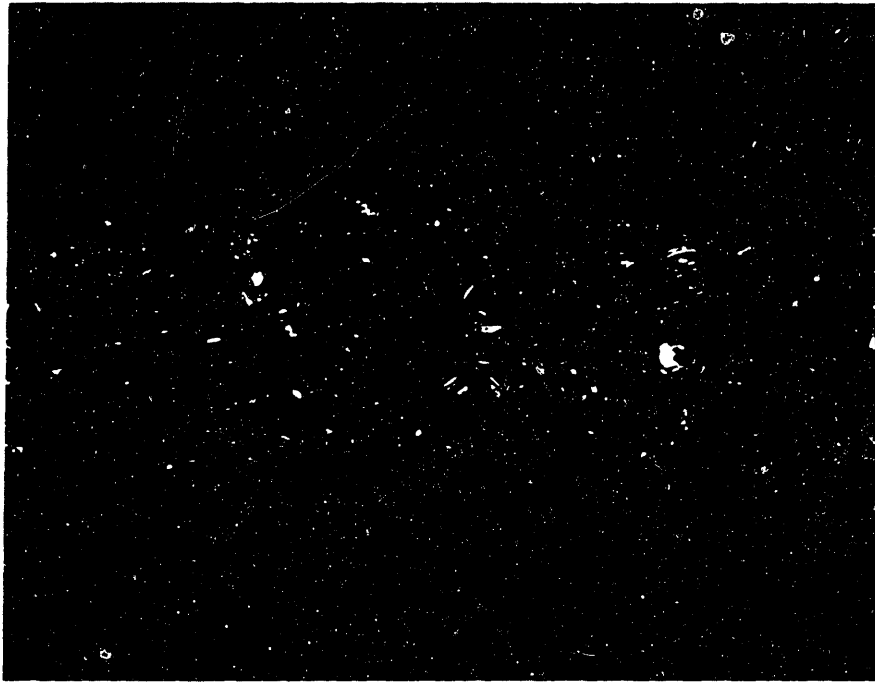


Figure 4-8: Optical microscope photograph of foam slice cross-section for comparison with micrometer thickness measurements.

was decided that the maximum counting error would be one intersection in both positive and negative directions. The difficulty in counting arises because the positions of cell walls are vague in many photographs. It may be difficult to tell whether a cell wall is in the top layer of cells, and a line passing very close to a three-way junction of walls as in Figure 4.10 may be counted as one or two intersections, depending on the clarity

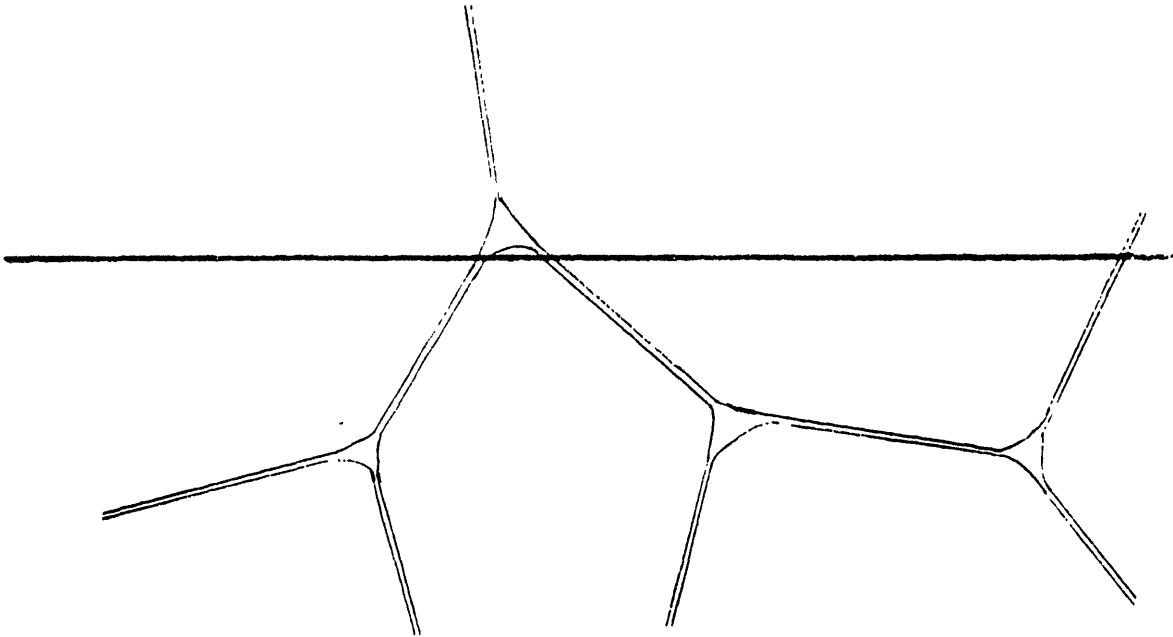


Figure 4-9: Test line passing close to a strut.

of the photograph. If the mean cell diameter is given by

$$d = 1.5\ell = 1.5\frac{L}{n}, \quad (4.4)$$

where L is the length of the test line and n is the number of intersections, then error analysis produces

$$\frac{\Delta d}{d} = \frac{\Delta n}{n}. \quad (4.5)$$

The value of n was chosen from an SEM photograph of a foam with cell diameters in the middle range (approximately .35 mm), and was taken to be 9.6. With $\Delta n = 1$, the error was calculated to be about ten percent. This may seem high, but it is a conserva-

tive estimate, and in addition represents one of the most accurate visual techniques for measuring cell size.

4.4.4 Density

When calculating the density error, it was determined that the percent error in mass is much smaller than the percent error in the length measurement. This is due to the accuracy of the balance used to weigh the plugs. The length and diameter of the cylinders were measured with a ruler graded in mm; the measurements were estimated to the nearest .1 mm. Though a caliper was available, its use proved no more convenient or accurate. The error in both diameter and axial length was estimated to be .5 mm, which produced a density error of four percent when 37.2 mm was used as the standard length dimension.

The results of the error analysis are summarized in Table 4.5, and the plot of K vs. $\sqrt{\rho}/d$ with error bars is shown in Figure 4.11. The larger negative error in the extinction coefficient is due to the skewed error in slice thickness. Of importance is which measurements have the dominant error in each parameter. In the extinction coefficient, the slice thickness error dominates the transmissivity error; in the parameter $\sqrt{\rho}/d$, the cell diameter error dominates the density error.

4.4.5 Further Considerations

The error analysis described above includes only measurement errors, so the error bars of Figure 4.11 do not include the effects of approximations made in the foam radiation model. Two quantities, f_s and the foam density, were assumed constant in the upper line of Figure 4.2. The densities are known to vary as much as 20 percent from the mean, and f_s was calculated from widely varying cell wall thicknesses. Another consideration is the disregarding of the scattering coefficient, which makes up a small part of the extinction coefficient. The spectrometer measures transmitted radiation, but not all of the scattered radiation, since only a small solid angle of outgoing radiation is collected.

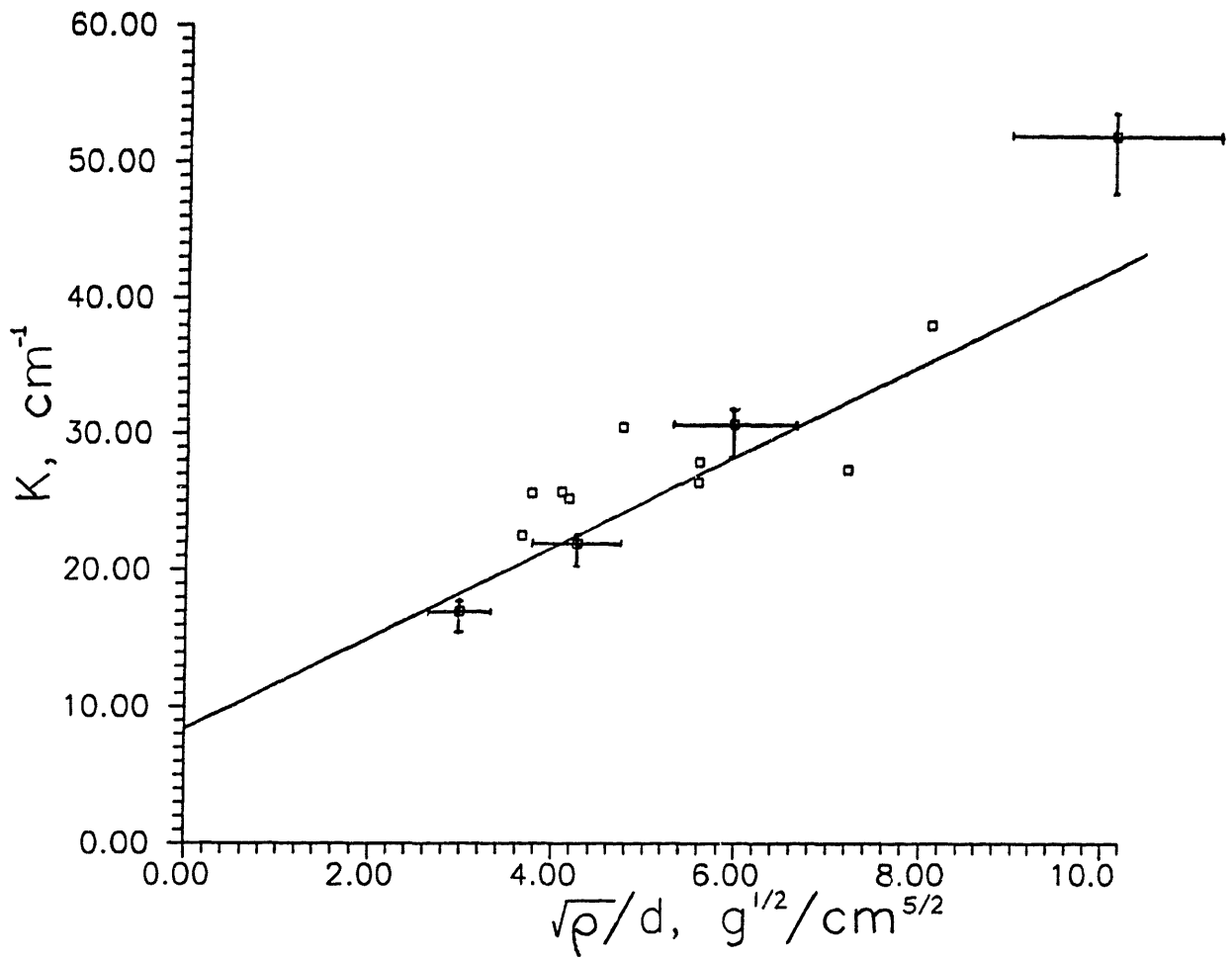


Figure 4-10: Best-fit extinction coefficient data with error bars.

Schuetz has shown that if the collection angle of a spectrometer is five degrees, the foam extinction coefficient is overestimated by approximately 11 percent. This error may not be significant, however, because scattering was neglected in the foam radiation model as well as in the spectrometer measurements. In addition to these factors, cell elongation may also have a significant effect on the radiation theory.

$d, \text{ mm}$	$\rho, \text{ g/cm}^3$	$\sqrt{\rho}/d, \text{ g}^{1/2}/\text{cm}^{5/2}$	$K_b, \text{ cm}^{-1}$	r_b	$K_f, \text{ cm}^{-1}$	r_f
.55	.0269	2.98	17.0	.9466	21.0	.9140
.47	.0294	3.65	22.5	.9919	26.0	.9755
.43	.0261	3.76	25.6	.9592	25.0	.9568
.40	.0268	4.09	25.7	.9777	32.6	.9351
.39	.0264	4.17	25.2	.9841	28.8	.9715
.38	.0262	4.26	21.9	.9897	30.7	.8824
.36	.0293	4.75	30.5	.9778	35.0	.9664
.31	.0300	5.59	26.4	.9844	33.1	.9392
.34	.0363	5.60	27.9	.9899	33.8	.9623
.29	.0300	5.97	30.7	.9757	47.6	.7534
.26	.0531	7.21	27.3	.9299	48.3	.3377
.21	.0289	8.10	38.0	.9934	55.8	.8387
.22	.0497	10.13	51.8	.9789	65.2	.9386

Table 4.1: Extinction coefficient, density, and cell diameter data for polyurethane foams. The "b" subscript is for best-fit slopes, and the "f" subscript is for force-fit slopes.

Foam #	Cell wall thicknesses, microns
1a	.21, .30
1b	.40, .66
1d	.20, .35
2a	.20, .40
2b	.20, .69
3a	.24, .28
3b	.27, 1.0
4	.27, .48

Table 4.2: Measured cell wall thicknesses for eight foams (two measurements for each foam). See Appendix B for more information on foam numbers listed.

Foam #	Slice left in place (% error)	Slice moved around (% error)
1	.04	4.2
2	.05	10.6

Table 4.3: Uncertainty in spectrometer measurement of transmissivity. Repeated spectra taken for a single foam slice.

Slice #	Micrometer measurement, in	Microscope measurement, in	Deviation	Percent Deviation
1	.014	.016	-.002	-12.5
2	.034	.038	-.004	-10.5
3	.069	.071	-.002	-2.8
4	.041	.038	+.003	7.9
5	.043	.043	0	0
6	.039	.042	-.003	7.1
7	.035	.037	-.002	5.4

Table 4.4: Error in paper micrometer measurements.

	K	$\sqrt{\rho}/d$
First component	$\tau: \pm 7.3\%$	$\rho: \pm 4\%$
Second component	$t: +2.6\%$ -7.7%	$\pm 11\%$
Combined error	$+3.3\%$ -8%	$\pm 11\%$

Table 4.5: Final results of error analysis.

Chapter 5

Foam Production

Now that the data has supported the theoretical relationship between the extinction coefficient and cell size, the problem now remains to create foams with small cells. This must be done without reducing f_v or the void fraction, or else by Eqn. (1.2) conduction through the solid will increase. The foam industry cannot presently produce foam insulations with mean cell diameters less than 0.2 mm without decreasing the void fraction substantially (as is done in microcellular foams) [14]. Photographs of some foam cross-sections may appear to have smaller cell sizes, but the cells are probably elongated in planes perpendicular to the photograph, making the mean cell size larger. If the foam industry is to compensate for the absence of low conductivity gases, it must consider producing foams with smaller, thin-walled cells.

The ultimate goal of this research is to determine what can be done to produce foam insulations with smaller cells so that the foam industry can use the information obtained. It is desired to test methods such as increasing pressure and adding chemicals to the foam mix. The initial goals, however, begin with the learning of foam mixing in the laboratory, and the macroscopic observation of the foaming process. Once foam mixing becomes more familiar, the research then focuses on whether the process can be viewed with a microscope, and how the microscope must be set up. The setup would undoubtedly involve photographic equipment (possibly a video camera) to record stages of cell

nucleation and growth. Such experiments have not been performed to any significant extent in the foam industry. This is because foam manufacturers rely mainly on the final cured form of the foam to determine how to produce smaller cells, rather than on the process itself. It should be noted that most commercial lab tests involve some analysis of the foaming process. It is common for a lab technician to mix certain foam chemicals and record the time after mixing for a foam to reach a certain appearance or texture. This test does not focus directly on controlling cell size, however. A visual test using a microscope may make it possible to explain how changes made to a foam mix affect cell size, and what stages in the foam formation are crucial in governing the final cell size.

This chapter will describe experiments performed on foam mixtures in various containers. The purpose of the experiments is to determine whether foam viewed through a glass surface will be representative of what takes place farther inside the foam. The concern here is that the effects of wetting or heat loss at a container boundary may retard cell growth, or may encourage the formation of a thick “skin” at the container boundaries similar to what forms at a free boundary. To prepare the reader for considering these possibilities, background information on foam production will first be presented. Fundamentals of polyurethane foam chemistry will first be discussed, briefly describing the various components present in a typical foam mix. The discussion will then turn to the mechanics of foam formation, including an introduction to classical nucleation and bubble growth theory. General methods of reducing cell size will be presented, along with potential problems with each method. Finally, The chapter will describe how polyurethane foam insulation is commercially produced.

5.1 Background

5.1.1 Foam Chemistry

Polyurethane foam is generally the reaction of a polyol with a polyisocyanate. The polyol is an alcohol with two or more hydroxyl (OH) groups attached to each molecule, and the

polyisocyanate molecule will have two or more isocyanate (NCO) groups attached. Upon reaction the hydroxyl and isocyanate radicals break up, and the molecules combine in chains of two or more units called urethanes. Another important reaction occurs if water is present in the reaction: water reacts with the polyisocyanate to form urea and carbon dioxide. Though many different secondary reactions take place, the two mentioned are of primary importance. The polyurethane that forms may be either in long chains with little branching, as in flexible foams, or highly cross-linked, as in rigid insulating foams. An illustration of the difference in structure is shown in Figure 5.1.

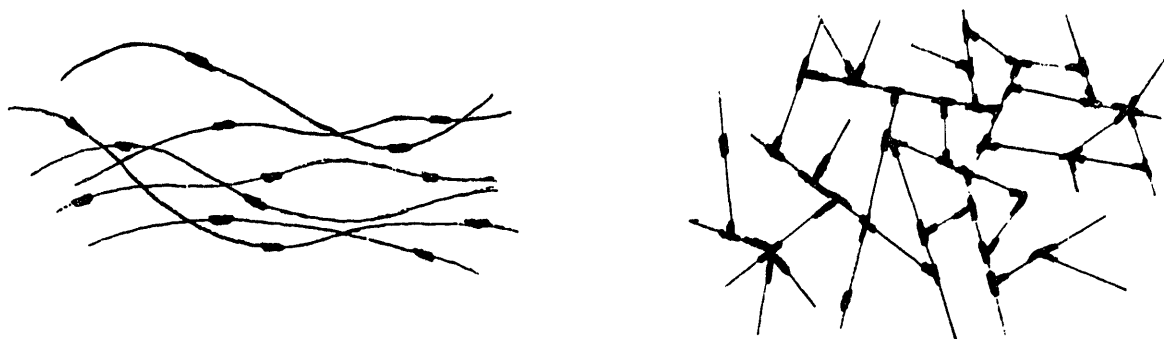


Figure 5-1: Comparison of elongated (left) and cross-linked (right) polymer molecules, showing locations of urethane linkages (heavy portions of lines).

The reactions described above form the basis for the solid polymer, but other components are necessary in a foam mix. The most essential of these is the blowing agent, or the component that eventually creates a gaseous phase and creates voids in the foam. The blowing agent can be dissolved in one of the polymer reactants. Since the polyurethane reaction is exothermic, the blowing agent vaporizes while the reaction is taking place, and comes out of solution in the form of bubbles. The most important examples of this

type of blowing agent are the CFC's mentioned in Chapter 1. In another type of blowing agent, the gas is formed as the product of a reaction occurring during polymerization. The primary example of this is the water-isocyanate reaction described above, releasing carbon dioxide into the bubbles. Water and CFC-11 are the primary blowing agents used in the foam industry, and are typically added to the polyol if the foam chemicals are supplied as a two-component system. Other chemicals are also typically added to the polyol which either affect cell structure or some other physical property. One example of an additive that can affect cell structure is the catalyst, usually another organic or organo-metallic compound. Another example is the surfactant, typically a silicon-based compound, which relieves surface tension when cell walls are thinning out. Components such as fire retardants and pigments are also often added to change other foam properties.

5.1.2 Foam Dynamics and Cell Size Control

Once the polymerization reaction has begun, gas bubbles begin to form in the liquid polymer around nucleation sites. Classical nucleation theory can be used to approximate the system initially as a gas dissolved in a fluid. This theory only serves as a rough approximation, and does not apply to later stages of foam formation where the polymer viscosity and surface tension become sufficiently high as the foam cures. Nevertheless, it serves as a valuable tool for understanding the basic dynamics of cell growth.

Hobbs [21] derived the work necessary to create a spherical bubble in a pure liquid:

$$W = P\Delta V - \gamma\Delta A = P \left(\frac{4\pi r^3}{3} \right) - \gamma(4\pi r^2) \quad (5.1)$$

where the first term is due to volume expansion, and the second term is the free energy from the creation of a new surface (γ is the surface tension). Differentiation with respect to radius r produces the radius at which the work is maximized:

$$r = \frac{2\gamma}{P} \quad (5.2)$$

Substituting this into Eqn. (5.1) yields

$$W_{max} = \frac{16\pi\gamma^3}{3P^2} \quad (5.3)$$

From this equation we can see that smaller bubbles have higher gas pressures. This means that if two bubbles of unequal size are separated by a sufficiently thin wall of liquid, gas will diffuse from the smaller bubble to the larger one. As a result, bubble size will increase with time and the number of bubbles will decrease.

To produce fine-celled foam, the process described above must be counteracted by bubble stabilization. Saunders and Hansen [22] suggest various means of reducing cell size, some of which are described in the remainder of this section. One suggestion is the increasing of nucleation sites, which increases the number of bubbles and thus makes the average bubble size smaller. Small solid particles or existing bubbles are usually necessary in the unreacted foam mix to provide outlets for gas diffusion. This is because spontaneous nucleation in a pure liquid requires high pressures for a small initial radius from Eqn. (5.2), and such pressures are highly unlikely. Self-nucleation may occur, however, if the surface tension is sufficiently low in the initial stages of polymerization; this lowers the required nucleation pressure for a given bubble size. A lower surface tension also decreases the pressure difference between bubbles of unequal size, providing an additional stability advantage. The surface tension may be lowered by the addition of a surfactant such as silicone oil, or by sufficiently catalyzing the reaction such that the surface tension and viscosity are still low when polymerization takes place.

As mentioned above, controlling bubble stability is another consideration in addition to increasing nucleation sites. Care must be taken that the bubbles do not grow too large before foam cure, and that cell walls do not become so thin that they eventually rupture. Saunders and Hansen discuss several points on controlling the thinning of cell walls. One important point is temperature control. An increase in temperature will tend to decrease viscosity as well as surface tension, and promote flow of polymer away from the cell wall due to capillary action. Preventing local areas of high temperature will thus minimize the amount of cell wall rupture. A silicone surfactant will also tend to keep surface tension low and viscosity high, thus stabilizing the cell. Another factor to consider is that attempting to create low-density foams with fine cells may make struts thin as

well as cell walls, which may lead to complete foam collapse. On the opposite end, an overzealous attempt to stabilize bubbles may lead to foams that are too dense, which would increase solid conduction. Tests must thus be run to determine optimum foaming conditions which will balance the effects described above.

5.1.3 Foam Board Production

A typical method of production for polyurethane foam insulation in board form is shown in Figure 5.2. The process is known as continuous lamination and consists of foam mixed on a sheet of facing material such as paper or metal foil and moved on a conveyor belt. The top surface is covered with another sheet of facing and constrained to produce even surfaces. The constraint also prevents excessive cell elongation from a unidirectional rise. The foam components are reacted by static (or impingement) mixing, in which two thin high-velocity jets are aimed at each other in a mixing chamber of small volume. The mixture deposited on the facing is heated as it enters the constraining belt to reduce heat loss on the outside of the foam near the facings. The continuous board that results is cut into desired lengths as it leaves the conveyor [1].

5.2 Foam Mixing Experiments

The method for small-scale foam production in the laboratory requires mechanical mixing rather than static mixing. The two foam components are poured in the proper weight ratios into a single container and mixed using a rotor at speeds of at least 1,000 RPM. Although this method does not produce foams of the same uniformity and cell quality as static mixing, it is sufficient for laboratory purposes and is the method used in the following experiments. The experiments will determine the feasibility of observing foam under a microscope, and if such observation is practical, methods of setting up a microscope will be suggested.

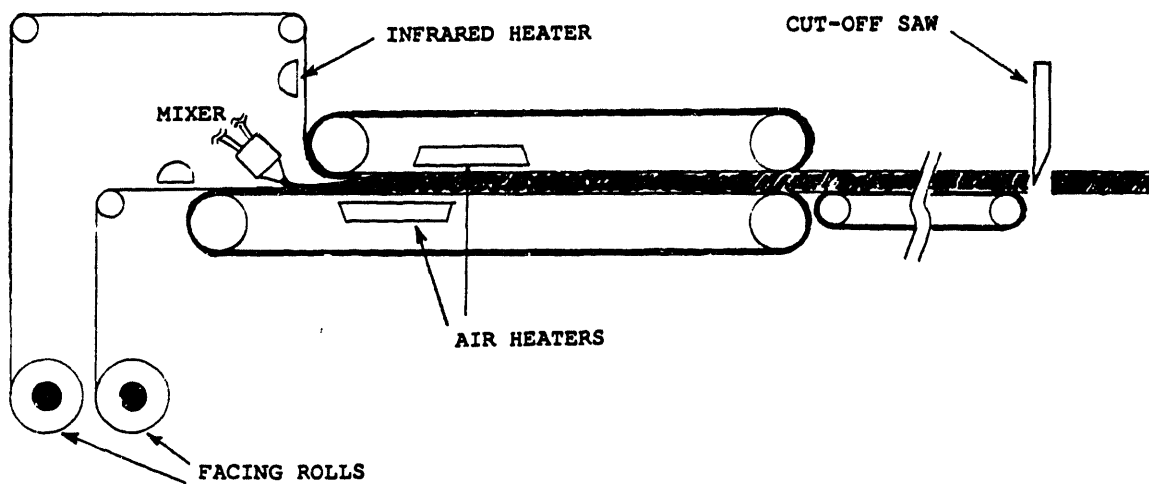


Figure 5-2: Industrial apparatus for manufacturing foam board [1].

5.2.1 Preliminary

Foam chemicals were received from ICI Polyurethanes and equipment was purchased for mixing. The first of the two foam components received was a form of methylene diisocyanate (MDI), a reactant commonly used for polyurethanes. The other component was a combination of high molecular weight polyols, catalysts, and a blowing agent, in this case CFC-11. Both components had densities of around 1 g/cm^3 . The mixer used was a Cole-Parmer Stir-Pak general purpose stirrer. This was a simple propeller-type low torque mixer which could provide up to 10,000 RPM in air. This mixer was adequate, since the foam mixture had a sufficiently low viscosity. The chemicals were to be mixed at a specific weight ratio, so a scale was used to measure the component amounts. Since no quantitative experiments would be performed, accuracy in measuring chemical amounts was not particularly important at this point, so a dietary scale was used, accurate to 1 gram.

Trial foams were initially mixed in one-pint ice-cream containers to determine the rate of volume expansion, which will be useful in future observation experiments. Under normal conditions the foam expanded from 25 to 30 times its original volume. This means that small amounts of each component are required to produce volumes of foam sufficient for most experiments. The amount of foam chemicals used also had a lower limit, as the propeller could not properly mix liquids that were too shallow in the container. It was decided that 45 g of total reactants (or about 45 ml) was an acceptable amount. The reactants were mixed for 3-5 seconds and within a few seconds after mixing the foam took on a creamy appearance due to the formation of small bubbles (in industrial tests the time after mixing that the appearance changes is known as the cream time). Immediately afterward the foam expanded rapidly in the next 30 seconds, and reached its final volume about 90 seconds after mixing. Within five minutes the foam reached its final state of rigidity.

The first foams produced showed two notable characteristics. The first is the "skin" that formed at the top of the free-rising surface. The skin is actually a top layer of

thickened cell walls and is generally attributed to rapid heat loss at the foam surface, which contracts cells and consolidates material. It is evident from the SEM photographs of Figure 5.3 that the thickness of this top layer is several times that of a typical cell wall. The second phenomenon observed occurs when the foam rises above the lip of the container while it is still fluid. The foam above the lip expands outward, which puts a radial stress on the foam as it is curing. This effect, aided by further expansion of the blowing agent, may create large voids in the foam like those shown in Figure 5.4. To control these voids it may be necessary to use smaller amounts of foam mix, or at least pour some of the mix into a similar container immediately after mixing. Another solution is to pour the foam in a wider, more shallow container, which was done in the next experiments.

5.2.2 Boundary Experiments

Once several trial batches of foam were produced, attention could be focused on obtaining a microscope for viewing the foaming process. Before this was done, however, it was necessary to determine whether such viewing would provide sound conclusions. The primary concern is that the foam would have to be viewed through a transparent surface, and that effects such as surface wetting and boundary heat loss would affect the cell size or structure at that surface. Surface friction and wetting effects were neglected on the assumption that such effects are also present between cells and are similar. The heat transfer characteristics, however, are not the same at the interior as they are at the surface, so thermal boundary experiments were of the greatest importance. The probable effect of heat loss at the viewing surface and the free rise surface is that rapid boundary heat loss would produce lower temperatures at these surfaces. The blowing agent would vaporize more slowly, resulting in smaller cells and thicker cell walls.

To test the presence of this effect, a number of foams were blown under different thermal conditions, and density and cell diameter measurements were taken for some of them. The first test performed was foam mixed and poured into a shallow thin-walled

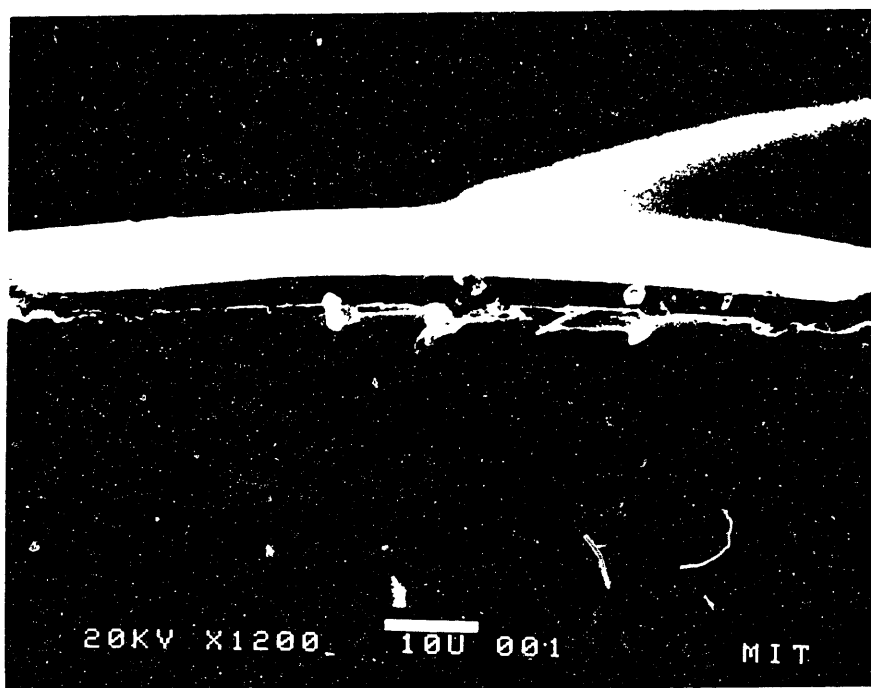
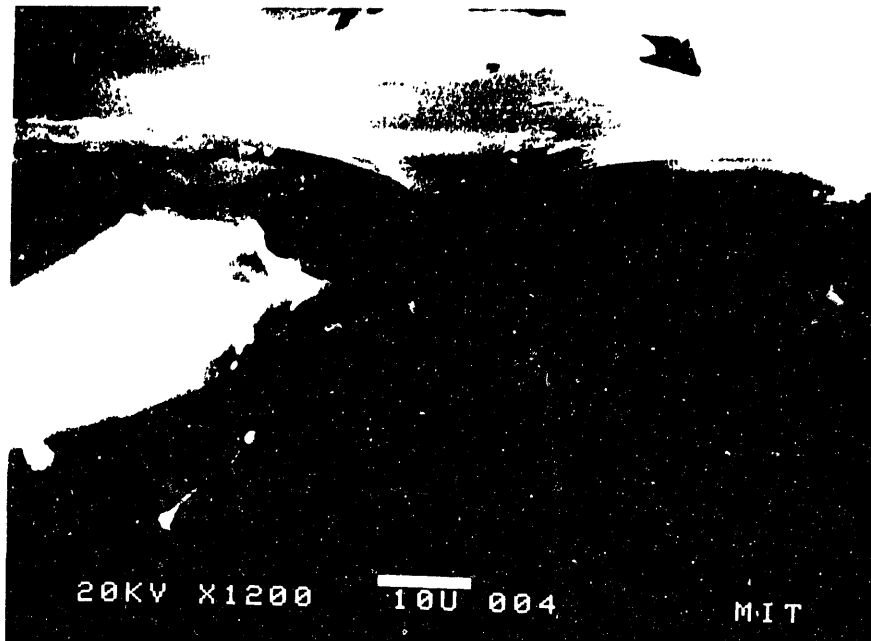


Figure 5-3: SEM cross-sectional photographs of free-rise surface skin (both photos 1200X). Skin thickness for both photos is approximately 3 μm .

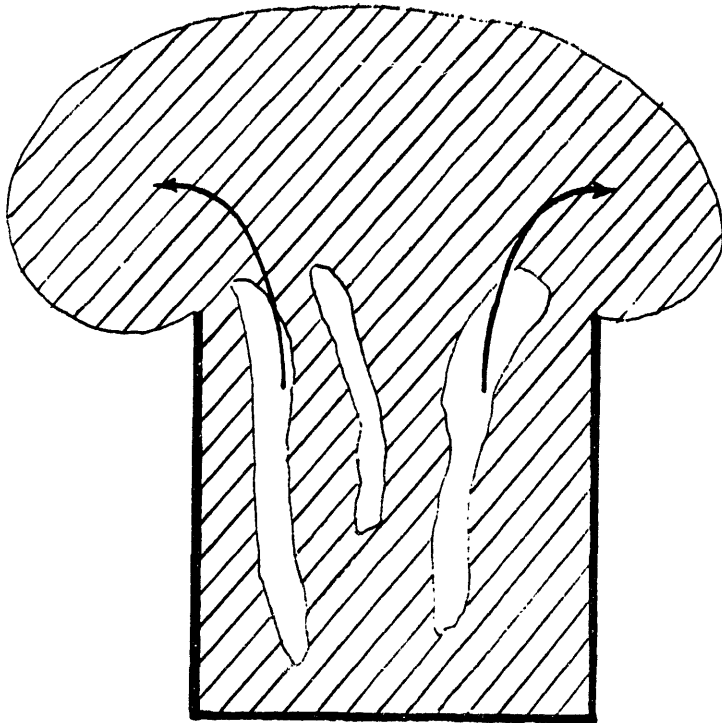


Figure 5-4: Void formation in lab-blown foams.

cardboard box, with half of the box surface insulated with commercial foam board. The experiment is sketched in Figure 5.5. Plugs were taken from the insulated end, uninsulated end, and center of the box near the bottom insulated surface, and density measurements were taken. Small cross-sections were also observed under an optical microscope for each location. The results were inconclusive; the center plug had the lowest density ($.0189 \text{ g/cm}^3$), and the densities of the insulated and uninsulated ends ($.0198$ and $.0205 \text{ g/cm}^3$, respectively) had error ranges that overlapped. Microscopic inspection of the cell structure also revealed little variation. Since the cardboard surface completely adhered to the foam, it was impossible to view the cells immediately adjacent to the boundary, so containers with smooth transparent surfaces were used in subsequent tests.

A second test was run by pouring the foam mix into a transparent polyethylene box of dimensions 5"x7" and 1" depth; a sketch of this experiment is shown in Figure 5.6. There were no special thermal conditions placed on the box; the purpose of this test was to measure the density and cell diameter variations with vertical distance from the bottom surface. The foam rise height was approximately 2.6 in. Five small cubes were cut from the foam at half-inch intervals from the bottom surface; these cubes were weighed and measured for dimensions. Slices were then cut from each cube in planes parallel to the foam rise (vertical) for viewing in the SEM. Two slices were also cut in planes perpendicular to the foam rise (horizontal), or the plane which would be seen when viewing the foaming process with a microscope. One slice was taken within .5 mm of the bottom surface, and the other was taken 1 in (25.4 mm) above the bottom. SEM photographs of the two slices are shown in Figure 5.7. The pictures look identical, and cell diameter analysis shows an identical cell size of .43 mm. Table 5.1 shows the density variation with distance, along with the variation of cell size and degree of elongation, or the ratio of the major cell axis to the minor axis. The densities and elongations roughly follow the predicted pattern that the foam should be most dense and least elongated near the boundaries. The elongated cell diameters calculated by Eqn. (3.5), however, do not

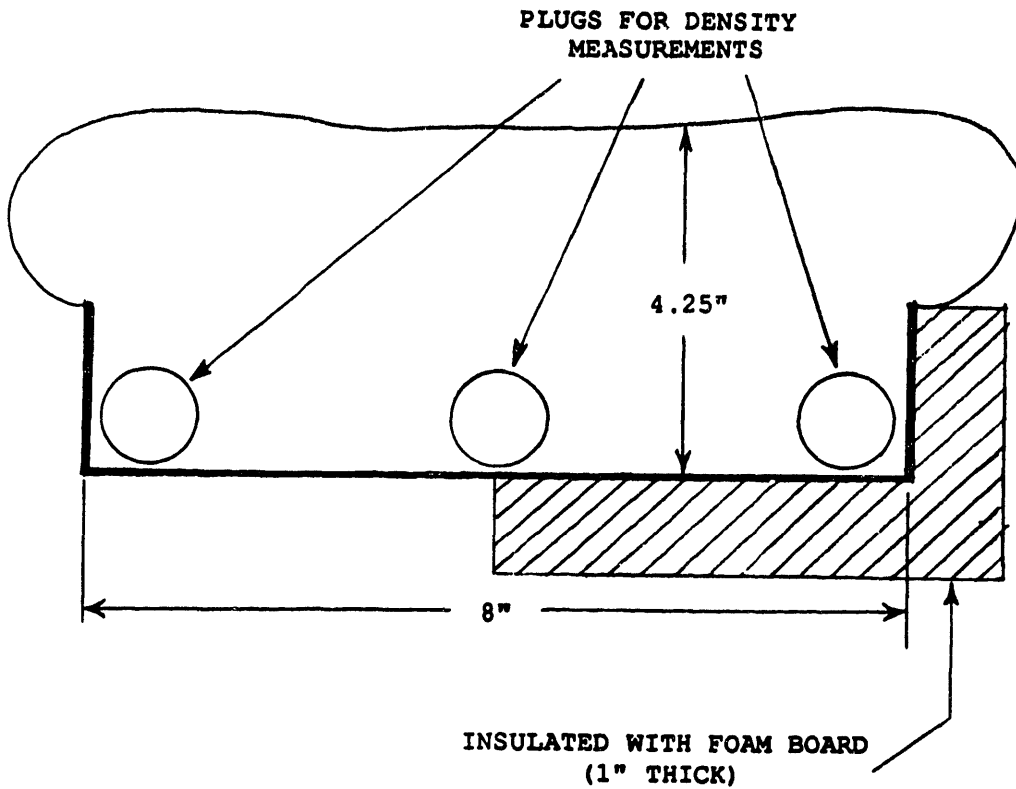


Figure 5-5: Sketch of foam blown in cardboard box, with locations of plugs.

SAMPLES FOR DENSITY
MEASUREMENTS

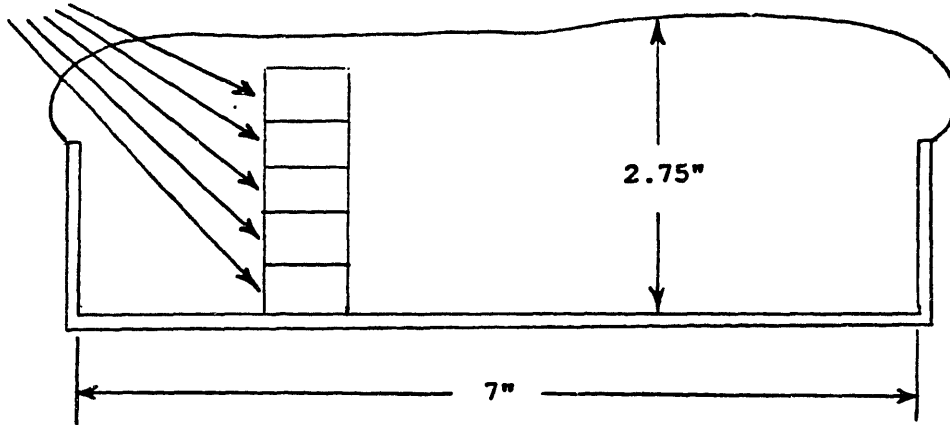
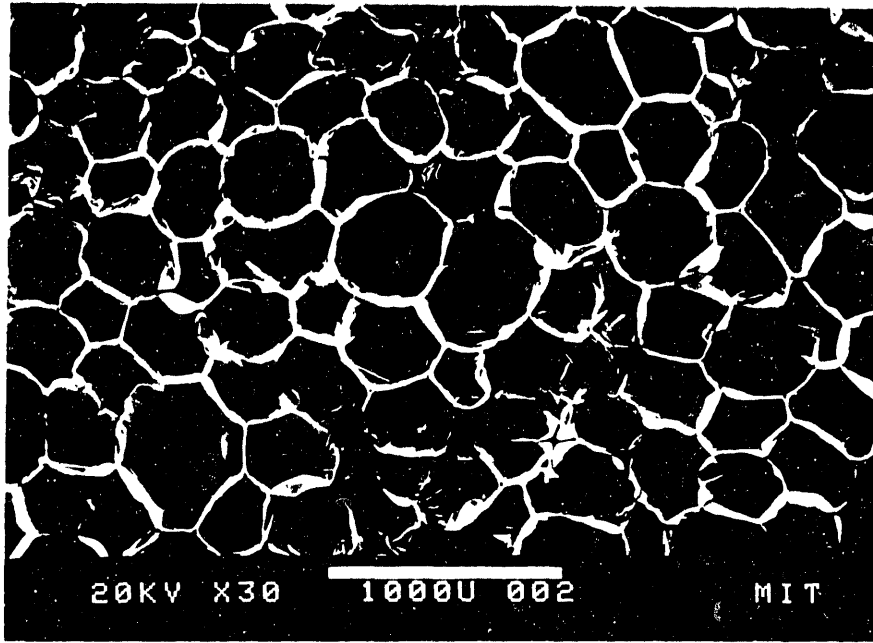
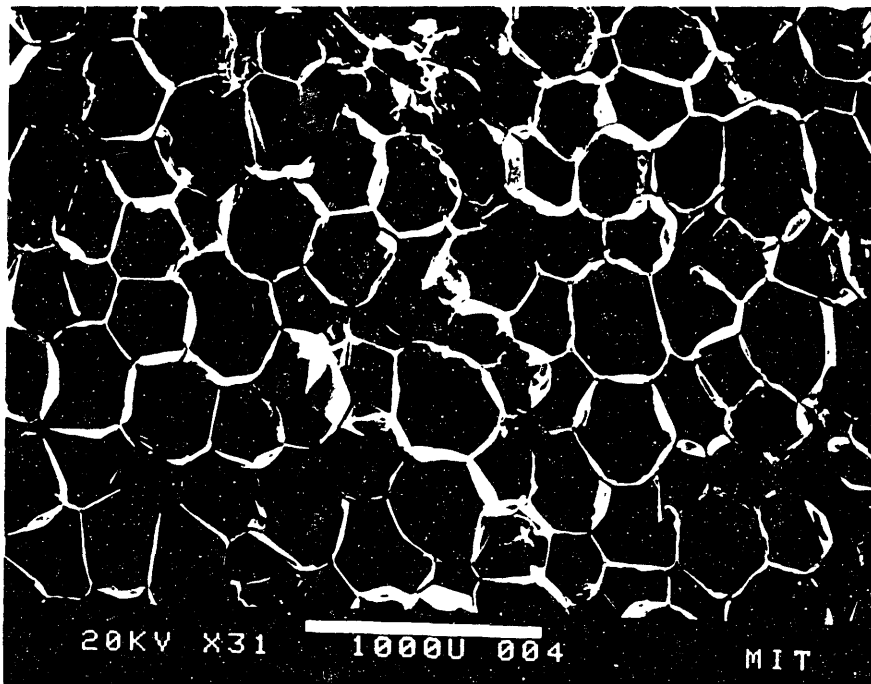


Figure 5-6: Sketch of foam blown in plastic box, with location of samples cut for density measurements.



Bottom surface



1" from bottom

Figure 5-7: SEM photographs of foam cells from foam blown in plastic box. In planes perpendicular to rise direction, magnification 30X.

follow the predicted trend, and seem to be affected more by local variations than by heat loss.

Concern also arose over the polyethylene box experiments because of the possibility of reaction between the foam polymer and the box polymer at elevated reaction temperatures. This did not seem likely at first, because the foam separated readily from the box after curing and formed a smooth transparent surface where it made contact with the box. Nevertheless, it was decided to view the foam in a glass container as a safeguard. The first containers used were Pyrex culture dishes of 5.5 in diameter and .75 in depth. Experiments were devised to alter the thermal conditions of one of these dishes before the foam mix was poured in. The first dish was to be insulated and heated to near maximum reaction temperature, which was found from a thermocouple measurement to be 296° F. Another dish was to be left uninsulated and at room temperature. Four small plugs were taken from each foam at approximately .7 in intervals from the bottom surface, and weighed for density. Cell diameter measurements were then taken at the bottom surface and 1 in from the bottom, with photographs in planes parallel and perpendicular to the rise direction for each location.

A listing of the density measurements for the Pyrex dish experiments is given in Table 5.2, and the complete set of cell diameter measurements is given in Table 5.3. A comparison of photographs taken at the bottom surface and perpendicular to the rise direction for each dish is also shown in Figure 5.8, demonstrating the great difference in cell sizes. It appears that heating the dish to near reaction temperature adds too much heat to the foam mix before it completely reacts. This makes the blowing agent vaporize prematurely and create bubbles much larger than would be found farther inside the foam. From Table 5.3 it can be seen that while the foam from the heated dish had boundary cells that were too large, the boundary cells of the unheated dish were slightly undersized. This suggests that some intermediate boundary temperature is desired, or that better insulation is needed for the boundary temperature to match the foam interior temperature.

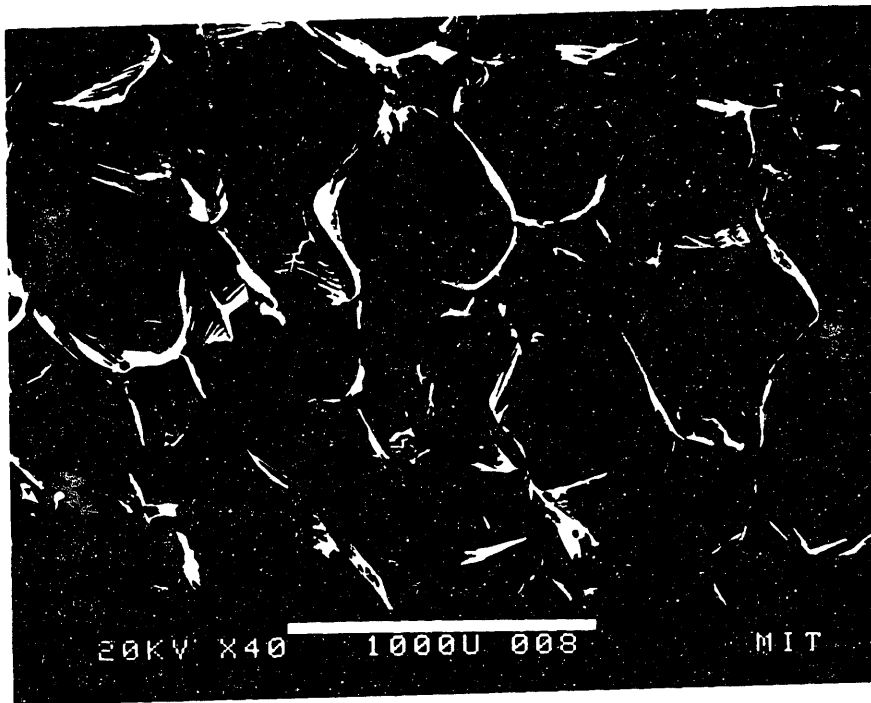
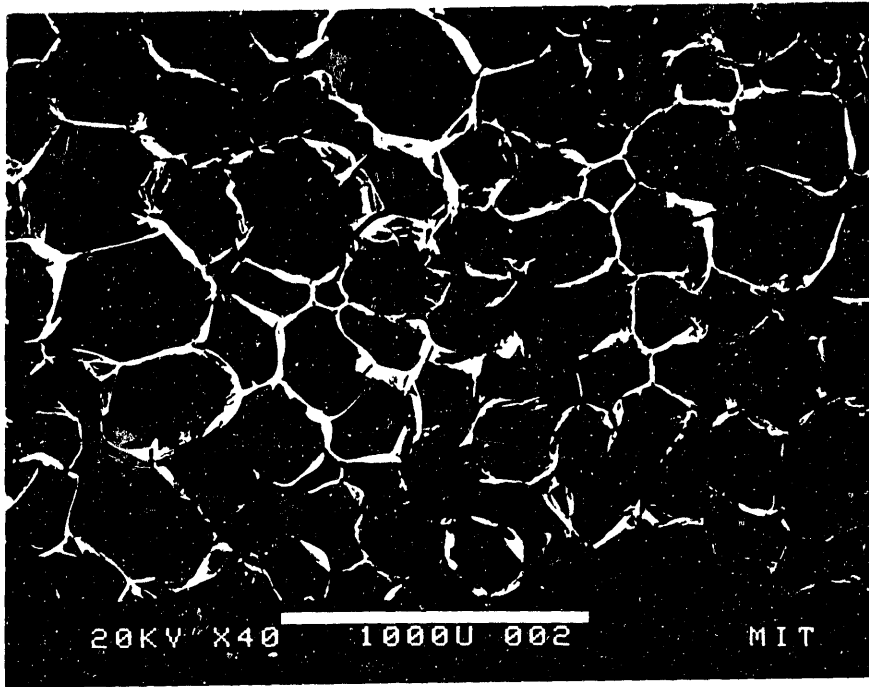


Figure 5-8: SEM photos of foam cells at the bottom surface of unheated (top) and heated (bottom) Pyrex dishes. In planes perpendicular to the rise direction, 40X magnification.

One possible consideration for insulating the boundary more efficiently is finding a container with thinner glass. Pyrex has a high heat capacity and the dishes were about .06 in thick, which may be enough for the glass to draw excess heat from the foam mix while it is reacting. To solve this problem, the container drawn in Figure 5.9 was devised, which consists of two ice-cream containers stacked on top of each other and glued together. The bottom is cut out of the top container so that the foam will be allowed to rise higher without reaching the top and expanding radially, causing the voids described earlier. At the bottom of the container is a half-inch thickness of pre-formed foam insulation with a hole of approximately one half inch diameter in the center. The purpose of the hole is to simulate viewing the bottom of the container with an inverted microscope, so that the objective peers up through the hole. Covering some of the insulation, including the hole, is a .006-inch thick sheet of cover glass, attached to the insulation with rubber cement. After the foam is poured into the container and allowed to cure, the rubber cement can be easily peeled away from the glass, allowing the foam to be viewed by removing the bottom insulation.

The foam cells were viewed in the two usual planes and at four different locations. Along the bottom surface viewing samples were taken directly over the hole and about .75 in away from the hole. For each of these locations samples were also taken one half inch above the glass. For the photographs at the bottom surface and perpendicular to the rise direction, optical microscope photographs were taken as well as SEM photographs. The results of the cell diameter analysis are shown in Table 5.4. The cells show greater elongation than the foams from the Pyrex dishes because of the greater vertical expansion of the foam. Comparisons of cell photographs in different positions are illustrated in Figures 5.10 and 5.11. The data did not seem to follow a particular trend, except that in the perpendicular plane photographs, the cell sizes were somewhat smaller at the bottom surface than farther into the foam. This was particularly evident with samples from over the hole. This result was not supported by earlier experiments, however, and was considered insignificant for the purposes of this research.

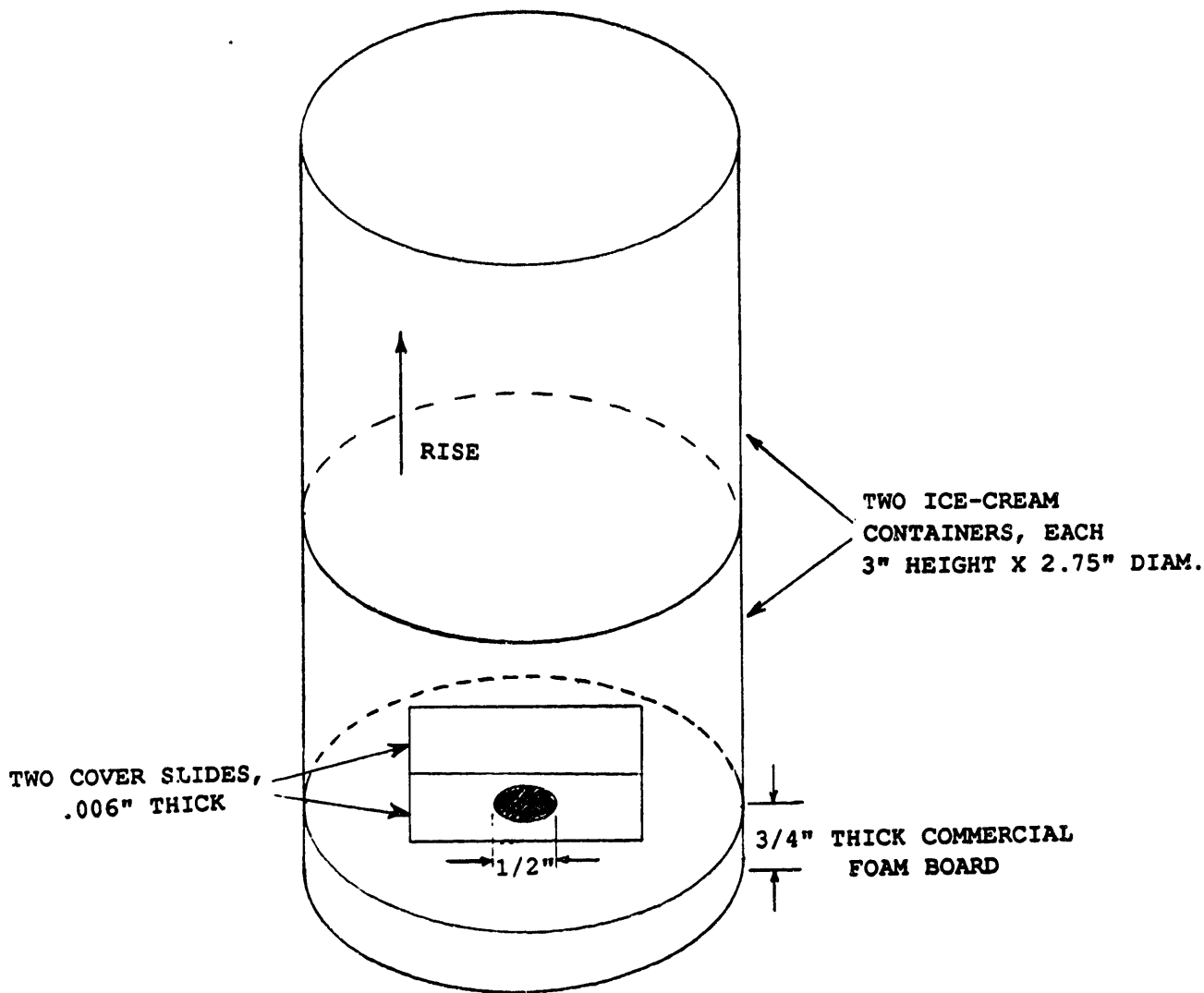


Figure 5-9: Sketch of thin-glass viewing experiment.

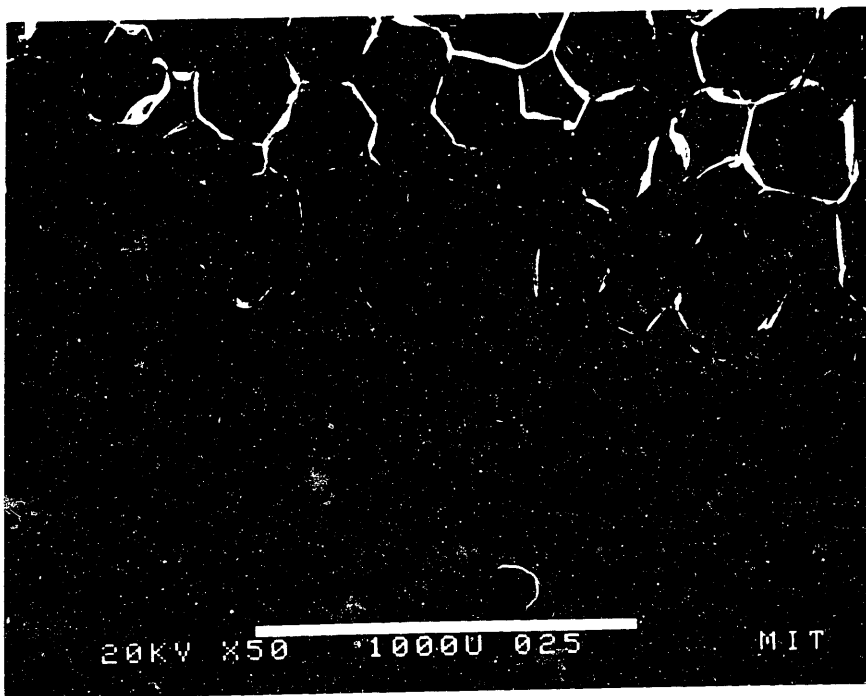
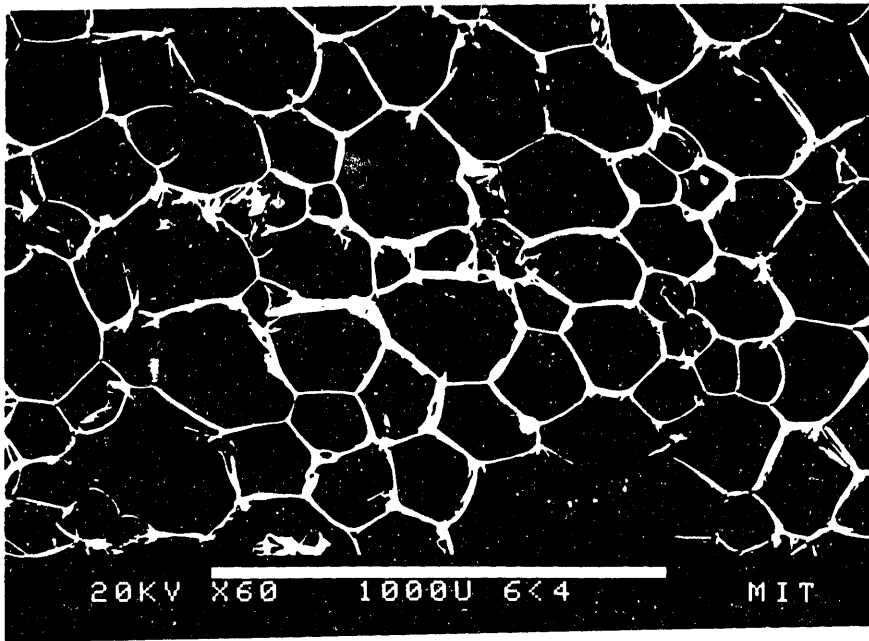


Figure 5-10: Comparison between cell sizes at glass surface (top) and 1/2" up from surface (bottom), thin-glass viewing experiment, away from hole. Magnifications are 60X (top) and 50X (bottom). Planes shown are perpendicular to the rise direction.

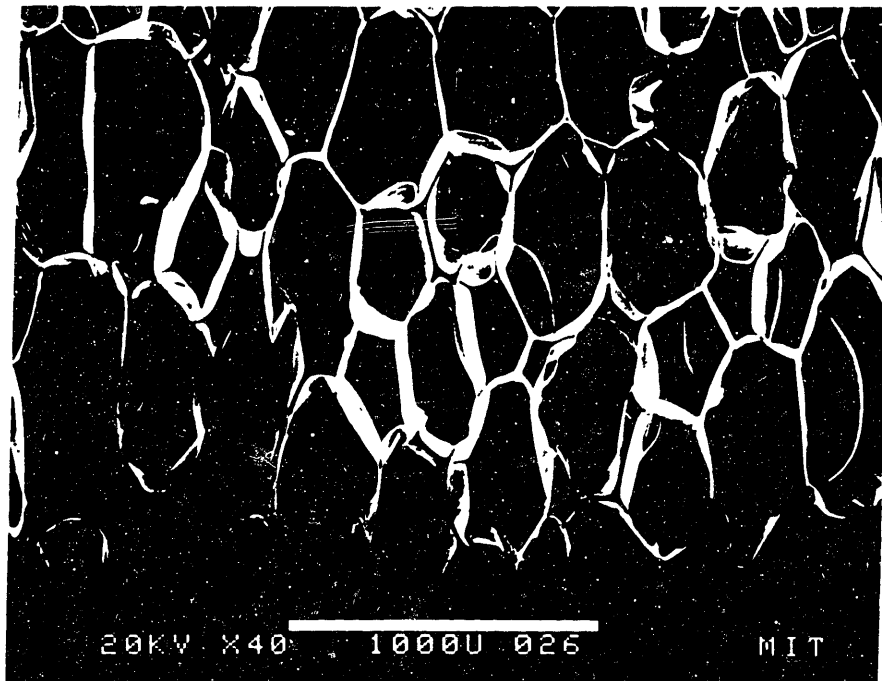
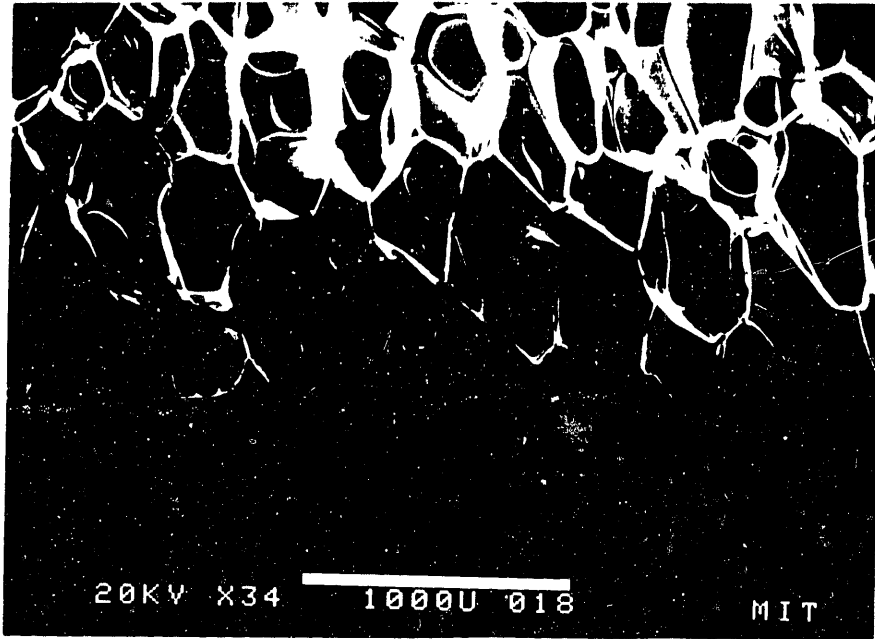


Figure 5-11: Comparison between cell sizes at glass surface (top) and 1/2" up from surface (bottom), thin-glass viewing experiment, over hole. Magnifications are 34X (top) and 40X (bottom). Planes shown are parallel to the rise direction.

The general conclusion drawn from this experiment was that boundary heat loss effects create some disparity in cell size. This disparity can be minimized by making the container boundary as thin as possible and insulating it. While the thin-glass experiment showed that the boundary cell sizes were somewhat smaller at the glass surface than farther inside the foam, the difference in cell size was less than in the Pyrex dish experiments. The skin that forms at the free-rise surface is probably not due to heat loss, since such a skin did not appear along the bottom of the foam blown in the unheated Pyrex dish. It is probably more due to lack of movement of the polymer at the free-rise surface, as compared to the container boundaries, where fluid friction may tend to thin out the polymer. If the foam is viewed with a microscope apparatus and a container similar to the one in Figure 5.7, one can expect to see cell growth reasonably close to what takes place at the interior of the foam.

5.2.3 Suggested Viewing Apparatus

Figure 5.12 shows a setup for microscopic viewing of foam based on the experimental results. A biological inverted microscope is suggested so that a stationary surface can be observed. A small amount of foam mix will be poured into a cardboard cylinder with a thin sheet of glass at its base. The glass will be adhered to a slice of preformed foam, no more than 0.5 in thick. The thickness of the insulation is limited by the working distance of the objective, which may have to extend above the hole in the stage in order to focus on the glass. The biological inverted microscope uses transmitted light for illumination, which would be adequate if the foam rise height were one inch or less. Such a rise height is difficult to obtain because of the foam's great volume expansion, so it may be more practical to use reflected light. The main problem with this is that biological inverted microscopes are not generally equipped to supply light from the objective; this feature can only be found in metallurgical microscopes which are more costly and precise than is required. It is possible, however, to fit a fiber-optic ring light source around the objective. Both types of illumination will be tested in future experiments.

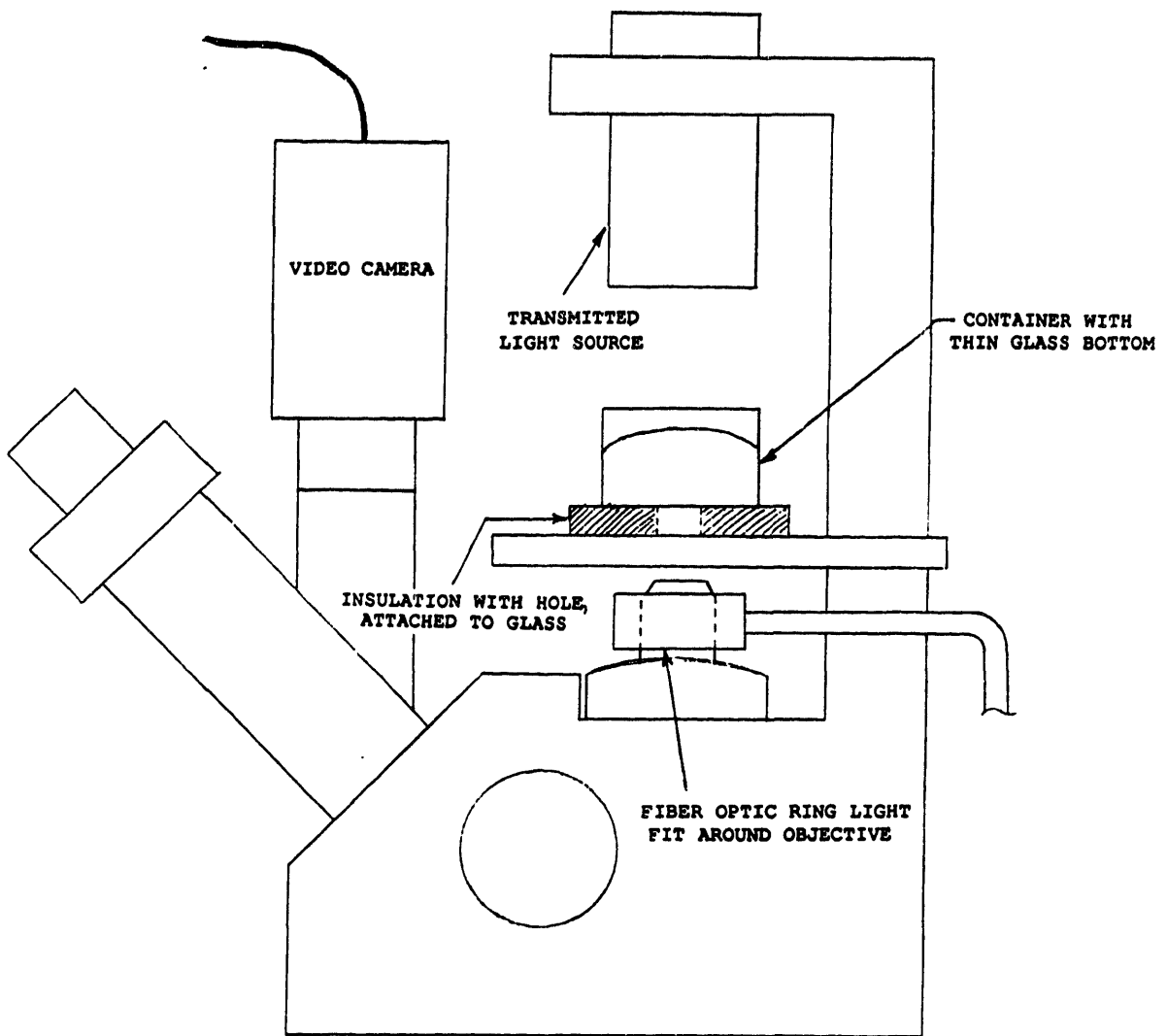


Figure 5-12: Proposed microscope setup for viewing foam.

To record the process, a video camera will be fitted on the microscope, along with a black-and-white monitor and videocassette recorder. Using quick multiple exposures of 35 mm still film was also considered. The camera would have to take at least one exposure per second, since the cell growth processes of interest take place in the first ten seconds of mixing. With this amount of time, the video camera must take a number of frames per second sufficient for review in slow motion. It is desired to view the foam at as early a stage as possible so the number of nucleation sites can be counted.

Distance from bottom, in	Mean cell Diameter, mm	Elongation	Density, g/cm^3
0	.57	1.12	.0227
.5	.48	1.32	.0200
1.0	.46	1.18	.0190
1.5	.53	1.15	.0183
2.0	.52	1.01	.0204

Table 5.1: Data for foam blown in plastic box.

	Distance from bottom, in			
	.3	1.0	1.7	2.4
Unheated dish	.0229	.0213	.0208	.0211
Dish at 280°F	.0216	.0206	—	.0210

Table 5.2: Density measurements for Pyrex dish foams, in g/cm^3 . The missing density was discarded because of excessive voids in the foam plug.

	Parallel to rise			Perpendicular to rise, mm
	Major axis, mm	Minor axis, mm	Elongation	
Unheated dish, bottom surface	.53	.39	1.36	.24
Unheated dish, 1" from bottom	.56	.44	1.27	.36
Dish at 280°F, bottom surface	.64	.58	1.10	.69
Dish at 280°F, 1" from bottom	.63	.50	1.26	.41

Table 5.3: Cell diameter data for foams blown in heated and unheated Pyrex dishes.

	Parallel to rise			Perpendicular to rise, mm
	Major axis, mm	Minor axis, mm	Elongation	
Over hole, bottom surface	.70	.39	1.79	.24
Over hole, 1/2" up from glass	.70	.36	1.94	.32
Away from hole, Bottom surface	.54	.43	1.26	.26
Away from hole, 1/2" up from glass	.63	.33	1.91	.30

Table 5.4: Cell diameter data for foams blown in the container of Figure 5.9.

Chapter 6

Conclusions

1. The model for the radiative portion of the effective conductivity of foam insulation has been improved. This was done by including the effect of cell walls as well as struts in the derivation of the extinction coefficient.
2. At low optical thickness, the high absorptivity cell wall model for the extinction coefficient simplifies to the original optically thin equation. This suggests that the high absorptivity model may also hold for intermediate optical thicknesses.
3. The Isomet saw was an adequate instrument for cutting foam samples for the spectrometer, but the tearing of cell walls may have an effect on the transmissivity measurements.
4. An improved but simple formula has been derived to determine the mean cell diameter from SEM photographs of foam cross-sections. This formula assumes spherical uniform cells.
5. From the spectrometer and computer data, it can be seen that the foam cannot be assumed a gray medium; the transmissivity, and thus the extinction coefficient, are not constant with wavelength.
6. The improved formula for the extinction coefficient fit the experimental data rea-

sonably well when used with best-fit values of K . When applied to radiative conductivity, the formula also fit data from another source.

7. Though the data from the best-fit extinction coefficient was compatible with the derived formula, it is still uncertain whether K should be defined by a force-fit or a best-fit slope from $-\ln \tau$ vs. t data.
8. Cell wall thickness may vary considerably within a given foam.
9. Foams with smaller cells will have smaller effective conductivities as long as the void fraction or fraction of solid polymer in struts is not also decreased.
10. Increasing the number of nucleation sites is of primary importance in producing fine-cell foam.
11. The cell walls in a fine-cell foam should be thin, but care must be taken that cell walls do not thin out to the point of rupture during foaming. Methods of controlling this include adding a surfactant and preventing local areas of high temperature.
12. A microscope can be used to view cell nucleation and growth during foaming. Cells viewed through an insulated thin glass surface are representative of cells farther inside the foam if the surface is adequately insulated.

Appendix A

Computer Code with Input and Output

The following program computes the Rosseland mean extinction coefficient for spectrometer data. The input to the program is a modified form of the ASCII file recorded by the spectrometer for each foam slice. The original form of the file is shown in Figure A.1, and the input file (modified form) is shown in Figure A.2. In the input file, the first number is the thickness of the foam slice, and the transmissivities for successive wavenumber intervals are listed from left to right in successive rows. The length of each wavenumber interval can be calculated from

$$\Delta\eta = \frac{FIRSTPT - LASTPT}{\#POINTS - 1}$$

where “FIRST PT” and “LAST PT” are the starting and ending wavenumber, respectively, and are read from the original file, as is “# POINTS”. Since the program can only read the first transmissivity in each row, the interval used by the program in the numerical integration is actually six times the value obtained above.

The output for the program is shown in Figure A.3. The best-fit and force-fit extinction coefficients are displayed for successive wavenumber intervals, along with their respective correlation coefficients. The final Rosseland mean values are then displayed,

along with the average correlations. The extinction coefficients for each interval was found to correspond with the transmissivity spectrum of Figure 3.3. In general, the extinction coefficient increases as the transmissivity decreases.

```

INSTRUMENT = IR44
FILETYPE = UNSPECIFIED
FIRST PT = 4800.47
LAST PT = 399.32
# POINTS = 4564
# SCANS = 256
DATE = 03/24/1989
TIME = 11:41:34
SAMPLE NAME =
SAMPLE FORM =
CHEMIST NAME =
ZEROFILL = 1
APODIZATION = HAPP GENZEL
DATA =
.081      .082      .081      .083      .086      .082
.085      .085      .084      .078      .080      .080
.081      .080      .081      .079      .082      .081
.
.
.       761 ROWS OF TRANSMISSIVITIES
.
.
.035      .034      .033      .033      .034      .033
.033      .035      .036      .034      .034      .036

```

Figure A-1: Original ASCII transmissivity file from Nicolet IR44.

SAMPLE THICKNESS (in)

.035					
.081	.082	.081	.083	.086	.082
.085	.085	.084	.078	.080	.080
.081	.080	.081	.079	.082	.081
		.			
		.			
		.			
		.			
		.			
.035	.034	.033	.033	.034	.033
.033	.035	.036	.034	.034	.036

Figure A-2: Transmissivity file modified for input into FORTRAN program.

K(forced)	Corr.	K(best fit)	Corr.	WAVENUMBER, cm^{-1}
74.59	0.9108	55.54	0.9827	2000
74.57	0.9107	55.54	0.9825	
74.52	0.9107	55.48	0.9828	
74.51	0.9112	55.53	0.9827	
74.49	0.9108	55.47	0.9828	
74.42	0.9103	55.39	0.9826	
74.41	0.9113	55.47	0.9825	
74.39	0.9117	55.48	0.9828	
74.37	0.9128	55.53	0.9832	
74.35	0.9123	55.51	0.9827	
74.31	0.9128	55.51	0.9830	
74.28	0.9130	55.50	0.9831	
74.30	0.9144	55.65	0.9830	
74.30	0.9164	55.81	0.9835	
74.34	0.9184	56.02	0.9836	
74.37	0.9193	56.12	0.9838	
74.31	0.9182	55.99	0.9835	
74.23	0.9155	55.95	0.9837	1900
74.04	0.9151	55.52	0.9831	
73.83	0.9154	55.35	0.9835	
73.65	0.9136	55.08	0.9832	
73.49	0.9134	54.93	0.9832	
73.28	0.9122	54.67	0.9832	
73.14	0.9113	54.50	0.9829	
73.01	0.9110	54.38	0.9827	
72.91	0.9113	54.36	0.9826	
72.79	0.9124	54.33	0.9831	
72.70	0.9140	54.39	0.9832	
72.60	0.9140	54.33	0.9831	
72.50	0.9162	54.41	0.9837	
72.39	0.9172	54.41	0.9839	
72.31	0.9170	54.36	0.9836	
72.23	0.9185	54.43	0.9837	
72.16	0.9202	54.53	0.9840	
72.07	0.9210	54.53	0.9841	1800
72.03	0.9233	54.72	0.9842	
71.88	0.9236	54.64	0.9843	
71.71	0.9244	54.58	0.9845	
71.79	0.9278	54.96	0.9849	
71.67	0.9295	55.08	0.9846	
71.15	0.9316	54.90	0.9847	
70.87	0.9350	55.09	0.9847	
71.18	0.9393	55.85	0.9848	Units of K: in^{-1}
73.27	0.9465	58.40	0.9856	
78.77	0.9563	64.18	0.9874	
87.25	0.9628	72.32	0.9884	
95.36	0.9665	79.91	0.9889	
100.69	0.9685	84.84	0.9895	
104.53	0.9713	88.64	0.9905	
108.30	0.9715	92.16	0.9898	
109.46	0.9725	93.26	0.9906	
106.75	0.9683	90.01	0.9890	1700
101.90	0.9645	84.96	0.9883	
96.92	0.9623	80.10	0.9888	
92.45	0.9570	75.40	0.9878	
88.89	0.9519	71.62	0.9869	
86.22	0.9499	69.00	0.9875	
84.15	0.9442	66.65	0.9859	
82.66	0.9412	64.99	0.9859	
81.50	0.9393	63.84	0.9856	
80.54	0.9385	63.00	0.9854	
79.78	0.9376	62.24	0.9857	
79.21	0.9362	61.63	0.9854	
78.77	0.9370	61.38	0.9856	

Figure A-3: Sample program output for polyurethane foam of density $.0300 \text{ g/cm}^3$ and cell diameter $.31 \text{ mm}$. Wavenumber values are not part of the actual output.

78.62	0.9376	61.33	0.9857	
78.59	0.9394	61.53	0.9860	
79.74	0.9429	62.92	0.9861	
80.84	0.9453	64.05	0.9868	
81.31	0.9464	64.60	0.9868	
83.32	0.9490	66.59	0.9871	1600
83.92	0.9491	67.05	0.9873	
81.60	0.9443	64.49	0.9868	
79.31	0.9395	62.07	0.9862	
77.77	0.9377	60.67	0.9858	
76.15	0.9343	59.07	0.9851	
75.33	0.9347	58.51	0.9848	
75.21	0.9390	58.95	0.9850	
76.37	0.9440	60.47	0.9857	
79.25	0.9510	63.71	0.9868	
83.45	0.9551	67.80	0.9871	
87.65	0.9581	71.74	0.9876	
90.49	0.9600	74.43	0.9880	
92.19	0.9618	76.11	0.9886	
92.52	0.9617	76.38	0.9885	
93.98	0.9607	77.46	0.9880	
92.76	0.9605	76.26	0.9886	
88.36	0.9526	71.28	0.9872	1500
85.18	0.9503	68.32	0.9870	
83.36	0.9471	66.41	0.9864	
81.88	0.9441	64.81	0.9859	
80.37	0.9422	63.34	0.9859	
79.58	0.9438	62.92	0.9862	
79.23	0.9437	62.62	0.9862	
79.19	0.9428	62.59	0.9853	
79.86	0.9458	63.49	0.9859	
80.57	0.9479	64.36	0.9862	
81.45	0.9501	65.41	0.9863	
83.20	0.9531	67.30	0.9866	
86.10	0.9571	70.31	0.9874	
89.76	0.9587	73.67	0.9874	
92.80	0.9625	76.94	0.9881	
99.76	0.9668	83.58	0.9892	
101.22	0.9653	84.39	0.9892	
96.05	0.9590	78.67	0.9883	1400
90.94	0.9537	73.54	0.9874	
87.42	0.9504	70.11	0.9871	
85.01	0.9478	67.75	0.9870	
83.90	0.9457	66.63	0.9862	
83.18	0.9458	66.06	0.9864	
81.78	0.9422	64.41	0.9862	
81.16	0.9404	63.70	0.9859	
80.48	0.9389	62.97	0.9857	
79.27	0.9385	61.96	0.9858	
78.71	0.9389	61.59	0.9857	
78.63	0.9406	61.80	0.9854	
78.85	0.9411	62.09	0.9852	
79.02	0.9433	62.49	0.9855	
80.60	0.9476	64.38	0.9859	
83.37	0.9515	67.14	0.9867	
85.03	0.9531	68.75	0.9868	
86.34	0.9548	70.06	0.9873	
87.60	0.9568	71.49	0.9874	1300
89.39	0.9579	73.18	0.9873	
90.96	0.9577	74.42	0.9874	
91.85	0.9589	75.22	0.9883	
92.18	0.9590	75.46	0.9885	
91.48	0.9543	74.19	0.9870	
90.21	0.9545	73.16	0.9872	
88.95	0.9535	71.99	0.9869	
88.29	0.9550	71.72	0.9871	

88.11	0.9537	71.38	0.9867	
88.59	0.9553	72.00	0.9872	
89.40	0.9556	72.68	0.9874	
91.44	0.9574	74.73	0.9874	
94.18	0.9610	77.54	0.9887	
94.80	0.9581	77.53	0.9879	
92.82	0.9552	75.29	0.9878	
90.79	0.9518	73.07	0.9872	
88.69	0.9495	70.98	0.9870	
86.21	0.9452	68.34	0.9865	1200
84.58	0.9439	66.82	0.9866	
83.81	0.9444	66.30	0.9866	
82.71	0.9399	64.90	0.9854	
81.38	0.9388	63.72	0.9853	
80.70	0.9379	63.14	0.9847	
80.64	0.9411	63.45	0.9855	
82.00	0.9458	65.19	0.9859	
83.94	0.9481	67.05	0.9863	
85.60	0.9502	68.71	0.9867	
86.93	0.9516	70.04	0.9866	
87.78	0.9511	70.63	0.9867	
88.64	0.9519	71.45	0.9868	
89.55	0.9528	72.39	0.9866	
89.33	0.9539	72.34	0.9871	
88.68	0.9544	72.10	0.9862	
89.20	0.9624	74.33	0.9863	
89.89	0.9711	77.27	0.9870	1100
90.58	0.9768	79.66	0.9880	
98.82	0.9885	96.43	0.9888	
98.51	0.9872	92.77	0.9894	
99.42	0.9833	90.88	0.9886	
98.24	0.9780	86.75	0.9885	
93.42	0.9657	78.40	0.9877	
89.27	0.9559	72.81	0.9865	
86.76	0.9494	69.64	0.9858	
86.09	0.9476	68.79	0.9857	
85.08	0.9437	67.48	0.9847	
83.30	0.9421	65.73	0.9853	
82.66	0.9422	65.23	0.9854	
84.02	0.9433	66.51	0.9851	
83.47	0.9395	65.55	0.9847	
81.35	0.9332	63.11	0.9838	
80.63	0.9330	62.52	0.9838	
80.22	0.9311	62.01	0.9834	1000
79.64	0.9302	61.51	0.9828	
78.94	0.9290	60.81	0.9829	
78.52	0.9290	60.52	0.9826	
78.37	0.9275	60.26	0.9823	
78.30	0.9275	60.25	0.9819	
78.41	0.9276	60.36	0.9818	
78.45	0.9302	60.62	0.9826	
78.66	0.9307	60.86	0.9825	
79.21	0.9354	61.88	0.9828	
79.76	0.9416	63.10	0.9836	
80.03	0.9428	63.55	0.9834	
79.86	0.9409	63.14	0.9831	
79.30	0.9339	61.80	0.9823	
78.79	0.9281	60.72	0.9818	
78.18	0.9273	60.09	0.9823	
77.91	0.9277	59.93	0.9823	
77.96	0.9280	60.05	0.9819	900
77.85	0.9262	59.79	0.9815	
77.74	0.9283	59.85	0.9825	
77.72	0.9266	59.73	0.9815	
78.07	0.9277	60.22	0.9809	
78.76	0.9347	61.44	0.9828	

79.93	0.9435	63.51	0.9837	
84.28	0.9680	72.04	0.9852	
99.96	0.9867	105.39	0.9882	
113.76	0.9672	132.07	0.9786	
108.35	0.9782	120.75	0.9845	
95.28	0.9877	93.30	0.9879	
89.07	0.9783	79.23	0.9874	
86.43	0.9630	72.64	0.9846	
85.51	0.9566	70.35	0.9843	
84.63	0.9529	68.76	0.9849	
83.26	0.9465	66.68	0.9837	
82.56	0.9451	65.96	0.9832	
82.64	0.9433	65.84	0.9825	800
82.73	0.9417	65.76	0.9818	
83.10	0.9453	66.38	0.9835	
83.90	0.9469	67.08	0.9848	
85.51	0.9468	68.38	0.9846	
86.76	0.9429	68.91	0.9834	
86.91	0.9467	69.45	0.9848	
87.28	0.9447	69.46	0.9844	
86.10	0.9448	68.38	0.9854	
86.22	0.9415	68.15	0.9839	
84.86	0.9384	66.69	0.9832	
84.22	0.9378	66.12	0.9830	
83.28	0.9351	65.08	0.9823	
83.02	0.9327	64.60	0.9818	
83.15	0.9326	64.61	0.9824	
83.93	0.9356	65.52	0.9833	
84.05	0.9295	65.08	0.9809	
83.54	0.9272	64.51	0.9798	700
83.43	0.9300	64.62	0.9813	
82.92	0.9235	63.56	0.9798	
83.09	0.9277	64.19	0.9801	
83.08	0.9261	64.03	0.9795	
83.40	0.9259	64.05	0.9813	
83.54	0.9239	64.01	0.9803	
83.76	0.9260	64.34	0.9812	
84.35	0.9295	65.25	0.9814	
84.20	0.9288	64.96	0.9819	
84.44	0.9298	65.30	0.9818	
84.44	0.9264	64.88	0.9815	
84.34	0.9272	64.68	0.9833	
84.51	0.9216	64.30	0.9816	
84.72	0.9258	64.81	0.9831	
84.88	0.9217	64.61	0.9815	
84.94	0.9242	64.86	0.9823	
85.05	0.9270	65.23	0.9830	600
84.87	0.9195	64.37	0.9812	
85.03	0.9266	65.13	0.9834	
85.23	0.9264	65.27	0.9832	
85.40	0.9330	66.19	0.9841	
85.81	0.9371	67.04	0.9845	
86.46	0.9373	67.83	0.9829	
86.78	0.9339	67.66	0.9821	
87.02	0.9385	68.39	0.9833	
86.95	0.9375	68.27	0.9827	
86.92	0.9332	67.84	0.9810	
86.99	0.9376	68.28	0.9829	
86.94	0.9334	68.07	0.9797	
87.41	0.9418	69.40	0.9823	
88.29	0.9389	70.17	0.9789	
88.84	0.9375	70.16	0.9801	
89.22	0.9271	69.27	0.9771	
88.57	0.9282	68.80	0.9780	500
87.98	0.9253	67.75	0.9792	
87.43	0.9207	66.81	0.9783	

86.72	0.9134	65.21	0.9797	
86.49	0.9083	64.88	0.9757	
86.12	0.9149	65.12	0.9780	
85.67	0.9085	64.05	0.9778	
85.52	0.9135	64.20	0.9807	
85.01	0.9086	63.55	0.9781	
85.05	0.9135	64.23	0.9772	
84.87	0.9218	64.79	0.9800	
84.11	0.9082	62.68	0.9795	
83.89	0.9108	62.96	0.9780	
83.04	0.8954	60.99	0.9753	
83.19	0.8962	61.54	0.9714	
82.93	0.9087	61.61	0.9821	
82.62	0.9117	62.43	0.9751	400

extinction coefficient - force fit: 84.47
average correlation: 0.9392

extinction coefficient - actual fit: 66.96
average correlation: 0.9844


```

do 30 iw=1,760
  do 20 is=10,nsam+9
    il=is-9
    i2=iw-484
*
* The spectrometer file contains transmissivities at wavenumbers outside
* the desired range. These values are read into a dummy variable (q).
*
    if(iw .le. 484) then
      read(is,*)q
    else
      read(is,*)tr(il,i2)
    endif
20  continue
30  continue
*
* The following loop numerically integrates wavenumber-specific
* extinction coefficients to obtain two Rosseland mean coefficients:
* one for the force-fit slope and one for the actual-fit slope.
*
  do 50 j1=1,n
    do 40 j2=1,nsam
      trs(j2)=tr(j2,j1)
40  continue
*
* Obtain the extinction coefficient for each wavenumber interval.
*
  call exc(trs,w,nsam,kfeta,corrf,kbeta,corrb)
*
  eta=2000.-j1*deta
  a=(pi*c1*c2*(eta**4))/(2.*sb*(t**5))
  b=exp(c2*eta/t)
  sumkb=sumkb+((a*b)/(kbeta*(b-1.)*(b-1.)))*deta
  sumkf=sumkf+((a*b)/(kfeta*(b-1.)*(b-1.)))*deta
  sum=sum+((a*b)/((b-1.)*(b-1.)))*deta
*
* Sum correlation coefficients for force-fit and actual-fit extinction
* coefficients to be averaged later.
*
  sumcorrf=sumcorrf+corrf
  sumcorrb=sumcorrb+corrb
*
  write(6,45) kfeta,corrf,kbeta,corrb
45  format(t6,f6.2,t17,f6.4,t33,f6.2,t44,f6.4)
50  continue
*
* The Rosseland mean extinction coefficient is actually the ratio of
* two integrals (see analysis).
*
  krf=sum/sumkf
  krb=sum/sumkb
*
  write(6,60)krf
  write(6,70)sumcorrf/n
  write(6,80)krb
  write(6,70)sumcorrb/n
60  format(//,t3,'extinction coefficient - force fit: ',f6.2)
70  format(t3,'average correlation: ',f6.4,/)
80  format(t3,'extinction coefficient - actual fit: ',f6.2)
  stop
  end
*
*
* Subroutine exc calculates the extinction coefficient from the slopes
* of lines fitting the -ln(transmissivity) vs. thickness data in two
* ways: one (kf) uses a line that is forced through the origin, and the

```



```

* other (kb) uses the conventional least-squares best-fit line without
* regard to its intercept. The correlation coefficients for these two
* cases (rf, rb) are also calculated.
*
      subroutine exc(tau,x,n,kf,rf,kb,rb)
      real kb,tau(15),x(15),kf,icept
      sumx2=0.
      sumxy=0.
      sumx=0.
      sumy=0.
      sumym=0.
      sumycb=0.
      sumycf=0.
*
* Obtain sums from data points for force-fit and best-fit slope
* equations
*
      do 100 j=1,n
          if(tau(j) .le. .0001) tau(j)=.0001
          y=-log(tau(j))
          sumx2=sumx2+(x(j)*x(j))
          sumxy=sumxy+(y*x(j))
          sumy=sumy+y
          sumx=sumx+x(j)
100    continue
*
      kf=sumxy/sumx2
      kb=(n*sumxy-sumx*sumy)/(n*sumx2-sumx*sumx)
*
* 'icept' is the y-intercept of the best-fit line. It is not needed in
* this program, but is included for completeness.
*
      icept=(sumy*sumx2-sumxy*sumx)/(n*sumx2-sumx*sumx)
      ym=sumy/n
*
* Obtain sums of deviations to obtain correlation coefficients
*
      do 110 i=1,n
          if(tau(i) .le. .0001) tau(i)=.0001
          y=-log(tau(i))
          ycf=k*x(i)
          ycb=kf*x(i)+icept
          sumym=sumym+(y-ym)*(y-ym)
          sumycb=sumycb+(y-ycb)*(y-ycb)
          sumycf=sumycf+(y-ycf)*(y-ycf)
110    continue
      sigy2=sumym/(n-1)
      sigyxb2=sumycb/(n-2)
      sigyxf2=sumycf/(n-2)
      if(sigyxf2 .ge. sigy2) then
          rf=0.
          go to 120
      endif
      rf=(1.-(sigyxf2/sigy2))**.5
120    rb=(1.-(sigyxb2/sigy2))**.5
      return
      end

```

Appendix B

Summarized Extinction Coefficient Data for Polyurethane Foams

Source	Foam number	d , mm	ρ , g/cm ³	$\sqrt{\rho}/d$, g ^{1/2} /cm ^{5/2}	K_b , cm ⁻¹	r_b	K_f , cm ⁻¹	r_f
1	1a	.21	.0289	8.10	38.0	.9934	55.7	.8387
	1b	.29	.0300	5.97	30.7	.9757	47.6	.7534
	1c	.47	.0294	3.65	22.5	.9919	26.0	.9755
	1d	.34	.0363	5.60	27.9	.9899	33.8	.9623
	1e	.31	.0300	5.59	26.4	.9844	33.3	.9392
	1f	.36	.0293	4.75	30.5	.9778	34.4	.9664
	1g	.38	.0262	4.26	21.9	.9897	30.7	.8824
2	2a	.43	.0261	3.76	25.6	.9592	25.3	.9568
	2b	.26	.0351	7.21	27.3	.9299	48.3	.3377
3	3a	.55	.0269	2.98	17.0	.9466	21.0	.9140
	3b	.40	.0268	4.09	25.7	.9777	32.6	.9351
4	4	.22	.0497	10.13	51.8	.9879	65.2	.9386
5	5	.39	.0264	4.17	25.2	.9841	28.9	.9715

Table B.1: Cell size, density, and extinction coefficient data for polyurethane foams from five different sources. Also included are the correlation coefficients r_b , r_f for the best-fit and force-fit methods, respectively.

Foam number	K_b, cm^{-1}	K_{pred}, cm^{-1}	Percent difference
1a	38.0	34.2	-10.0
1b	30.7	27.5	-10.4
1c	22.5	19.7	-12.4
1d	27.9	28.0	+0.4
1e	26.4	26.3	-0.4
1f	30.5	23.3	-23.6
1g	21.9	20.9	-4.6
2a	25.6	19.2	-25.0
2b	27.3	33.0	+20.9
3a	17.0	16.9	-0.6
3b	25.7	20.5	-20.2
4	51.8	46.4	-10.4
5	25.2	20.7	-17.9

Table B.2: Comparison of best-fit extinction coefficient with the value predicted from Eqn. (4.1). The difference is compared to the best-fit (measured) value to obtain the percentage.

Bibliography

- [1] Woods, G., The ICI Polyurethanes Book, John Wiley and Sons, New York, 1987.
- [2] Schuetz, M.A., and Glicksman, L.R., "A Basic Study of Heat Transfer in Foam Insulation," *Journal of Cellular Plastics*, pp. 114-121, March-April 1984.
- [3] Glicksman, L.R., and Torpey, M., "Radiation in Foam Isulation," Proceedings of the Polyurethane World Congress, 1987.
- [4] Skochdopole, R.E., "The Thermal Conductivity of Foamed Plastics," *Chemical Engineering Progress* No. 57, p. 57, 1961.
- [5] Doherty, D.C., Hurd, R., and Lester, G.R., "The Physical Properties of Rigid Polyurethane Foams," *Chemistry and Industry*, p. 1343, 1962.
- [6] Schuetz, M.A., "Heat Transfer in Foam Insulation", M.S.Thesis, Department of Mechanical Engineering, Massachusetts Institute of Technology, 1982.
- [7] Williams, R.J.J., and Aldao, C.M., "Thermal Conductivity of Plastic Foams," *Polymer Engineering and Science* 23, No. 6, pp.293-298, April 1983.
- [8] Siegel, R., and Howell, J.R., Thermal Radiation Heat Transfer, Hemisphere Publishing Corp., New York, 1981, pp. 412-504.
- [9] Glicksman, L.R., Mozgowiec, M., and Torpey, M., "Radiation Heat Transfer in Foam Insulation," to be presented at the Ninth International Heat Transfer Conference, 1990.

- [10] Torpey, M., "A Study of Radiation Heat Transfer Through Foam Insulation," M.S. Thesis, Department of Mechanical Engineering, Massachusetts Institute of Technology, 1987.
- [11] Hottel, H.C., and Sarofim, A.F., Radiative Transfer, McGraw-Hill, New York, 1967, p. 379.
- [12] Saltykov, S.A., *Stereometric Metallography*, second edition, *Metallurgizdat*, Moscow, 1958.
- [13] Underwood, E.E., Quantitative Stereology, Addison-Wesley, Reading, Mass., 1970, pp, 31,68.
- [14] Cunningham, A., Personal Communication, ICI Polyurethanes, Kortenberg, Belgium, 1989.
- [15] Schael, G.W., "Characterization of the Structure of Cellular Plastics," *Journal of Applied Polymer Science*, Vol. 11, pp. 2131-2142, 1967.
- [16] Michalski, W.J., and Hubeny, H. "Statistic Examination of Cell-Size Distribution in Structural Polyurethane Foam," *Kunststoffe* 68, No. 8, pp. 479-483, 1978.
- [17] Reitz, D.W., "A Basic Study of Gas Diffusion in Foam Insulation," M.S. Thesis, Department of Mechanical Engineering, Massachusetts Institute of Technology, 1983.
- [18] Ozisik, M.N., Radiative Transfer and Interactions with Conduction and Convection, John Wiley and Sons, New York, 1973, pp. 24-25, 316-319.
- [19] Sinofsky, M., "Property measurement and Thermal Performance Prediction of Foam Insulations," M.S. Thesis, Department of Mechanical Engineering, Massachusetts Institute of Technology, 1984.
- [20] Cunningham, A., and Sparrow, D.J., "Rigid Polyurethane Foam: What Makes it the Most Effective Insulant?" *Cellular Polymers*, Vol. 5, pp. 327-342, 1986.

- [20] Cunningham, A., and Sparrow, D.J., "Rigid Polyurethane Foam: What Makes it the Most Effective Insulant?" *Cellular Polymers*, Vol. 5, pp. 327-342, 1986.
- [21] Hobbs, S.Y., "Bubble Growth in Thermoplastic Structural Foams," *Polymer Engineering and Science*, Vol. 16, No. 4, 1976.
- [22] Saunders, J.H., and Hansen, R.H., "The Mechanism of Foam Formation," Plastic Foams, Frisch, K., ed., M. Dekker, New York, 1972, pp. 24-59.